공학박사학위논문

압력구배가 거친 표면 위 난류경계층 특성에 미치는 영향

Pressure Gradient Effects on Smooth and Rough Surface Turbulent Boundary Layers

2014년 8월

서울대학교 대학원

기계항공공학부

신 주 현

압력구배가 거친 표면 위 난류경계층 특성에 미치는 영향

Pressure Gradient Effects on Smooth and Rough Surface Turbulent Boundary Layers

지도교수 송 성 진

이 논문을 공학박사학위논문으로 제출함

2014년 4월

서울대학교 대학원

기계항공공학부

신 주 현

신주현의 박사학위 논문을 인준함

2014년 6월

위 원 장 : _____ (인)

부 위 원 장 : _____ (인)

위 원 : _____ (인)

위 원 : _____ (인)

위 원 : _____ (인)

Abstract

Pressure Gradient Effects on Smooth and Rough Surface Turbulent Boundary Layers

Ju Hyun Shin

Mechanical and Aerospace Engineering

The Graduate School

Seoul National University

The present study investigates the effects of streamwise pressure gradients on turbulent boundary layers over smooth and rough surfaces. For smooth surfaces, even with a higher wall shear stress, favorable pressure gradient barely changes friction coefficient due to the increases freestream velocity. Adverse pressure gradient decreases friction coefficient slightly. For smooth surfaces, favorable pressure gradient increases streamwise normal Reynolds stress near the surface because

FPG confines high-turbulence vortices to a narrow region near the surface and reduces outward movement of vortices. On the contrary, adverse pressure gradient decreases streamwise normal Reynolds stress near the surface by enhancing the outward movement of near-surface vortices. Under zero pressure gradient, by generating additional coherent unsteady vortices, surface roughness increases mean velocity defect throughout the boundary layer. The surface roughness also increases streamwise normal Reynolds stress and friction coefficient. Combined effects of roughness and pressure gradients have been investigated. For rough surfaces, favorable pressure gradient enhances the roughness effects of increasing mean velocity defect, streamwise normal Reynolds stress, and friction coefficient. Also, favorable pressure gradient increases roughness-induced streamwise turbulent kinetic energy production. The FPG effects are due to 1) near-surface confinement of roughness-generated vortices and 2) strengthened roughness-induced vortices due to an increased velocity gradient. On the contrary, near the surface, adverse pressure gradient reduces the roughness effects on mean velocity defect, streamwise normal Reynolds stress because APG enhances outward convection of roughness-induced vortices and decreases the velocity gradient. Consistently, adverse pressure gradient decreases friction coefficient and streamwise turbulent kinetic energy production in the rough surface boundary layer. The results show that

favorable pressure gradient increases the roughness effects while adverse pressure gradient decreases the roughness effects. From the results, mean velocity and friction coefficient estimation methods are proposed. Irrespective of the Reynolds number, pressure gradient, and surface roughness, the ratio of displacement thickness to boundary layer thickness provides appropriate scaling for collapsing the mean velocity profiles in flat plates, axial compressor blade boundary layers, and axial turbine blade boundary layers. A new power law mean velocity estimation method, applicable to smooth and rough flat plate boundary layers with and without pressure gradient, is proposed. The new power law can also accurately estimate mean velocity profiles in axial compressor and turbine blade boundary layers. Finally, a new friction coefficient correlation is proposed for smooth and rough surface turbulent boundary layers with and without pressure gradient. The proposed correlation can also estimate the friction coefficients in smooth axial turbine blades.

Keywords: Flat plate, Friction coefficient, Mean velocity, Pressure gradient, Scaling, Surface Roughness, Turbomachinery blade, Turbulent boundary layer

Student number: 2009-20692

Contents

List of Figures

List of Tables

Nomenclature

C	Blade chord
C_{ax}	Axial blade chord
C_f	Friction coefficient, $\tau_w/(0.5\rho U_\infty^2)$
d_p	Wire diameter of hot-wire probe
H	Shape factor, δ^*/θ
K	Acceleration parameter, $(\nu/U_\infty^2)(dU_\infty/dx)$
k	Nominal roughness height
k_i	Height of each peak and valley for rough surface
k_r	Nominal height of the sandgrain roughness
k_s	Equivalent sandgrain roughness
k^+	Roughness Reynolds number based on k, ku_τ/ν
k_s^+	Roughness Reynolds number based on k_s, $k_s u_\tau/\nu$
L	Length of the flat plate
l_p	Wire length of hot-wire probe
l_p^+	Dimensionless hot-wire probe wire length, $l_p u_\tau/\upsilon$
Ma	Mach number
p	Pitch (streamwise spacing among the roughness elements)
P	Local static pressure
P^+	Pressure gradient parameter, $\nu(dP/dx)/\rho u_\tau^3$

q	Streamwise turbulent kinetic energy flux, $\int_0^{\delta} u'^2 U_{\infty} dy$
R	Radius of streamline curvature
Ra	Centerline averaged roughness, $\frac{1}{N}\sum_{i=0}^{N} \lvert k_i \rvert$
Re_c	Reynolds number based on the blade chord, $U_0 C/\nu$
Re_L	Reynolds number based on the length of flat plate, $U_0 L/\nu$
Re_x	Reynolds number based on the streamwise distance from the leading edge, $U_{\infty} L/\nu$
Re_{θ}	Reynolds number based on the local momentum thickness, $U_{\infty}\theta/\nu$
s	Suction surface distance from the stagnation point
st	Stanton number
T_t	Total temperature
T_w	Wall temperature
Ti_{∞}	Turbulence intensity upstream of the flat plate
TKE	Integrated streamwise turbulent kinetic energy, $(\int_0^{\delta} u'^2 dy)/(U_0^2 L)$
u	Time mean velocity in the x direction
u'	Fluctuating velocity in the x direction
$<u'>$	Root-mean-square of the u'
$\overline{u'u'}$	Mean value of the normal Reynolds stress ($u'u'$)
u^+	Dimensionless streamwise velocity, u/u_{τ}

u_τ	Friction velocity, $\sqrt{\tau_w/\rho}$
U_∞	Local freestream velocity
U_0	Inlet freestream velocity
v'	Fluctuating velocity in the y direction
$\overline{v'v'}$	Mean value of the normal Reynolds stress ($v'v'$)
x	Streamwise distance from the flat plate leading edge
x_{ax}	Axial distance from the blade leading edge
y	Normal distance from the surface
y^+	Dimensionless distance from the surface, yu_τ/ν
z	Spanwise distance from the flat plate midspan
α	Inclination angle of the vortices downstream of the roughness elements
β	Pressure gradient parameter, $\delta^*(dP/dx)\tau_w$
δ	Boundary layer thickness, $y_{u=0.99U_\infty}$
δ^*	Displacement thickness, $\int_0^\delta (1-u/U_\infty)dy$
θ	Momentum thickness, $\int_0^\delta (u/U_\infty)(1-u/U_\infty)dy$
Π	Wake parameter
ρ	Fluid density
τ_w	Wall shear stress
ν	Fluid kinematic viscosity

ψ	Stream function, $\int_0^y u dy$
ω_z	Spanwise vorticity
ω_x'	Vorticity fluctuation in the x direction
ω_y'	Vorticity fluctuation in the y direction
ω_z'	Vorticity fluctuation in the z direction

Chapter 1. Introduction

1.1 Motivation

Gas turbine is a air-breathing internal combustion engine which is commonly used to produce electric energy in combined-cycle power plants and to generate thrust for aircraft. It consists of compressor, combustor, and turbine (Fig. 1.1). Compressor increases pressure upstream a combustor. Thermal energy is added to the flow by supplying fuel in the combustor. The energy is converted to the shaft work in the turbine stage and the shaft work is used to drive the compressor and electric generator. To operate such system at the best efficiency, it is important to maintain the design total pressure and axial velocity [1]. Aerodynamic loss in compressor and turbine stages reduces total pressure and axial velocity. Denton [2] catagorized the loss sources into three- profile loss, secondary loss, and leakage loss (Fig. 1.2). Profile loss arises from the 2-dimensional blade boundary layers developing over blades suction and pressure surfaces. Secondary loss arises from the secondary flows near the endwall. Leakage loss is generated from the 3-dimensional leakage flows near the blade tips and

hub clearances. Each loss source is responsible for one-third of the total pressure loss. According to Curtis et al. [3], 60% and 20% of the total pressure loss arise from the suction and pressure surface boundary layers, respectively. Over a compressor blade, boundary layer is transitional or turbulent for x/C > 0.3 [4, 5] and most of the suction surface loss arises from turbulent boundary layer which is under adverse pressure gradient (APG, $dP/dx > 0$) (Fig. 1.3). Under APG, freestream velocity decreases with increasing streamwise location x. According to Mayle [6], for a controlled-diffusion compressor airfoil with Re_c = 300,000, the acceleration parameter K [7] ranged from -2.0×10^{-6} to 0 on suction surfaces and was inversely proportional to Re_c.

As efficiency becomes ever more important in gas turbine, surface quality of compressor and turbine blades have increasingly grained attention [8] due to its significant impact on the profile loss. Figure 1.4 shows (a) fouled second stage compressor rotor blades and (b) roughened third stage turbine rotor blades of a heavy duty gas turbine [9]. In compressors, ingestions of salt, dust, oily smoke increases surface roughness [10]. Shin et al. [11] measured heights of surface roughness over a rotor blade of a heavy-duty gas turbine compressor and found that the maximum roughness height for fouled compressor is

centerline averaged roughness *Ra*, average of the absolute heights of roughness peaks and valleys (Fig 1.5), is 16.93 μm. In turbines, deposition of fuel particles, erosion and corrosion of blade surfaces, and thermal barrier coating (TBC) spallation can increase surface roughness [12]. Bons et al. [12] and Taylor [13] measured surface roughness on in-sevice turbine blades. The maximum turbine surface roughness was *Ra* = 41.3 μm. Those compressor and turbine roughnesses are 3-dimensional and randomly distributed throughout the blade surfaces. Koch and Smith [14] proposed a correlation between *Ra* and 'equivalent sandgrain roughness' *Ks*. *Ks* is average height of sandpaper roughness or height of densely packed spheres on smooth surfaces [15]. physically, *Ks* is the roughness height that causes the same friction for a surface roughened by sand grains [16]. According to Koch and Smith [14], *Ks* is 6.2 times the centerline averaged roughness *Ra*. Such roughness increases profile loss and decreases mass flow rate and system efficiency. According to Millsaps et al. [10], roughness in compressor stage can decreases efficiency, mass flow rate, and power output by 1%, 1%, and 3%, respectively, and increases fuel consumption by 2%. The compressor roughness causes additional fuel and maintenance costs of US$ 2,000,000 per gas turbine per year [17]. Yun et al. [18] found that the normalized efficiency of a single-stage

axial turbine can decrease by up to 19% with 400-μm blade roughness. Back et al. [19] found that the mass-averaged loss and deviation of a compressor cascade can increase as *Ks/C* increases from 0.0006 to 0.00425. Leipold et al. [20] found a increased boundary layer on a rough compressor blade. Zhang et al. [21] and Lorenz et al. [22] also found that surface roughness increases total pressure loss and boundary layer thickness in a turbine cascade. According to Back et al. [23] the roughness effect of increasing aerodynamic loss is mainly due to the roughness in the aft half-chord (x/C = 0.5 ~ 1.0) where turbulent boundary layer develops under APG. Therefore, to understand the mechanism of such roughness effect and to estimate the roughness effect on aerodynamic loss, it is necessary to investigate the individual and combined effects of pressure gradient and surface roughness effects on flat plate turbulent boundary layers. Also, to estimate the profile loss arises from such flows, it is required to develop mean velocity and friction coefficient estimation methods which are applicable to both smooth and rough surface turbulent boundary layers with and without pressure gradient and turbomachinery blade turbulent boundary layers. In this study, "flat plate boundary layer" refers to turbulent boundary layer developing over flat plates without 1) streamwise curvature effect which induces pressure gradient in wall normal direction ($\partial P/\partial y$), 2) no

relaminarlization, and 3) no flow separation. "pressure gradient" refers to streamwise pressure gradient which consists of favorable pressure gradient (FPG, $dP/dx < 0$), zero pressure gradient (ZPG, $dP/dx = 0$), and APG. "turbomachinery blade boundary layer" refers to attached axial compressor and turbine blade boundary layers.

1.2 Background

In this section, previous researches on FPG and APG effects on smooth surface turbulent boundary layer are introduced. Next, researches on surface roughness on boundary layer under zero pressure gradient (ZPG, $dP/dx = 0$) are introduced. Figure 1.6 shows schematic of boundary layers over (a) smooth surface under ZPG, (b) smooth surface under FPG, (C) smooth surface under APG, and (d) rough surface under ZPG. Combined effects of pressure gradients and surface roughness on rough surface boundary layers in the literature are also introduced. Finally, mean velocity estimation and friction coefficient estimation methods in the literature are introduced.

1.2.1 FPG effects on smooth surface boundary layer

Attention has also been paid to favorable pressure gradient (FPG)

effects on the smooth plate turbulent boundary layers [24]. Compared to ZPG flow, for smooth surfaces, FPG decreased the mean velocity defect [25, 26] and shape factor [25, 27]. However, regarding turbulence quantities (e.g., $\overline{u'u'}$), there is still a discrepancy that arises from normalizing factors - 1) *local* freestream velocity (U_∞) and 2) *inlet* freestream velocity (U_0). FPG decreased $\overline{u'u'}/U_\infty^2$ throughout the boundary layer in Joshi et al. [24]. However, according to Escudier et al. [25], FPG decreased u'/U_∞ only in the outer layer (ψ/ν > 400) and barely affected the maximum u'/U_∞ near the surface (ψ/ν < 400). Yet, both studies [24, 25] showed that FPG increases $\overline{u'u'}/U_0^2$ near the surface (y/δ < 0.1 in Joshi et al. [24] and ψ/ν < 2,000 in Escudier et al. [25]) and decreases it in the outer region. Joshi et al. [24] also presented contours of spanwise vorticity ($\omega_z\delta/U_0$) for both ZPG and FPG boundary layers. Compared to the ZPG boundary layer, most of the vortices existed near the surface (y/δ < 0.1) under FPG ($K\times10^6$ = 0.6 ~ 1.1), suggesting that FPG suppressed the outward migration of the coherent structures and aligned the vortices more parallel to the surface.

1.2.2 APG effects on smooth surface boundary layer

A number of studies have been conducted to identify the APG effects on smooth surface turbulent boundary layers on flat plates. Spalart and Watmuff [28] conducted experiments and Direct Numerical Simulation (DNS) studies of non-equilibrium turbulent boundary layers under an APG. With APG, the growth rates of displacement (δ^*) and momentum thickness (θ) increased with increasing *x*. In addition, as *x* increased, the shape factor (*H*) also was increased, and the friction coefficient (C_f) was decreased with increasing *x*. Krogstad and Skare [29] conducted an experimental investigation of equilibrium turbulent boundary layers with a strong APG (β = 20). Unlike the zero pressure gradient (ZPG) boundary layers with only one peak near y/δ = 0.03, APG boundary layers had two - "inner" and "second" - peaks inthe turbulent production profiles, and the "second" peak existed at y/δ = 0.45. The C_f under APG was smaller than that under ZPG. Nagano et al. [30] measured non-equilibrium, APG turbulent boundary layers with P^+ = 0 ~ 2.87×10^{-2} (β = 0 ~ 5.32). For y/δ < 0.4, $<u'>/U_0$ decreased as P^+ increased. At y/δ = 0.03, compared to the ZPG boundary layer, the fluctuating velocity component changed more slowly

with time under APG, indicating APG reduced turbulent energy production. Recently, Lee and Sung [31] conducted a DNS investigation of APG turbulent boundary layers. They showed that APG enhanced vorticity fluctuations (ω'_x, ω'_y and ω'_z) for y/δ > 0.2 but decreased them for y/δ < 0.2. For the mean velocity distribution, both Nagano et al. [30] and Lee and Sung [31] found a downward shift (Δu^+) of the mean velocity profiles in the logarithmic layer.

1.2.3 Roughness effects on boundary layers under ZPG

The impact of surface roughness on turbulent boundary layers has been investigated by many researchers. Acharya et al. [32] and Brzek et al. [33] showed that surface roughness increases the friction coefficient (C_f) in ZPG boundary layers. For a rough surface, the total drag was composed of the pressure drag on roughness elements and friction drag on the surface [34, 35]. Growth rates of δ^* and θ increased as C_f was increased [32]. Pipe flow study of Nikuradse [36] and ZPG plate boundary layer studies of Brzek et al. [33], Krogstad et al. [37], and Krogstad and Antonia [38] showed that roughness increases the normalized mean velocity defect ($1-u/U_\infty$). In the

logarithmic layer, surface roughness decreases y^+ and shifts the mean velocity profile downward [36]. The amount of shift (ΔB) is called "roughness function" or "roughness shift" (Eq. (1.1)).

$$u^+ = (1/\kappa)\ln(y^+) + B - \Delta B \tag{1.1}$$

where κ and B are 0.41 and 5.0, respectively. In Brzek et al. [33], roughness also increased the $\overline{u'u'}/U_\infty^2$ throughout the boundary layer. These observations [33, 36, 37, 38] at the boundary layer thickness (δ) scale were due to the vortical structures and shearing motions at the roughness height (k_r) scale [37]. Thus, the roughness effect became stronger as normalized roughness height (k_r/δ) increased. Jimenez [39] found that the roughness effects are visible in the outer layer for k_r/δ > 0.02.

Few studies have focused on the roughness effects on flow structures at the k_r scale. Furuya et al. [34] investigated two-dimensional wire roughness effects on the mean flow structure and drag. For their fully rough configuration (k^+ > 80), pressure drag contributed to 70% of the total drag. In addition, the pressure drag increased as the pitch to

roughness height ratio *p/k* was increased. The high pressure drag for *p/k* = 8 was related to the reattachment location of the separated flow between the two wires. Meinders and Hanjalic [40] visualized flows around a surface-mounted-array of cubes. Horseshoe vortices, generated near the frontal face, propagated downstream, and arc-shaped vortices were found in the wake downstream of the cubes. Also, flow separation and reattachment were found on and downstream of the cube surfaces. Laser Doppler Anemometry (LDA) measurements showed that the $\overline{u'u'}$ downstream of the cubes was significantly higher than in the freestream and wasmaximized in the shear layer near the separation and horseshoe vortex region. Djenidi et al. [41] showed vortices downstream of 2-dimensional square bars (k_r/δ = 0.026) and found turbulence intensity ($<u'>/U_\infty$) peaks near the roughness elements (y/k_r = 1 ~ 3).

1.2.4 Combined effects of FPG and roughness

Coleman et al. [42] and Chakroun and Taylor [43] measured higher Stanton number (*St*) for a rough surface with an FPG than with a ZPG. More recently, Bons and McClain [44] measured momentum thickness and streamwise turbulent kinetic energy flux (*q*) at a fixed

location($Re_x \approx$ 900,000) with “real” turbine surface roughnesses and pressure gradients. Roughness increased all of the measured parameters significantly. Furthermore, the roughness effects on momentum thickness and streamwise turbulent kinetic energy flux were enhanced by FPG.

Coleman et al. [45] made the first near surface velocity measurements of rough surface turbulent boundary layers under FPG. Their fully rough surface was composed of densely packed, uniform sized sphere elements with a diameter of 1.27 mm. For their rough surface non-equilibrium FPG ($K\times10^6$ = 0.29) boundary layer, the shape factor decreased as the streamwise distance (x) increased. Compared to the rough surface ZPG case, roughness decreased u^+ less under FPG. Cal et al. [46] presented mean velocity and Reynolds stress data for smooth and transitionally rough (k^+ = 16 ~ 72) surface turbulent boundary layers with mild non-equilibrium FPG ($K\times10^6$ = 0.017 ~ 0.26). The C_f was higher for the rough surface FPG boundary layers than for the smooth surface FPG boundary layers. For the rough surface FPG boundary layers, $\overline{u'u'}/U_\infty^2$ increased throughout the boundary layer with increasing k^+. Cal et al. [47] also investigated roughness and FPG effects on turbulent boundary layers with a fully roughened surface. With the same 24-grit sandpaper roughness, k^+

ranged between 49 ~ 54 and 103 ~ 248 for the rough surface ZPG and rough surface FPG boundary layers, respectively. C_f for the rough surface FPG boundary layer was higher than that for the rough surface ZPG boundary layer. For a rough surface, FPG decreased $\overline{u'u'}/U_\infty^2$ slightly for y/δ > 0.5. However, for y/δ < 0.5, FPG increased $\overline{u'u'}/U_\infty^2$ significantly.

Tay et al. [48] conducted particle image velocimetry (PIV) measurements in a turbulent channel flow with rough converging walls (non-equilibrium FPG). Two types of roughness - sandgrain with a 1.55-mm diameter and gravel with a mean diameter of 4.22 mm - were introduced. Both transitionally rough and fully rough conditions were generated. The *K* values were higher than those in previous studies [45 ~ 47] and ranged between 1.44 ~ 3.60×10^6 and 0.89 ~ 3.93×10^6 for the smooth and rough surfaces, respectively. In some limited cases, *K* values were beyond the criterion for relaminarization [49] (Eq. (1.2)).

$$K_{crit} \approx 2\times10^{-6} \tag{1.2}$$

C_f did not change but k^+ was decreased due to FPG in the rough surface boundary layer, and, thus, FPG made the surface “less rough”.

1.2.5 Combined effects of APG and roughness

A few studies investigated the combined effects of the APG and surface roughness. Perry and Joubert [50] provided the first measurements of rough surface APG turbulent boundary layers. Two-dimensional square bars with a pitch to height ratio (*p/k*) of 4 were used. Similar to the rough surface ZPG boundary layer data by Moore [51], the roughness shifts($\Delta u/u_\tau$) for rough surface APG boundary layers were linearly proportional to the normalized roughness height (k^+). Bons and McClain [44] performed heat transfer and boundary layer measurements for a rough patch with "real" turbine surface roughness at $Re_x \approx$ 900,000. Effects of surface roughness and APG ($K\times10^6$ = - 0.225) manifested themselves in the Stanton number, momentum thickness and turbulent kinetic energy flux. Compared to the ZPG boundary layer, the rough patch effect on the momentum thickness was reduced by 49.2% under APG. Thus, APG reduced the roughness effect of increasing θ.

Detailed boundary layer measurements of 3-dimensional, distributed roughness under APG were conducted by Pailhas et al. [52] and Tay et al. [53]. Pailhas et al. [52] performed turbulent boundary layer measurements with two rough surfaces (*k*=500-μm and 600-μm) and two different types of APG. C_f for the rough surface APG boundary

layers were higher than those for smooth surface APG boundary layers. However, for the same roughness, C_f decreased with increasing APG. Also, the roughness Reynolds numbers k_s^+, inferred from the measured Δu^+ and a correlation of Nikuradse (Pailhas et al. [52]), were smaller under APG than under ZPG.

Tay et al. [53] conducted turbulent flow measurements using Particle Image Velocimetry (PIV) in a diverging channel section ($K \times 10^6$ = - 0.435 ~ - 0.922). Both APG and surface roughness increased δ, δ^*, θ, and mean velocity defect ($1-u/U_\infty$). At y/δ=0.2, APG increased the mean velocity defect slightly more in the rough surface boundary layer than in the smooth surface boundary layer. For rough surfaces, C_f and k_s^+ increased significantly in the stronger APG region. Also, APG increased the Reynolds stress more in the rough surface boundary layers than in smooth surface boundary layers. Thus, they concluded that the effect of APG and roughness may “augment one another”.

1.2.6 Mean velocity and friction coefficient estimation methods

To estimate profile loss under pressure gradient and surface roughness, it is important to establish the scaling factor which correlates with such effects. Zagarola and Smits [54] proposed δ^*/δ as the scaling

factor for normalized mean velocity defect profiles in smooth pipe flows. For smooth surface ZPG flat plate turbulent boundary layers, the Reynolds number dependence (Re_θ = 460 ~ 48,300) of mean velocity defect profiles (1-u/U_∞ vs. y/δ) also scaled with δ^*/δ [55]. For a smooth plate, the effects of the adverse pressure gradient (APG) and favorable pressure gradient (FPG) also scaled with δ^*/δ [55].

In rough surface studies, Castillo et al. [56] conducted high-Reynolds number (Re_θ = 29,773~116,832) boundary layer measurements on a rough (block type roughness) flat plate without pressure gradients and showed that the mean velocity defect profiles scaled with δ^*/δ. Cal et al. [28] showed that mean velocity defect profiles in the rough plate cases scaled with δ^*/δ under FPG. Under APG, Tay et al. [53] found that mean velocity defect profiles in rough surface, channel flow cases scaled with δ^*/δ.

For outer layers of turbulent boundary layers, Eq. (1.3) has often been used to estimate velocity profile.

$$\frac{u}{U_\infty} = (\frac{y}{\delta})^\gamma \tag{1.3}$$

The conventional 1/7 power law assumes γ = 1/7. From the definition

of the displacement thickness and momentum thickness, γ = (*H*-1)/ 2 has also been proposed. However, in axial compressors and turbines, low (e.g., Re_θ = 680 in a smooth compressor [57] and Re_θ = 590 in a roughened turbine [58]) turbulent boundary layers have been found, and, for such boundary layers, depends on Re_θ [59]. Johnson and Bushnell [59] proposed $1/\gamma = m\log(Re_\theta) + b$ where *m* and *b* depend on the wall total temperature ratio (T_w/T_t) and Mach number (*Ma*).

For the velocity profile of overlap layers, Eq. (1.1) has been widely used. However, Ching et al. [60] showed that the log-law may not be appropriate for boundary layers at low Reynolds numbers (Re_θ = 400~1,320) because the logarithmic region becomes too thin to be clearly identified.

Alternatively, power laws which use wall variables have been proposed. George and Castillo [61] proposed power laws in both the inner and outer coordinates:

$$u^+ = C_i (y^+ + a^+)^\gamma \tag{1.4a}$$

$$\frac{u}{U_\infty} = C_o ((y + a)/\delta)^\gamma \tag{1.4b}$$

Here, C_i, C_o, and γ depend on Reynolds number, and a^+ and a are shifts in the origin ($y=y^+=0$).

Bergstrom et al. [62] tested Eqs. (1.4a) and (1.4b) with low (Re_θ = 1,080 ~ 3,920) turbulent boundary layers in an open channel flow and showed that the power laws match the experimental velocity profiles in the overlap and outer layers. According to Bergstrom et al. [62], for rough surfaces, the velocity profiles estimated by Eqs. (1.4a) and (1.4b) matched the measured velocity profiles better than the logarithmic law (Eq. (1.1)).

Studies have also proposed correlations for the skin friction coefficient (C_f). Most of the correlations consider the Re_θ effect only for smooth surfaces [63]. For Re_θ = 1,430 ~ 31,000, Bergstrom et al. [64] proposed a friction coefficient correlation applicable to both smooth and rough surface boundary layers without pressure gradients (Eq. (1.5)).

$$C_f^{0.5} = (0.360 \pm 0.025)(\delta^*/\delta) \tag{1.5}$$

According to Bergstrom et al. [64], C_f correlates with the mean velocity scaling factor δ^*/δ. However, the applicability of Eq. (1.5) to

turbulent boundary layers with FPG and APG has not yet been examined.

1.3 Research objectives

Despite such efforts, there is still a dearth of information about FPG and APG effects on turbulent boundary layers with and without surface roughness. First, the friction coefficient data for smooth surface FPG boundary layers are limited, and there is a divergence of opinion regarding the FPG effect on the distribution of the turbulence quantities in smooth surface boundary layers. Second, the effects of FPG on mean velocity defect and normal Reynolds stress are not fully understood for rough surface boundary layers. Such data are essential to understand the influence of FPG on flow structures near and far above the roughness elements. Third, previous rough surface, FPG boundary layer results show discrepancies. Cal et al. [46, 47] showed that FPG significantly increased the friction coefficient that is already increased by surface roughness. However, Tay et al. [48] did not show such a trend. Fourth, the FPG effects on the friction coefficient and integral boundary layer parameters (δ, δ^*, θ, H, and δ^*/δ) of rough surface boundary layers need to be further investigated. Fifth, the FPG effect

on the integrated streamwise turbulent kinetic energy (*TKE*) has not yet been investigated for either smooth or rough surfaces. Sixth, for rough surfaces, the APG effects on turbulence structures are not fully understood. Seventh, there is a divergence of opinion on the combined effects of roughness and APG. Pailhas et al. [11] showed that APG decreased C_f and k_s^+ in the rough surface cases, and Bons et al. [10] found that APG decreased the roughness effect on θ. However, contrary to Pailhas et al. [52], Tay et al. [53] showed that APG increased for rough surfaces. Eighth, there is still lack of information about the individual and combined effects of APG and roughness on friction coefficient and integral boundary layer parameters - δ, δ^*, θ, *H*, and δ^*/δ. Ninth, the APG effect on *TKE* in boundary layers has not yet been investigated for either smooth or rough surfaces. Tenth, a systematic comparison of the APG and FPG effects on turbulence structure and friction coefficient are scarce for either smooth or rough surfaces. Eleventh, there has not yet been a systematic evaluation of the applicability of the δ^*/δ to scale the individual and combined effects of Reynolds number, pressure gradient (ZPG, FPG, and APG), and roughness for flat plates. Furthermore, for rough flat plate turbulent boundary layers under pressure gradients, power laws for mean velocity estimation and correlations for C_f estimation do not yet exist. Finally,

the applicability of δ^*/δ-based estimation methods for mean velocity and C_f for turbomachinery boundary layers has not yet been examined. The study aims to answer the following questions.

1. How does FPG change the distribution of C_f for smooth surfaces?
2. For smooth surfaces, how do FPG and APG change the streamwise turbulence quantities in terms of $<u'>/U_\infty$ and $\overline{u'u'}/U_0^2$?
3. For rough surfaces, how does FPG change $1-u/U_\infty$ and $\overline{u'u'}/U_0^2$?
4. How does FPG change the distribution of C_f and integral boundary layer parameters - δ, δ^*, θ, *H*, and δ^*/δ - for rough surfaces?
5. How does FPG change *TKE* for both smooth and rough surfaces?
6. For rough surfaces, how does APG change $1-u/U_\infty$ and $\overline{u'u'}/U_0^2$?
7. How does APG change the distribution of C_f and integral

boundary layer parameters - δ, δ^*, θ, H, and δ^*/δ - for rough surfaces?

8. How does APG change *TKE* for both smooth and rough surfaces?
9. How different/similar are the effects of APG and FPG on smooth and rough surface turbulent boundary layers?
10. Do the mean velocities of the flat plate and turbomachinery boundary layers scale with δ^*/δ?
11. Can the mean velocity profiles of the flat plate and turbomachinery boundary layers be estimated in terms of δ^*/δ?
12. Can C_f for the flat plate and turbomachinery boundary layers be estimated with δ^*/δ?

1.4 Thesis organization

This thesis consists of seven chapters. Descriptions for each chapter are as follows.

Chapter 1 introduces issues on surface roughness in gas turbines. Previous researches on pressure gradients and roughness effects on turbulent boundary layers are reviewed. Also, researches on mean

velocity scaling, mean velocity estimation, and friction coefficient estimation methods are introduced. The objectives of the present study are presented.

Chapter 2 describes the experimental facility for the flat plate boundary layer measurements. Description of the test section, instrumentation, and test matrix are presented.

In Chapter 3, the test results for smooth surface turbulent boundary layers with and without pressure gradient are presented. The effect of pressure gradients on mean velocity, turbulence, friction coefficient, and integral boundary layer parameters of smooth surface turbulent boundary layers are discussed.

In Chapter 4, the test results for rough surface turbulent boundary layers with and without pressure gradient are presented. The effect of surface roughness on turbulent boundary layer under ZPG are discussed. Next, FPG and APG effects on rough surface turbulent boundary layers are discussed. The results shows that FPG increases the roughness effects, while APG reduces the roughness effects.

In Chapter 5, applicability of the δ^*/δ scaling to smooth and rough flat plate and turbomachinery boundary layers with and without pressure gradient is discussed. A new power law using δ^*/δ is proposed and the applicability of the power law is evaluated.

In Chapter 6, a new friction coefficient correlation, applicable to rough surface flat plate boundary layers with varying pressure gradients and smooth turbine blade boundary layers, is proposed.

Chapter 7 summarizes the new contributions of this research.

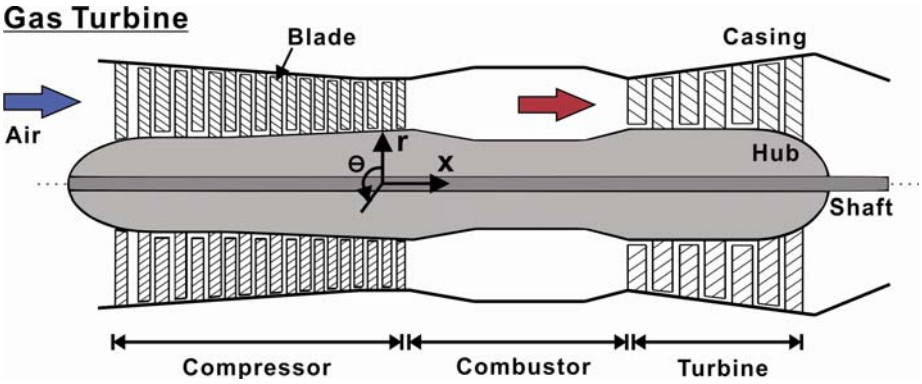

Fig. 1.1 A schematic of gas turbine.

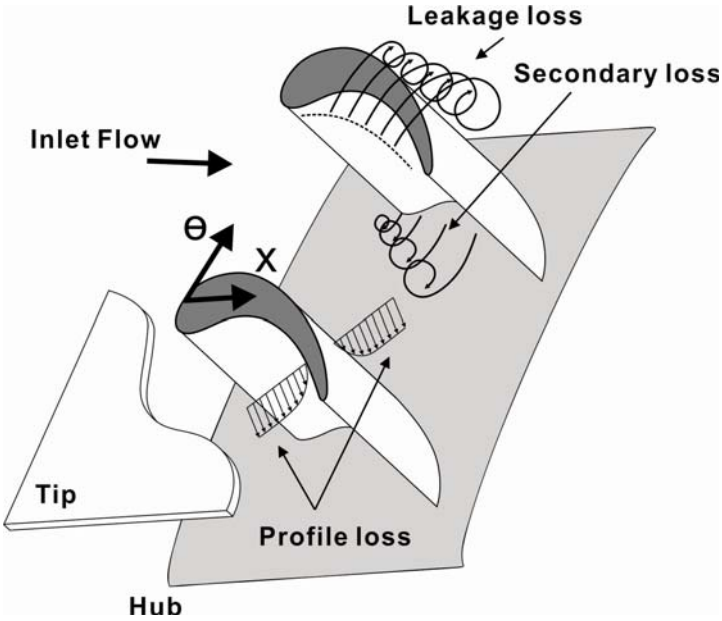

Fig. 1.2 Three loss sources in gas turbine.

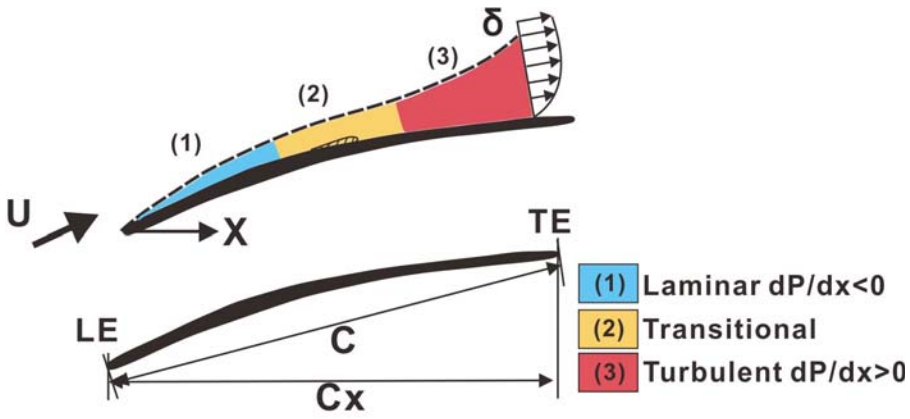

Fig. 1.3 Boundary layers in turbomachinery blades.

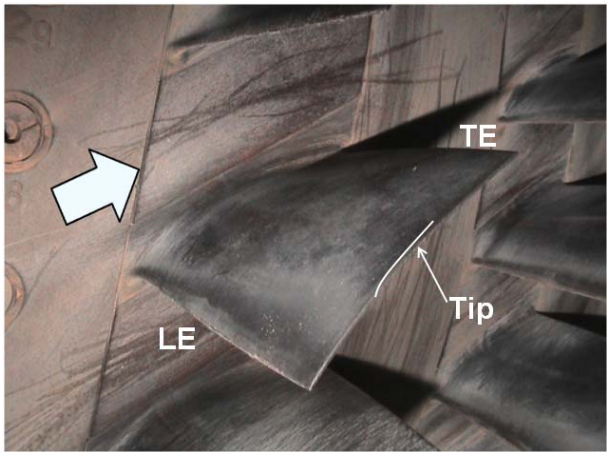

(a)

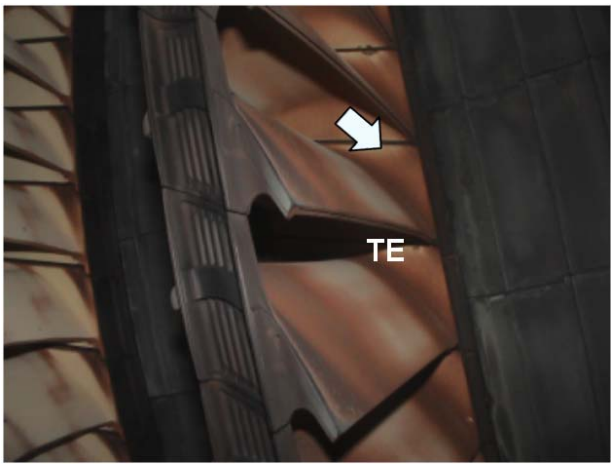

(b)

Fig. 1.4 Roughened heavy duty gas turbine blades:
(a) Second stage compressor rotor blade, (b) Third stage turbine rotor blades [9].

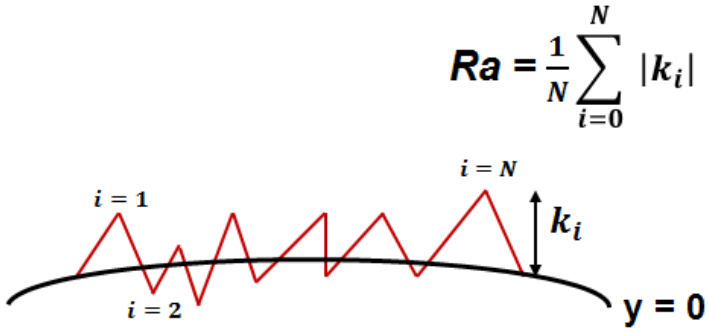

Fig. 1.5 A schematic of rough surface.

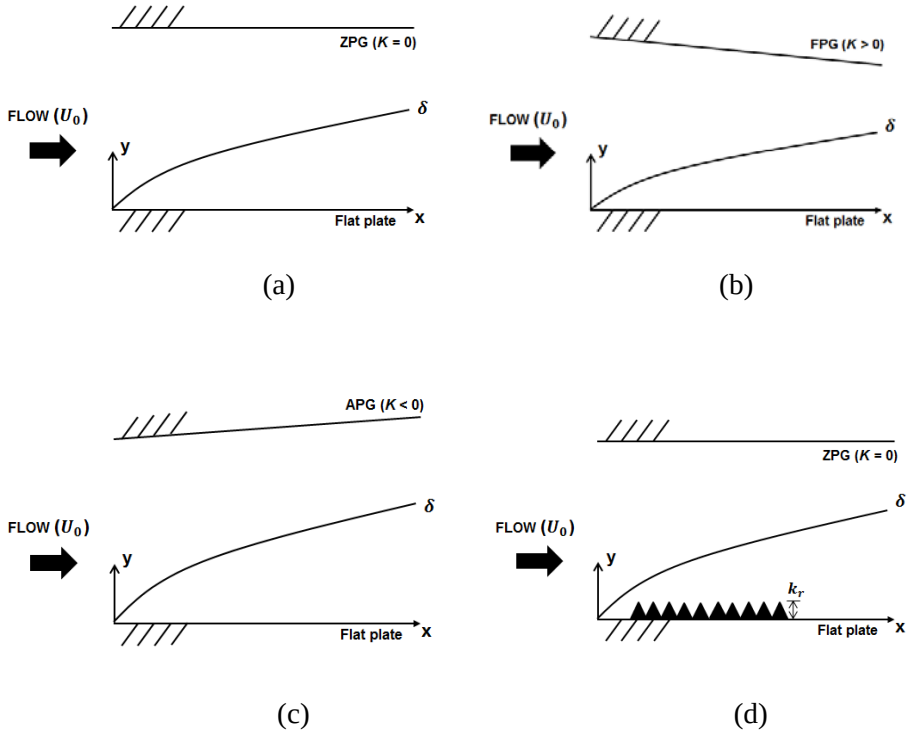

Fig. 1.6 Schematic of boundary layers over a flat plate: (a) Smooth surface zero pressure gradient, (b) Smooth surface favorable pressure gradient, (c) Smooth surface adverse pressure gradient, (d) Rough surface zero pressure gradient.

Chapter 2. Experimental Method

2.1 Test facility

2.1.1 Wind tunnel

Flat plate boundary layer measurements have been conducted in an open-type, low-speed wind tunnel at Seoul National University (SNU). The wind tunnel consists of a 45-kW blower, diffuser, settling chamber, contraction duct, and test section (Fig. 2.1). The maximum volume flow rate is 620 m^3/min, and flow speed is controlled by an inverter. The freestream turbulence intensity just upstream of the test section (Ti_∞) is 0.7 ~ 0.8%. The freestream velocity has been kept throughout the test section.

2.1.2 Test section

A 430 mm $\times$ 400 mm $\times$ 2,400 mm test section contains a 1,200 mm $\times$ 400 mm $\times$ 10 mm aluminum flat plate. The flat plate has an elliptic leading edge with a 120-mm major axis and a 10-mm minor axis and a 40-mm-long triangular trailing edge. The elliptic leading edge is used to prevent the leading edge separation.

An endwall of the test section is replaced by an adjustable wall to control the pressure gradient (Fig. 2.2). FPG has been imposed by reducing flow area using the adjustable wall. With an reduced flow passage, the flow has been accelerated in the streamwise direction. For APG, the flow area has been widen in the streamwise direction to decelerate the flow.

Surface roughness is simulated by using sheets of 40-grit (grit size, k = k_r = 400-μm) and 60-grit (k_r = 250-μm) sand papers which are composed of sand grits glued onto a 500-μm-thick base paper. The sandpaper is attached over the entire surface of the plate including the leading edge and the trailing edge, except at the 9 axial locations (S1~S9, Table 2.1) where boundary layers are measured. S1 is located 151.5 mm downstream from the leading edge, and the stations are 114.0 mm apart. These smooth measurement sections are 10 mm long and cover the entire plate span. The distance between the upstream roughness and measuring station is 5 mm, corresponding to $12.5k_r$. Such configuration is introduced to 1)minimize the error in the origin (y_0); and 2) measure reattached boundary layers downstream of roughness elements. Thus, the measured velocity profiles and turbulence structures reflect not only the local roughness effects but also the diffusion of the turbulence properties and mixing losses downstream of

the roughness elements. By attaching 500-μm-thick aluminum bars on the smooth regions, steps between the smooth and rough regions have been removed. Therefore, there is no step effect in the result. The roughness configuration for 40-grit roughness case is illustrated in Fig. 2.3. For smooth surface (k=2 μm), the 40-grit sandpaper is attached only on the leading edge to trip the boundary layer. The leading edge shape and trip mechanism are identical for both rough and smooth surfaces.

2.2 Instrumentation

A Pitot probe and PSI pressure transducer (0.05% full-scale accuracy) has been used to measure the inlet free-stream velocity (U_0) at the plate leading edge. Boundary layer has been measured using a Dantec Dynamics 55p15 single-sensor boundary layer type hot-wire probe with a constant temperature anemometer (CTA) at 9 stations (S1 ~ S9) in Table 2.1. Probe wire diameter (d_p) and length (l_p) are 5 μm and 1.25 mm, respectively (l_p/d_p = 250) and the probe wire is 42 viscous length long (l_p^+ = 42). At a given streamwise location, hot-wire voltage outputs have been measured at 50 ~ 150 positions in the y direction. A 2-axis traverse system with a resolution of 0.005 mm has been used to

position the probe. The traverse system has been controlled with a LabVIEW software. At each position, outputs have been sampled at 10 kHz for 10 seconds. The voltage outputs have been converted to velocities using 4th order polynomial fittings as in Fig. 2.4. The fitting curves have been determined via an in-situ calibration using the wind tunnel and pitot probe used in the present study. Uncertainty in the mean velocity measurement is 0.3% with a 95% confidence interval. Instrumentation is summarized in Table 2.2.

2.3 Test matrix

Boundary layer measurements have been made for 11 different Cases as listed in Table 2.3. In Chapter 3, smooth surface boundary layer data for Cases 1 (Smooth / ZPG), 2 (Smooth / FPG), and 3 (Smooth / APG) are used. In Chapter 4, rough surface boundary layer data for Cases 8 (Rough / ZPG), 9 (Rough / FPG), and 11 (Rough / APG) are used. To investigate the combined effects of pressure gradients and roughness, the acceleration parameter distributions in the rough surface pressure gradient boundary layers have been controlled to be similar to the smooth surface pressure gradient boundary layers. Also, the normalized local freestream velocity distributions for the rough surface

boundary layers are also similar to the smooth surface boundary layers (Fig. 2.5) In Chapter 5 and 6, all of the test cases (Cases 1~11) are used. The k_r/δ in the present study ranges from 0.015 to 0.049, from 0.020 to 0.075, and from 0.011 to 0.039 for the rough surface ZPG (Case 8), rough surface FPG (Case 9), and rough surface APG (Case 11) cases, respectively. The Roughness Reynolds number (k_s^+) ranges from 103 to 143, from 155 to 243, and from 60 to 112 for the rough surface ZPG (Case 8), rough surface FPG (Case 9), and rough surface APG (Case 11) cases, respectively. For all of the measurements, Reynolds number, based on the length of the flat plate and the free-stream velocity at the flat plate leading edge (Re_L), is 900,000.

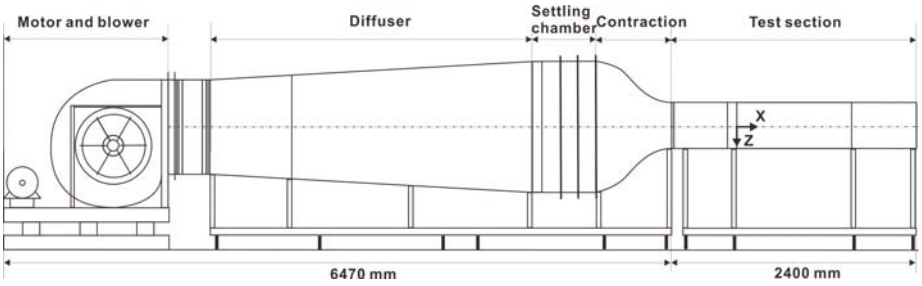

Fig. 2.1 A Schematic of wind tunnel.

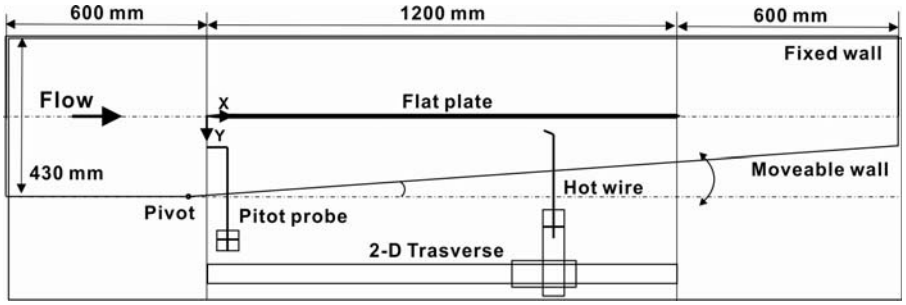

(a)

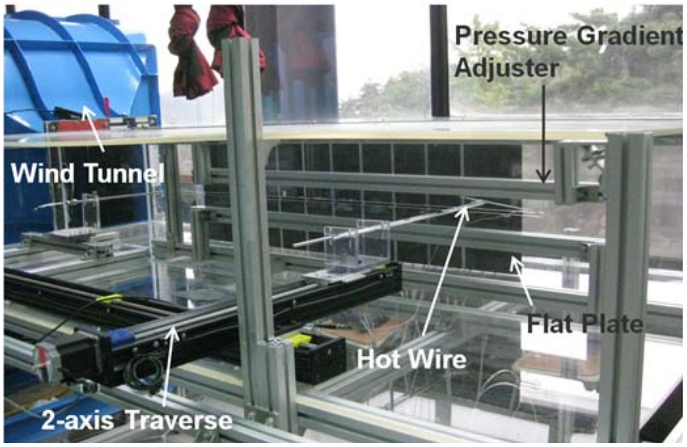

(b)

Fig. 2.2 Test section: (a)Schematic, (b)Picture.

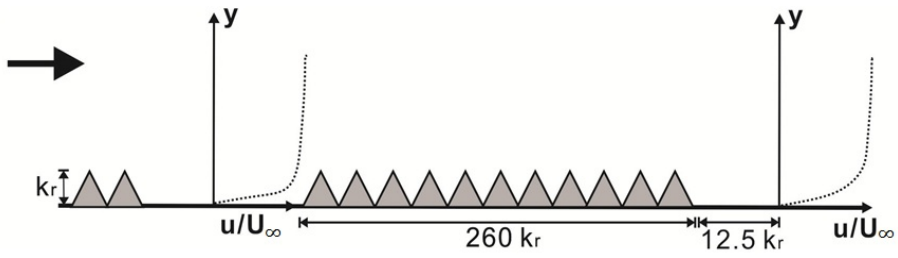

Fig. 2.3 Roughness configuration ($k_r = 400\,\mu m$).

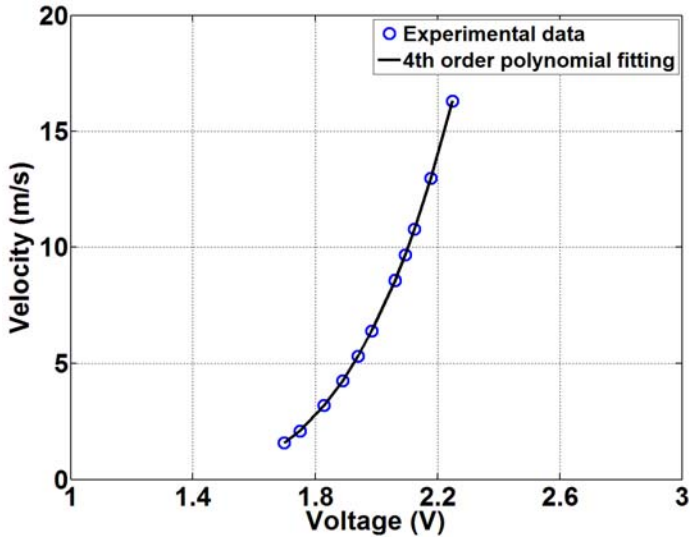

Fig. 2.4 Hot-wire cabliration curve.

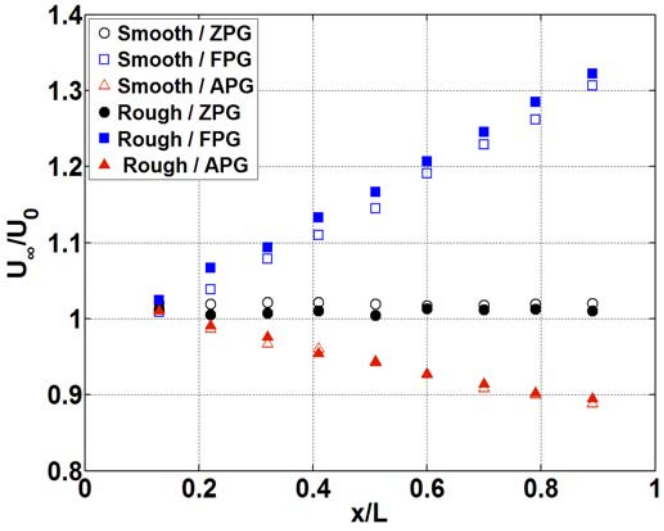

Fig. 2.5 Freestream velocity distributions.

Table 2.1 Locations of measuring stations.

	S1	S2	S3	S4	S5	S6	S7	S8	S9
x/L	0.13	0.22	0.32	0.41	0.51	0.60	0.70	0.79	0.89

Table 2.2 Instrumentation.

Instrument	Measuring location	Data
Pitot probe	Leading edge	Upstream velocity
Hot-wire anemometry	9 stations on flat-plate 50~150 points in the y direction at each station	Streamwise time-mean velocities Streamwise velocity fluctuations

Table 2.3 Test matrix.

No.	Case	$k \times 10^3/L$	$K \times 10^6$	$Re_x \times 10^{-3}$	Re_θ
1	Smooth / ZPG	0	-0.015 ~ 0.015	116 ~ 816	880 ~ 2,220
2	Smooth / FPG	0	0.377 ~ 0.284	115 ~ 1,046	540 ~ 1,510
3	Smooth / APG	0	-0.223 ~ -0.143	115 ~ 711	1,160 ~ 2,810
4	Smooth / APG2	0	-0.370 ~ -0.286	114 ~ 621	1,870 ~ 4,350
5	Smooth / APG3	0	-0.480 ~ -0.375	112 ~ 619	2,410 ~ 5,090
6	Rough #60 / ZPG	0.208	0.014 ~ -0.028	119 ~ 810	750 ~ 2,620
7	Rough #60 / APG	0.208	-0.244 ~ -0.158	113 ~ 711	1,130 ~ 3,450
8	Rough #40 / ZPG	0.333	-0.031 ~ -0.040	116 ~ 809	950 ~ 2,970
9	Rough #40 / FPG	0.333	0.355 ~ 0.269	116 ~ 1,058	620 ~ 2,640
10	Rough #40 / FPG2	0.333	0.650 ~ 0.512	110 ~ 1,220	420 ~ 2,400
11	Rough #40 / APG	0.333	-0.201 ~ -0.139	113 ~ 716	1,210 ~ 3,630

Chapter 3.

Pressure Gradient Effects on Smooth Surface Boundary Layers

3.1 Smooth surface boundary layers under zero pressure gradient

To validate the test configuration and investigate the mean velocity distribution, turbulence distribution, and boundary layer growth characteristics in the baseline case, mean velocity profiles, turbulence intensity profiles are measured. From the mean velocity profiles, friction coefficient, and boundary layer integral parameters are inferred.

Figure 3.1 shows the measured smooth surface ZPG mean velocity defects ($1-u/U_\infty$) versus non-dimensional surface normal distance (y/δ) at S8 (x/L = 0.79). The flows have conventional mean velocity characteristic of turbulent boundary layers. A high velocity gradient is shown for y/δ < 0.1 which consists of the viscous sublayer (y^+ < 5), buffer layer (5 < y^+ < 30), and lower part of the logarithmic layer (30 < y^+ < 70). For 0.05 < y/δ < 0.3, the velocity defect data show good

agreement with the smooth surface ZPG velocity defect measurements by Castillo and Johansson [65]. The mean velocity profile is also shown in inner coordinate (Fig. 3.2). The friction velocity (u_τ) for the inner variables u^+ and y^+ has been estimated from the C_f obtained from the slope of mean velocity profile via the Clauser chart technique [66] with the least square method. In this study, the upper limits of the log regions for the Clauser chart fitting are y^+ = 100 and y^+ = 200 at S2 and S9, respectively. At a given location, the lower limits of the log regions are y^+ = 30 and y^+ = 50 for smooth surface and rough surfaces, respectively. Despite the low Re_θ tested in the present study, there are more than 15 data points in clear log regions for all of the velocity profiles. For Re_θ>290, Tay et al. [48] also found that log regions in smooth and rough surface turbulent boundary layers with and without FPG. According to Nishizawa et al. [67] and Madad et al. [68], C_f inferred via the Clauser chart technique (with κ = 0.41 and B = 5.0) show good agreement with those directly measured using an oil film interferometry for smooth surface ZPG, FPG, and APG boundary layers. For $0.1 < y/\delta < 0.3$, the velocity profile shows good agreement with the logarithmic law (Eq. (1.1)) with ΔB = 0. The zero roughness shift indicates that the flat plate surface is hydraulically smooth.

Figure 3.3 shows the streamwise turbulence intensity profiles plotted versus (a) y/δ and (b) $y+$. In turbulence measurement with hot-wire probes, errors can increase near a surface [69]. The probe wire length in the present study (l_p^+ = 42) is longer than the Ligrani and Bradshaw's [69] recommended length of l_p^+ < 42. Yet, present study's turbulence intensity quantitatively show good agreement with the turbulence intensity profile measured by Ligrani and Bradshaw with l_p^+ = 3.3 (★ symbol) for $y+$ > 40, corresponding to y/δ > 0.05 and y/k_r > 2.7. For $y+$ < 40, the present study underestimates turbulence intensity slightly. However, the present study's turbulence intensity profile shows good agreement with result of Ligrani and Bradshaw [69] with l_p^+ = 12 (☆ symbol) throughout the boundary layer, and thus the present study's turbulence data are reliable. Turbulence intensity has its maximum at y^+ = 16 ~19 (buffer layer) where most of the turbulence production occurs by the "bursting motion" [70]. This turbulence production process is strongly related to vortex structures near the surface. For y/δ > 0.03, turbulence intensity gradually decreases and reaches $3\,Ti_\infty$ at y/δ = 1.0.

C_f distribution for the present smooth surface ZPG boundary layer is shown in Fig. 3.4. The friction coefficient C_f is defined as ratio of

wall shear stress (τ_w) to dynamic pressure of local freestream ($0.5\rho U^2$). Therefore, C_f indicates wall shear stress under ZPG. The friction coefficient decreases slightly with increasing Reynolds number Re_θ. This common Reynolds number dependence has previously been shown via Direct Numerical Simulation (DNS) by Spalart [71] and empirical correlation by Osaka et al. [63]. The friction coefficients from the present study show quantitatively good agreement with Spalart's result and Osaka's correlation. The C_f from correlation (Eq. (3.1)) of Ludwieg and Tillmann [72] has also been plotted. For Re_θ > 1,500 Eq. (3.1) shows good agreement with experimental result of present study. However, for Re_θ < 1,500, Eq. (3.1) slightly underpredicts C_f. Therefore, Eq. (3.1) does not estimate C_f for low-Re_θ turbulent boundary layers.

The boundary layer thickness (δ) and momentum thickness (θ) are presented versus the local Reynolds number based on the streamwise position (x) in Fig 3.5. Boundary layer thickness is defined as normal distance from the wall where local mean velocity (u) reaches 99% of the local freestream velocity (U_∞). Momentum thickness is calculated from the mean velocity profiles and it indicates momentum loss or local profile loss. Physically, boundary layer grows as the fluid in the

freestream enters the turbulent boundary layer at $y \approx \delta$. The interface is characterized by "bulges" which are strongly related to the vortices in the outer layer [70]. As boundary layer grows, boundary layer thickness and momentum thickness increases as Re_x increases.

From the boundary layer integral parameters, the shape factor (*H*) and ratio of the displacement thickness and boundary layer thickness (δ^*/δ) are calculated. Distribution of those parameters are plotted versus Re_θ in Fig 3.6. In Fig 3.6(a), shape factor data from purtell et al. [73] (experimental) and Spalart [71] (DNS) are also shown. Shape factor shows the ratio of mass defect and momentum defect in boundary layers and a conventional view of the shape factor is "indicator of the flow separation". For smooth surface turbulent boundary layer under ZPG, it ranges from 1.3 to 1.7. The shape factors in the present study ranges from 1.4 to 1.5. As Re_θ increases, *H* decreases gradually. Thus, relative to the mass defect, momentum defect increases more rapidly as Re_θ increases. The present study's shape factors show good agreements with data from Purtell et al. [73] and Spalart [71].

The ratio of the displacement thickness and boundary layer thickness (δ^*/δ) plotted versus Re_θ is shown in Fig. 3.6(b). Spalart and Watmuff [28] suggested δ^*/δ as the “centroid of vorticity” (Eq. (3.2)).

$$\omega_z \approx -du/dy, \quad U_\infty \equiv -\int_0^\infty \omega_z dy, \quad \delta^* \equiv -\frac{1}{U_\infty}\int_0^\infty y\omega_z dy \qquad (3.2)$$

Thus, δ^*/δ represents the location of the center of mean vorticity relative to the height of the boundary layer. δ^*/δ decreases gradually as Re_θ increases. Thus, location of the mean vorticity shift downward as Re_θ increases. Such Re_θ can also be found in the mean velocity profiles [74].

3.2 Favorable pressure gradient effects

Figure 3.7 shows the FPG effect on the mean velocity defect in the smooth surface boundary layer. FPG decreases the velocity defect significantly throughout the boundary layer. Such FPG effect can be found at all of the measuring stations and qualitatively similar FPG effect was shown by Herring and Norbury [26]. FPG also decreases the boundary layer thickness. Consequently, FPG increases the streamwise velocity gradient (*du/dy*), or shear stress, at the surface (y = 0).

Figure 3.8 shows the smooth surface ZPG and FPG mean velocity

profiles in the inner coordinate. Similar to the ZPG boundary layer, a clear logarithmic layer can be found. FPG slightly increases *B* in Eq. 1.1 and such result is consistent with the DNS result of Spalart and Watmuff [28].

Figure 3.9 shows (a) the turbulence intensity ($< u' > / U_\infty$) and (b) streamwise normal Reynolds stress ($\overline{u'u'} / U_0^2$) profiles for varying y/δ in the smooth surface FPG boundary layers. For y/δ < 0.02, FPG slightly increases $< u' > / U_\infty$ (Fig. 3.8(a)). In previous works, on the contrary, FPG either decreased $< u' > / U_\infty$ [24] or barely changed $< u' > / U_\infty$ [25] near the surface. The present result shows that FPG can increase near-surface $< u' > / U_\infty$ even with a higher freestream velocity U_∞. For y/δ > 0.02, FPG decreases $< u' > / U_\infty$ due to the increased freestream velocity. Figure 3.9(b) shows the effect of FPG on turbulence production. FPG increases streamwise turbulence production for y/δ < 0.6. The result shows that FPG enhances the near-surface turbulence production. On the contrary, for y/δ > 0.6, FPG barely changes $\overline{u'u'} / U_0^2$. The result is consistent with the observation of Joshi et al. [24] which showed that FPG can confine the vortices and

turbulence near the surface. Due to the confinement of vortices, turbulence production increases near the surface while the turbulence production reduces in the outer part of the boundary layer.

Despite the higher wall shear stresses in Fig. 3.7, the freestream velocity increases as well for the FPG boundary layer. Therefore, the C_f for the FPG boundary layer is almost the same as that for the ZPG boundary layer (Fig. 3.10). Thus, the low-Re_θ C_f correlation for smooth surface ZPG boundary layers [63] is also applicable to smooth surface FPG boundary layers. Eq. (3.1) overpredicts C_f slightly because Eq. (3.1) estimates C_f only with the shape factor. It implies that for low low Reynolds number, correlation between C_f and H is less strong than that for high Reynolds number.

Due to the increased freestream velocity and reduced turbulence energy in the outer region, FPG decreases boundary layer thickness growth rate and momentum thickness (Fig. 3.11).

Figure 3.12 shows FPG effects on H and δ^*/δ. FPG decreases both parameters throughout the measuring stations tested in this investigation. The decreased shape factor indicates that FPG decreases mass defect more than momentum defect and FPG can delay the flow separation.

The decreased δ^*/δ shows that FPG shifts the vorticity center to the surface.

3.3 Adverse pressure gradient effects

Measurements are conducted with APG to investigate the adverse pressure gradient effects on mean and turbulence properties for smooth surface boundary layers. Comparison between APG and FPG effects are also discussed in this section.

Figure 3.13 shows the APG effect on the mean velocity profile for smooth flat plates. APG increases the mean velocity defect throughout the boundary layer. The decreased mean velocity near the surface leads to reduced velocity gradient (*du/dy*) and wall shear stress. Consequently, the friction velocity is reduced by the APG. On the contrary, FPG decreased velocity defect and increased wall shear stress (τ_w) and friction velocity (u_τ) for smooth surface boundary layers. Thus, APG and FPG have the opposite influence on τ_w and u_τ. Figure 3.14 shows the smooth surface mean velocity profiles in the inner coordinate. The velocity profile in the APG boundary layer agree well

with the smooth surface ZPG boundary layer in the logarithmic (30 < y^+ < 300) and buffer (5 < y^+ < 30) layers. Nagano et al. [6] and Lee and Sung [7] showed that a sufficiently large ($\beta \geq 0.73$) APG may shift the mean velocity profile downward in the logarithmic region. Note that such APG effect is contrary to the FPG effect in Fig. 3.8.To compare the present APG with those in the previous works, β is calculated from the measured *K* using the bernoulli equation (Eq. (3.3)).

$$\beta = (\frac{\delta^*}{\tau_w})(\frac{dP}{dx}) = -\rho U_\infty (\frac{\delta^*}{\tau_w})(\frac{dU_\infty}{dx}) \qquad (3.3)$$

The β in the present study ranges from 0.28 to 0.44. Due to the weak APG in the present study, the downward shift is not visible. However, as expected, APG widens the wake region (y^+ > 300), corresponding to y/δ > 0.3. The velocity profile in the wake region can be expressed using the wake parameter (Π) proposed by Coles [75] (Eq. (3.4)).

$$u^+ = \frac{1}{\kappa}\ln(y^+) + B + \frac{\Pi}{\kappa}\omega(\frac{y}{\delta}) \qquad (3.4)$$

In the present study, Π is determined at $y = \delta$ with $\omega(y/\delta) = 1 - \cos(\pi y/\delta)$. The estimated Π in the smooth surface ZPG boundary layer is 0.57, showing good agreement with conventional value of Π=0.55. In the APG boundary layer, Π higher at 0.81.

Figure 3.15 shows distributions of streamwise turbulence intensity $< u' > / U_\infty$ and streamwise normal Reynolds stress $\overline{u'u'}/U_0^2$ versus y/δ. APG increases the turbulence intensity for y/δ > 0.1. For y/δ > 0.1, the current data show good qualitative agreement with those of Tay et al. [53]. Due to the stronger pressure gradient and higher local freestream turbulence intensity, turbulence intensities in Tay et al. [53] are higher than those in the present study. For y/δ < 0.1, the APG effect is barely shown. The increase in the turbulence intensity for y/δ > 0.1 can be due to either - 1) a decrease in the local freestream velocity (U_∞) or 2) an increase in the fluctuating velocity (u'). Figure 3.15(b) shows which one is responsible for the trends in Fig. 3.15(a). For y/δ > 0.4, APG slightly increases $\overline{u'u'}/U_0^2$ and decreases U_∞. Thus, both factors increase turbulence intensity. However, for 0.1 < y/δ < 0.4, APG decreases $\overline{u'u'}/U_0^2$, and, thus, the increased $< u' > / U_\infty$ in the region is only due to the decreased U_∞. Furthermore, the APG

effect of decreasing $\overline{u'u'}/U_0^2$ extends down to y/δ < 0.1, indicating that turbulence production is reduced in the region. As shown by Lee and Sung [31], the redistribution of the $\overline{u'u'}$ is strongly related to the vorticity distribution. They inferred that APG emancipated the near wall vortices and turbulence from the inner region (y/δ < 0.2) and transported them to the outer region. Contrary to the APG, FPG increases $/\overline{u'u'}/U_0^2$ near the surface. Thus, near the surface, APG decreases turbulence production and FPG increase it. Such contrast is due to the different roles of APG and FPG on convection of vortices near the surface.

Figure 3.16 shows friction coefficient distributions of smooth surface ZPG and smooth surface APG boundary layers. The correlation curve proposed by Osaka et al. [63] for the smooth surface ZPG boundary layer and the smooth surface APG data from Tay et al. [53] are also shown. Friction coefficients in the present smooth surface APG boundary layers and Tay et al. [53] are lower than those of the present smooth surface ZPG boundary layer and Osaka's correlation. Thus, APG decreases C_f. It is due to the decreased velocity gradient near the surface. With increased shape factors, C_f from Eq. (3.1) are also lower

than those in the smooth surface ZPG case.

Figure 3.17 shows the APG effects on boundary layer thickness and momentum thickness. Contrary to FPG, APG increases growth rates of both parameters due to the decreased mean velocity and increased turbulence energy in the outer region. Also, contrary to FPG, APG increases shape factor and δ^*/δ (Fig. 3.19). Thus, APG increases mass defect more than momentum defect, induces flow separation, and shifts the vorticity center outward.

3.4 Conclusions

The conclusions of this chapter can be summarized as follows.

1. Compared to the smooth surface ZPG boundary layer, for smooth surfaces, FPG decreases mean velocity defect throughout the boundary layer.
2. For smooth surfaces, FPG increases streamwise normal Reynolds stress near the surface.
3. FPG barely changes friction coefficient because the increased freestream velocity counteracts against the increased wall shear

stress.

4. FPG decreases growth rates of the boundary layer thickness and momentum thickness, shape factor, and δ^*/δ.
5. Compared to the smooth surface ZPG boundary layer, for smooth surfaces, APG increases mean velocity defect throughout the boundary layer.
6. For smooth surfaces, APG decreases streamwise normal Reynolds stress near the surface.
7. APG slightly decreases friction coefficient due to the decreased wall shear stress.
8. APG increases growth rates of the boundary layer thickness and momentum thickness, shape factor, and δ^*/δ.
9. The FPG effect of increasing near turbulence production is related to the confinement of vortices due to the FPG. On the contrary APG decreases the near-surface turbulence production because APG enhances the outward convection of near-surface vortices.

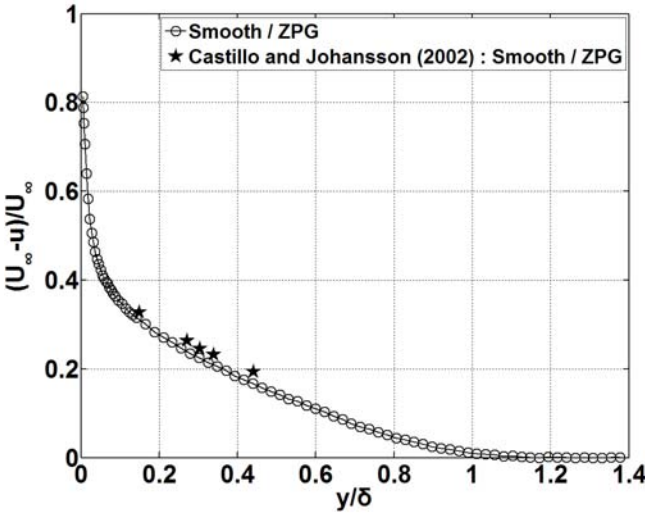

Fig. 3.1 Mean velocity defect profile in the smooth surface zero pressure gradient boundary layer. Smooth / ZPG: $K\times10^6$ = 0.01, Re_x = 729,000, Re_θ = 2,070,
Castillo and Johansson (2002): Re_θ = 1,497.

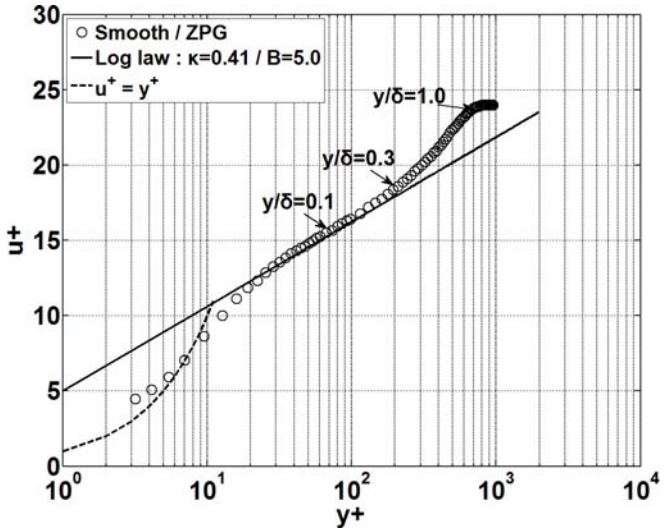

Fig. 3.2 Mean velocity profile (inner coordinate) in the smooth surface zero pressure gradient boundary layer. K, Re_x, and Re_θ are as in Fig. 3.1.

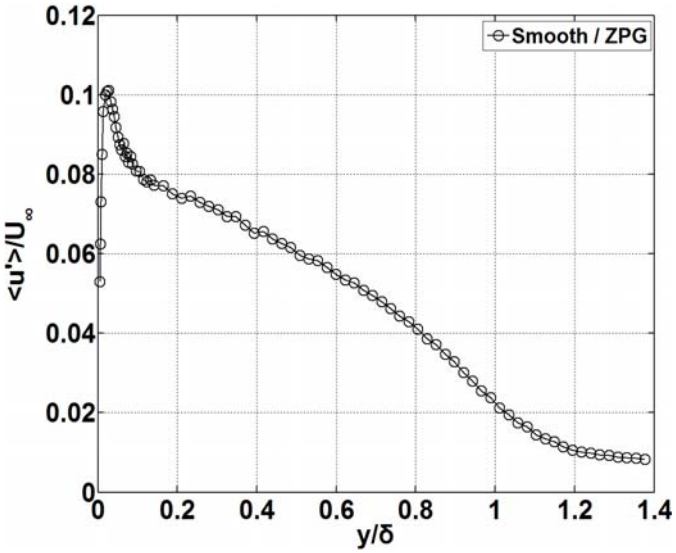

(a)

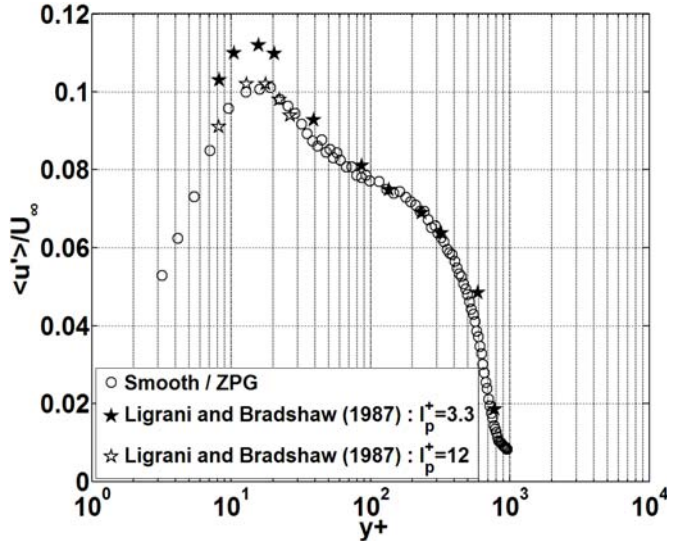

(b)

Fig. 3.3 Turbulence intensity profile in the smooth surface zero pressure gradient boundary layer: (a) Turbulence intensity vs. y/δ, (b) Turbulence intensity vs. $y+$.

K, Re_x, and Re_θ for Smooth / ZPG are as in Fig. 3.1.

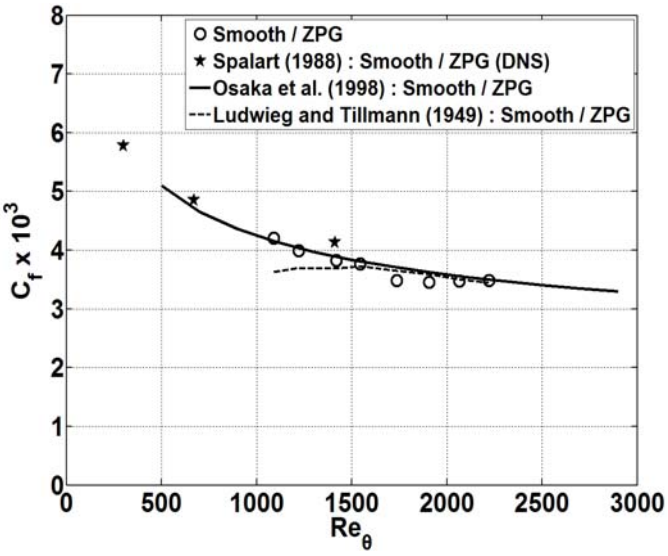

Fig. 3.4 Friction coefficients in the smooth surface zero pressure gradient boundary layers. Smooth / ZPG: $K \times 10^6$ = -0.02 ~ 0.01, Re_x = 203,000 ~ 816,000.

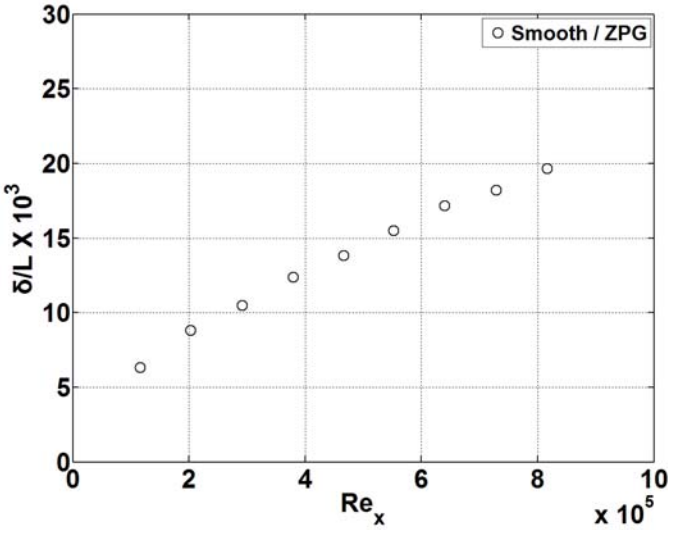

(a)

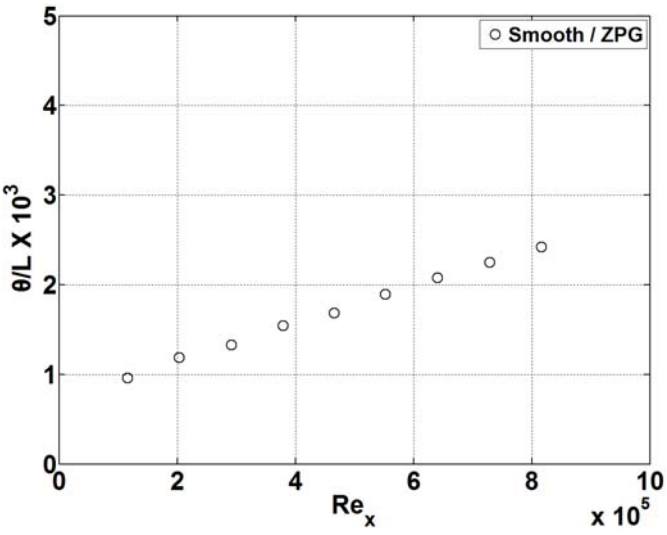

(b)

Fig. 3.5 Integral boundary layer parameters in the smooth surface zero pressure gradient boundary layers: (a) Boundary layer thickness, (b) Momentum thickness. Smooth / ZPG: $K \times 10^6$ = -0.02 ~ 0.01, Re_θ = 880 ~ 2,220.

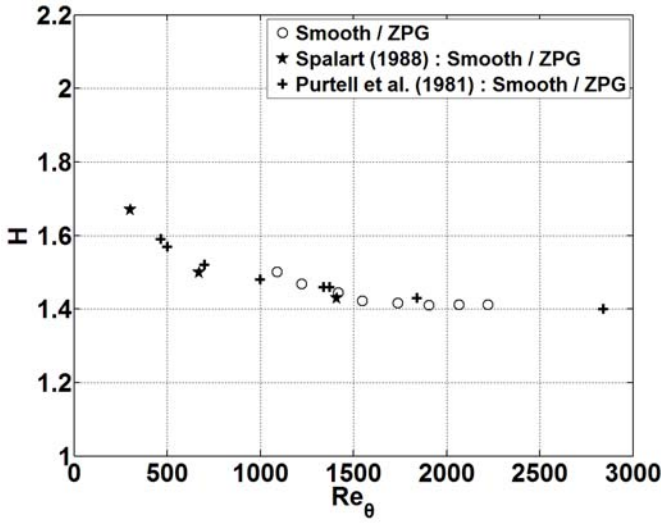

(a)

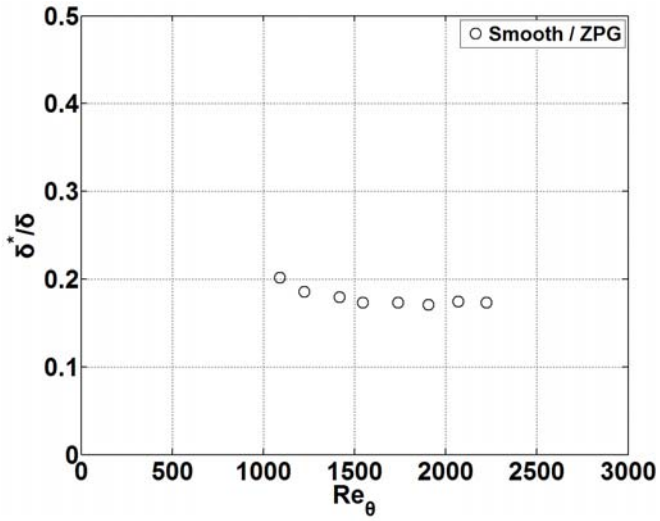

(b)

Fig. 3.6 Distribution of H and δ^*/δ in the smooth surface zero pressure gradient boundary layer: (a) H, (b) δ^*/δ. K and Re_x are as in Fig. 3.4.

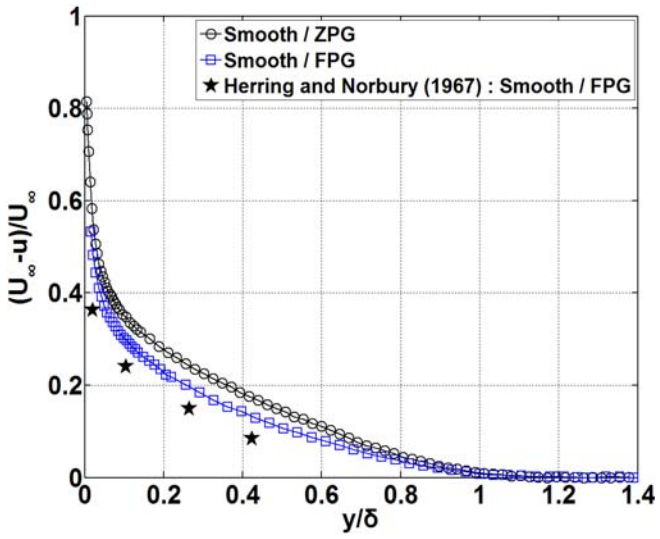

Fig. 3.7 Favorable pressure gradient effect on mean velocity defect. Smooth / ZPG: $K\times10^6$ = 0.01, Re_x = 729,000, Re_θ = 2,070, Smooth / FPG: $K\times10^6$ = 0.28, Re_x = 903,000, Re_θ = 1,420.

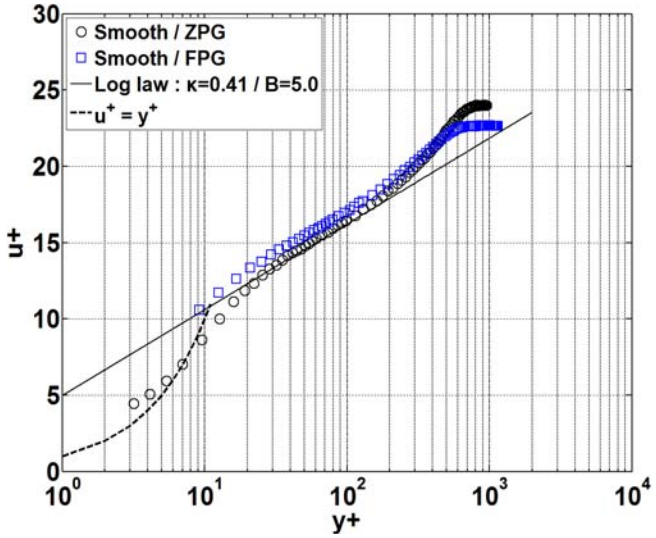

Fig. 3.8 Mean velocity profile (inner coordinate) in the smooth surface favorable pressure gradient boundary layer. K, Re_x, and Re_θ are as in Fig. 3.7.

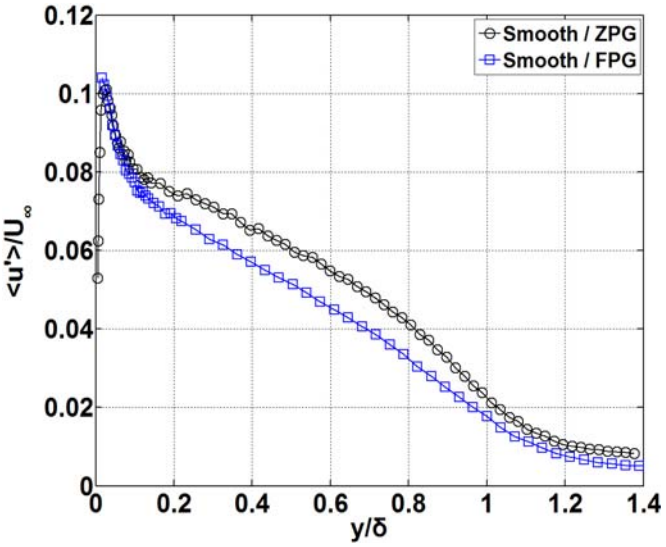

(a)

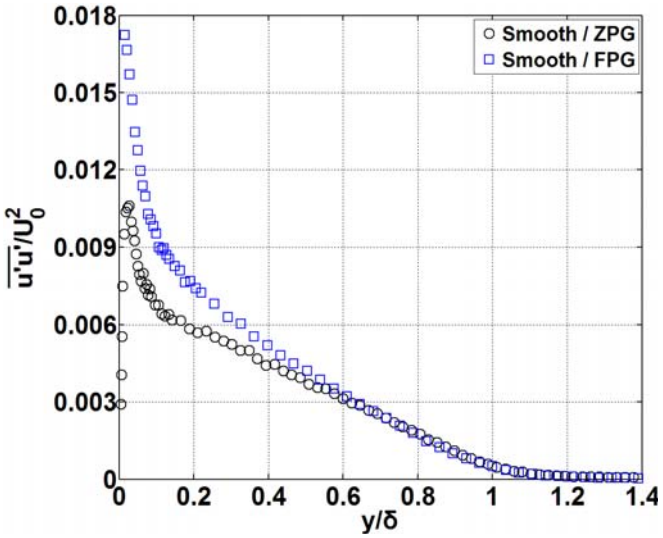

(b)

Fig. 3.9 Favorable pressure gradient effect on turbulence profiles: (a) Turbulence intensity, (b) Streamwise normal Reynolds stress. K, Re_x, and Re_θ are as in Fig. 3.7.

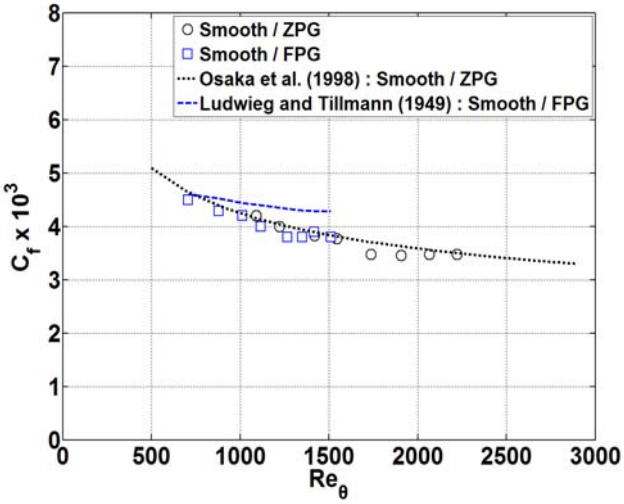

Fig. 3.10 Favorable pressure gradient effect on friction coefficient. Smooth / ZPG: $K\times10^6$ = -0.02 ~ 0.01, Re_x = 203,000 ~ 816,000, Smooth / FPG: $K\times10^6$ = 0.38 ~ 0.28, Re_x = 207,000 ~ 1,046,000.

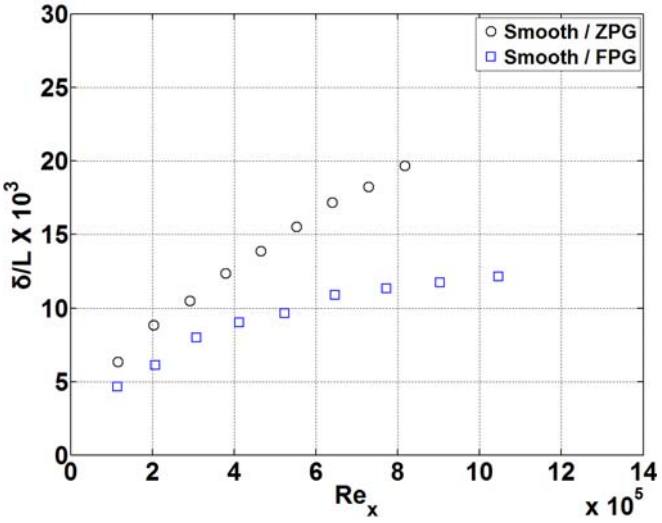

(a)

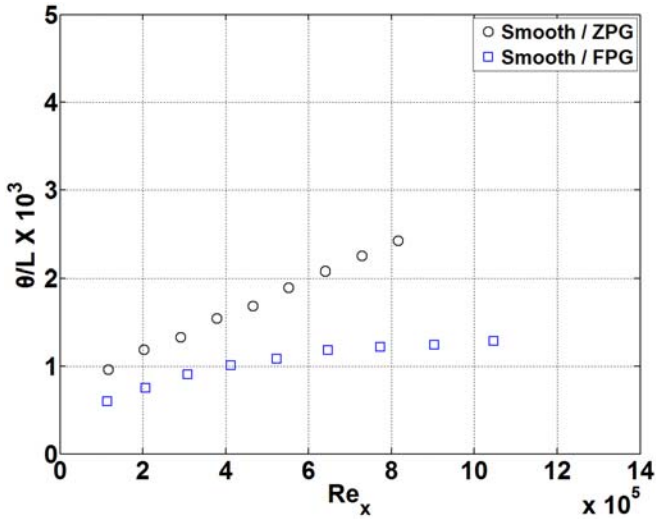

(b)

Fig. 3.11 Favorable pressure gradient effects on integral boundary layer parameters:
(a) boundary layer thickness, (b) Momentum thickness. Smooth / ZPG : $K\times10^6$ = -0.02 ~ 0.01, Re_θ = 880 ~ 2,220, Smooth / FPG: 0.38 ~ 0.27, Re_θ = 540 ~ 1,510.

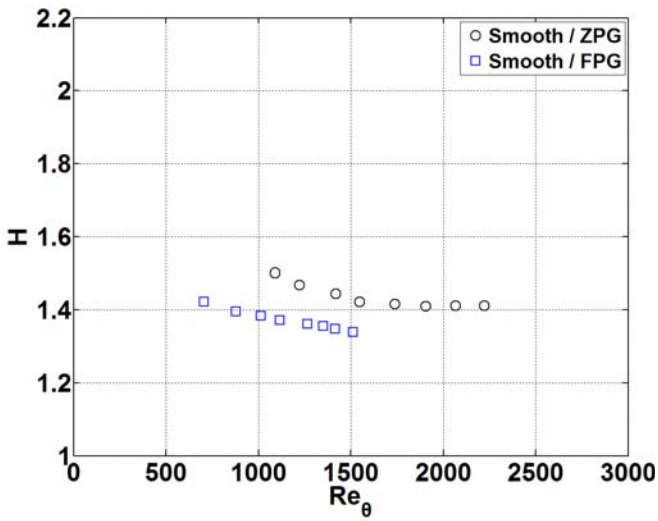

(a)

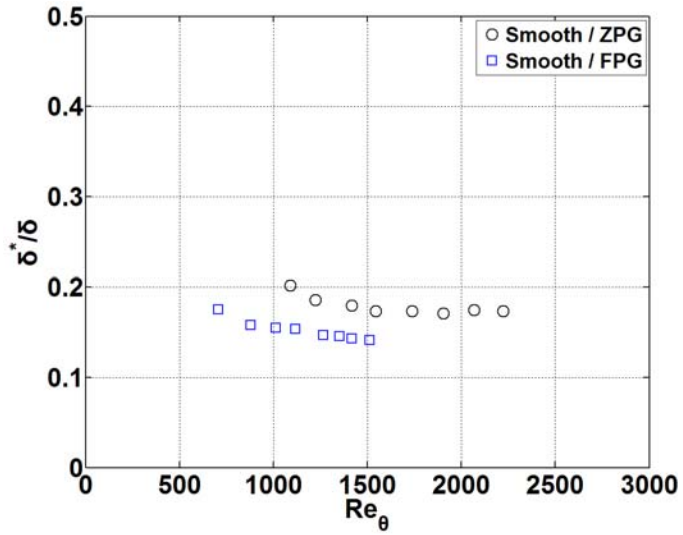

(b)

Fig. 3.12 Favorable pressure gradient effects on H and δ^*/δ: (a) H, (b) δ^*/δ.

K and Re_x are as in Fig. 3.10.

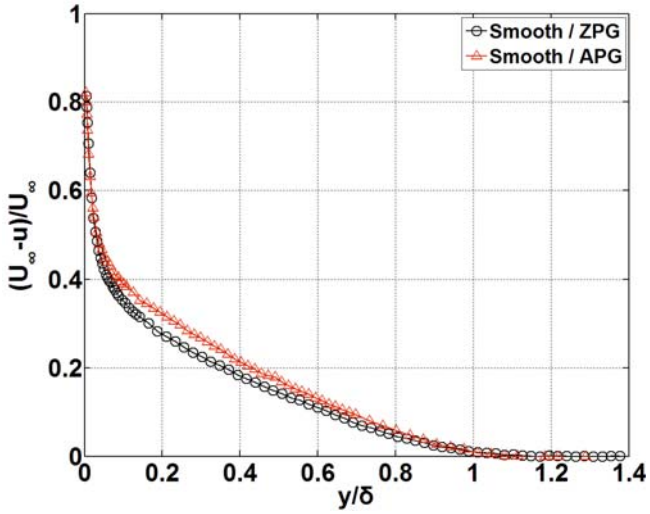

Fig. 3.13 Adverse pressure gradient effect on mean velocity defect.
Smooth / ZPG: $K\times10^6$ = 0.01, Re_x = 729,000, Re_θ = 2,070,
Smooth / APG: $K\times10^6$ = -0.14, Re_x = 644,000, Re_θ = 2,660.

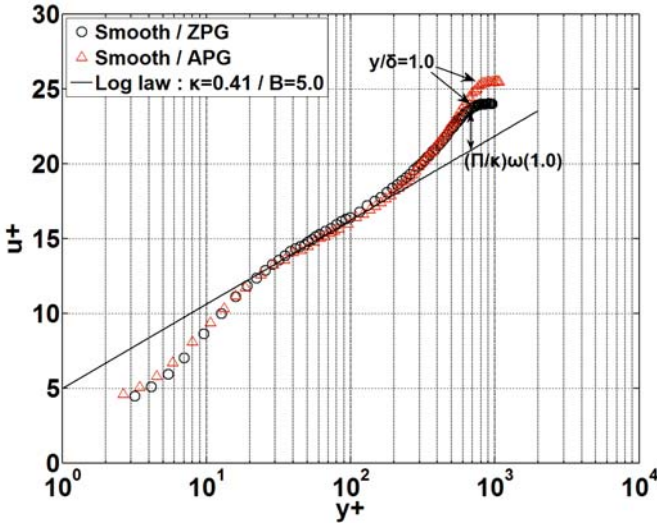

Fig. 3.14 Adverse pressure gradient effect on mean velocity profile in inner coordinate.
K, Re_x, and Re_θ are as in Fig. 3.13.

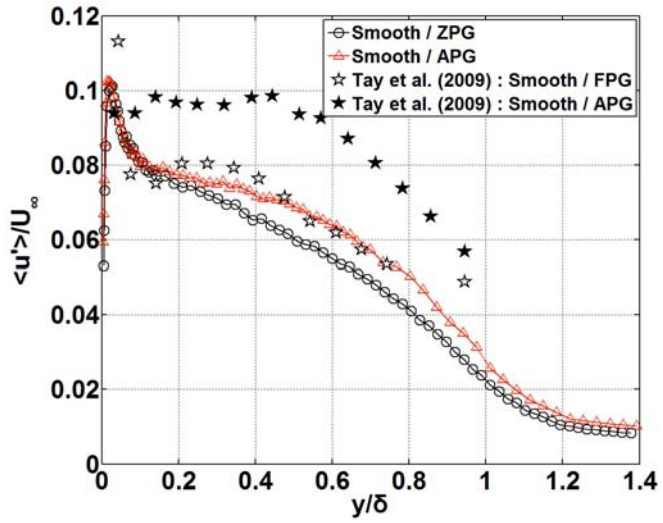

(a)

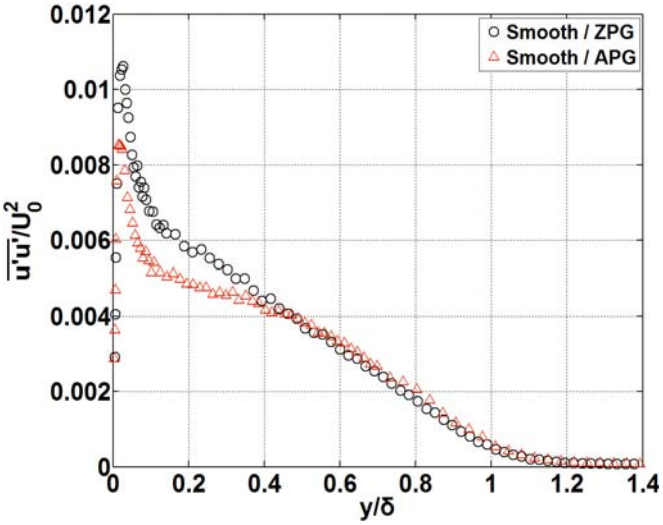

(b)

Fig. 3.15 Adverse pressure gradient effect on turbulence profiles: (a) Turbulence intensity, (b) Streamwise normal Reynolds stress. K, Re_x, and Re_θ are as in Fig. 3.13, Tay et al. (2009): $K\times10^6$ = 0.49, Re_θ = 914 (Smooth / FPG), $K\times10^6$ = -0.45, Re_θ = 2,182 (Smooth / APG).

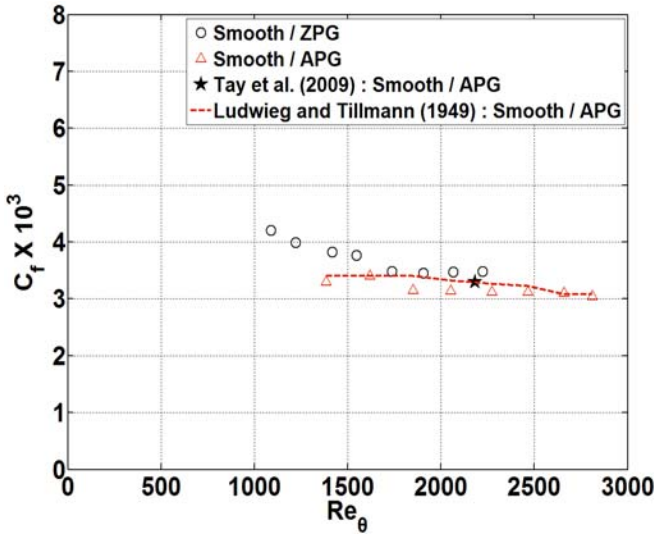

Fig. 3.16 Adverse pressure gradient effect on friction coefficient. Smooth / ZPG: $K\times10^6$ = -0.02 ~ 0.01, Re_x = 203,000 ~ 816,000, Smooth / APG: $K\times10^6$ = -0.22 ~ -0.14, Re_x = 196,000 ~ 711,000, Tay et al. (2009): $K\times10^6$ = -0.45.

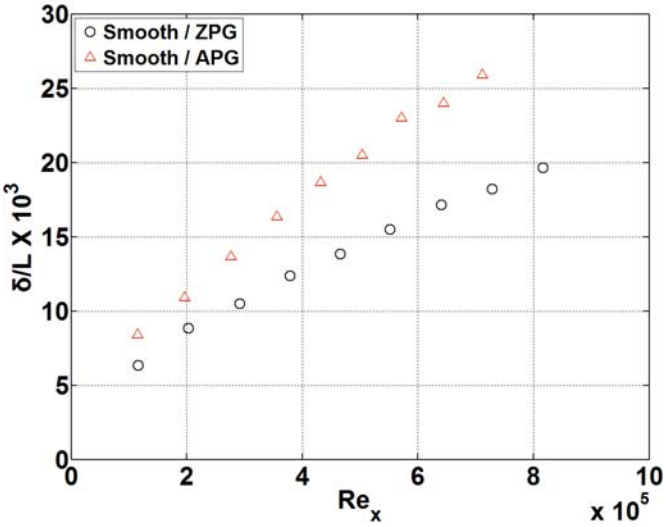

(a)

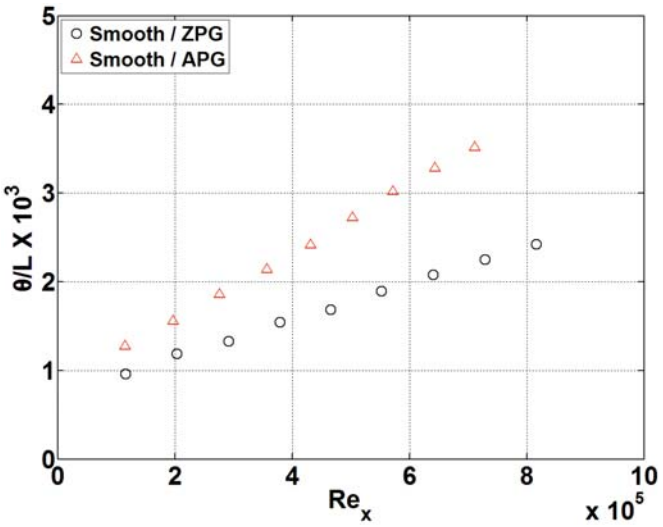

(b)

Fig. 3.17 Adverse pressure gradient effects on integral boundary layer parameters: (a) boundary layer thickness, (b) Momentum thickness. Smooth / ZPG: $K\times10^6$ = -0.02 ~ 0.01, Re_θ = 880 ~ 2,220, Smooth / APG: $K\times10^6$ = -0.22 ~ -0.14, Re_θ = 1,210 ~ 3,630.

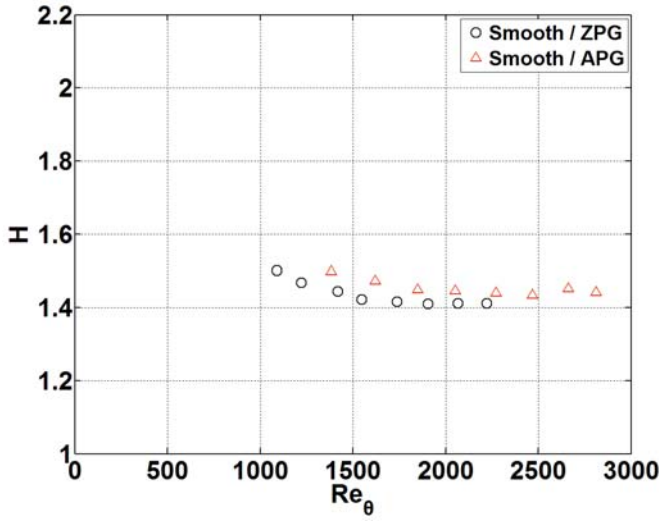

(a)

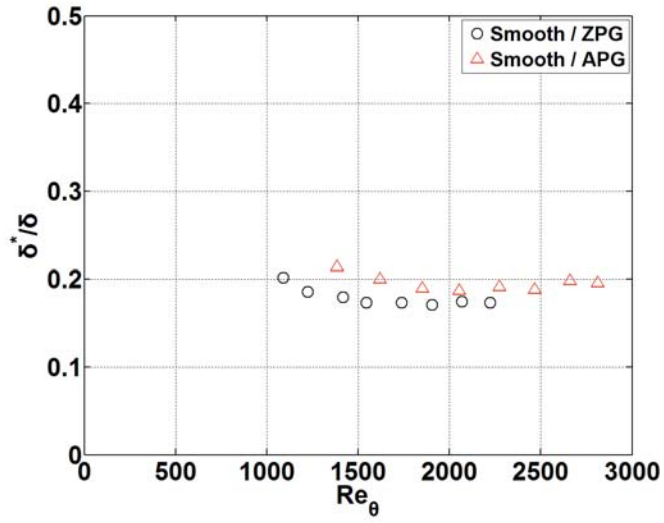

(b

Fig. 3.18 Adverse pressure gradient effects on H and δ^*/δ: (a) H, (b) δ^*/δ. K and Re_x are as in Fig. 3.16.

Chapter 4.

Pressure Gradient Effects on Rough Surface Boundary Layers

4.1 Roughness effects on zero pressure gradient boundary layers

To investigate the roughness effects on boundary layer growth and profile loss, mean and streamwise normal Reynolds stress profiles in the smooth and rough surface boundary layers are measured and plotted together versus y/δ and y/k_r. Surface roughness effect on the downstream mean velocity distribution is demonstrated in Fig. 4.1. As measurements have been made downstream ($12.5k_r$) of roughness elements, the rough surface boundary layers take the shape of reattached turbulent boundary layers. Roughness increases the mean velocity defect throughout the boundary layer, and the mean velocity defect extends to higher y/k_r than for a smooth surface. Figure 4.2 shows the rough surface ZPG mean velocity profile in the inner coordinate. A clear Roughness shift (ΔB) is shown in the mean

velocity profile. According to Schultz and Flack [76], Roughness Reynolds number based on the equivalent sandgrain roughness (k_s^+) can be estimated from the roughness shift (Eq. (4.1)).

$$\Delta u^+ = \frac{1}{\kappa} ln(k_s^+) - 3.5 \tag{4.1}$$

According to Perry and Joubert [50], the roughness shift may be linearly proportional to k^+ regardless of pressure gradient. Therefore, k_s^+ for rough surface ZPG, FPG, and APG boundary layer are estimated from Eq. 4.1. Based on Eq. (4.1), k_s^+ for the rough surface ZPG, FPG, and APG profiles range from 103 to 143, from 155 to 243, and from 60 to 112, respectively. Thus, the present study's rough plate is fully rough (k_s^+ > 60).

The surface roughness effect on the streamwise normal Reynolds stress ($\overline{u'u'}/U_0^2$) is plotted in Fig. 4.3. Surface roughness increases the turbulence intensity for y/δ > 0.04 and for y/k_r > 2. Compared with the smooth surface case, the value of the maximum $\overline{u'u'}/U_0^2$ is higher, and the position of the maximum $\overline{u'u'}/U_0^2$ (y/k_r = 3.25) is farther away from the surface. The result is due to the roughness-induced, high

turbulence coherent unsteady vortical structures in the "roughness sublayer" [77]. This 3-dimensional roughness result is similar to the 2-dimensional result of Djenidi et al. [41] which showed peak turbulence intensity (downstream of 2-dimensional square bars) at y/k_r = 1 ~ 3. According to Ryu et al. [78], vorticity spatially correlates with the velocity fluctuations, and the vorticity also correlates highly with the location of vortices [79, 80]. Thus, the high Reynolds stress at y/k_r = 3.25 shows the mean location of roughness-generated coherent unsteady vortices (which increase vorticity and streamwise turbulence production) near the surface. A schematic of the local flow structure in the present study's rough surface ZPG case is shown in Fig. 4.4. Similar to this 3-D result, numerical result of Lee et al. [81] also showed inclined vortices for 2-dimensional roughness.

The roughness effect on friction coefficient is shown in Fig. 4.5. Roughness increases the friction coefficient because the roughness increases pressure and friction drag by generating vortices. The difference in C_f between rough and smooth surfaces is decreased as Re_θincreases. Such trend occurs because δ increases with Re_θ, but k_r remains constant, resulting in a decreased k_r/δ. Such Re_θ effect is also shown in $\overline{u'u'}/U_0^2$ (Fig 4.6). Due to the decreased k_r/δ and less strong

vortical motions, roughness increases the maximum $\overline{u'u'}/U_0^2$ less for the higher Re_θ compared to that in for the lower Re_θ.

Figure 4.7 shows the roughness effect on boundary layer thickness and momentum thickness growth under ZPG. Compared to the smooth surface case, integral parameters for the rough surface case has higher thickness growth rates due to the roughness' flow displacement effect and increased momentum loss.

Figure 4.8 shows the roughness effect on H and δ^*/δ on ZPG boundary layers. Surface roughness increases both parameters, indicating that among δ, δ^*, and θ, δ^* is the most sensitive parameter to surface roughness. The increased H also shows that roughness may induce a premature flow separation. For a rough surface cylinder, Achenbach [82] showed that increased surface roughness shifts the separation point upstream. Also, increased δ^*/δ shows that the vorticity center moves upward as roughness increases. It is due to the strengthened vorticity above the roughness elements.

4.2 Favorable pressure gradient effects

Figure 4.9 shows the FPG and roughness effects on mean velocity

defect plotted versus (a) y/δ and (b) y/k_r. Throughout the boundary layer, the FPG effect of decreasing $1-u/U_\infty$ is smaller for a rough surface than for a smooth surface. For y/δ < 0.1, FPG does not decrease $1-u/U_\infty$ in the rough surface case. Therefore, for a given pressure gradient, surface roughness increases mean velocity defect more greatly in the rough surface case than in the smooth surface case. The pressure gradient and roughness effects on near-surface mean velocity defect can be seen in Fig. 4.9(b). For y/k_r < 30, the roughness effect of increasing mean velocity defect is greater for FPG flow than for ZPG flow. Figure 4.10 shows the roughness-induced change in mean velocity (mean velocity defect in the rough surface case minus that in the smoorh surface case) for smooth and rough surfaces. The roughness effect is stronger with FPG than with ZPG for y/k_r < 30, and the difference is maximized at y/k_r = 2. For y/k_r > 30, roughness effect is weaker with FPG than with ZPG.

Same trend is shown in the graph of streamwise normal Reynolds stress ($\overline{u'u'}/U_0^2$) plotted versus (a) y/δ and (b) y/k_r (Fig. 4.11). In Fig 4.11(a), the FPG effect of increasing $\overline{u'u'}/U_0^2$ is more greater in the

rough surface case than in the smooth surface case. FPG increases $\overline{u'u'}/U_0^2$ more greatly in a wider region in the rough surface case than in the smooth surface case. In Fig 4.11(b), compared to the rough surface ZPG boundary layer, FPG increases the maximum $\overline{u'u'}/U_0^2$ by 64% at y/k_r = 3.75 and enhances the roughness effect on turbulence production for y/k_r < 25. However, for y/k_r > 25, FPG decreases $\overline{u'u'}/U_0^2$ as FPG confines turbulence to the near surface region, and decreases rate of outward vortex convection. The results shows that for rough surfaces, FPG increases near-surface turbulence, however, the turbulence energy decreases more faster as y/k_r increases, results in a decreased boundary layer thickness. The significant increase in the normal Reynolds stress near the maximum turbulence location can be caused by 1) more concentrated vortical structures near the maximum turbulence (y/k_r = 3.75) and 2) strengthened horseshoe vortices and associated shear due to the elevated velocity gradient *du*/*dy*. The latter effect produce additional streamwise turbulence kinetic energy. Similar trend is observed at all measurement locations, and the FPG effect on the near surface turbulence becomes bigger as Re_θ increases. The Re_θ

effect is shown in plots of $\overline{u'u'}/U_0^2$ (Fig. 4.12). As Re_θ, The maximum $\overline{u'u'}/U_0^2$ increases.

Integrated streamwise turbulent kinetic energy (*TKE*) has been calculated and the difference in *TKE* between S1 and S9 is listed in Table 4.1. *TKE* represents the production rate of the overall turbulence energy which is generated and accumulated in the boundary layer. For a smooth surface, there is little difference between FPG and ZPG boundary layers. Increased turbulence near the surface ($y/\delta \approx 0.03$) is counterbalanced by decreased boundary layer thickness and turbulence in the outer region. Thus, FPG redistributes but does not increase the total streamwise turbulent kinetic energy in a smooth surface boundary layer. Compared to the smooth surface ZPG boundary layer, rough surface ZPG boundary layer has higher *TKE* production rate due to the turbulence generated by the roughness elements. The same roughness increases *TKE* production rate more with FPG than with ZPG. Thus, FPG enhances the roughness effect of increasing total turbulence energy in the boundary layer.

Friction coefficient is plotted versus Re_θ in Fig. 4.13. Throughout the present Re_θ range, for rough surfaces, FPG further increases the friction

coefficient which has already been significantly increased by surface roughness. The findings consistently show that FPG strengthens the vortical motions which increase the total drag. The friction coefficient and wall shear stress correlate with k_s^+, and k_s^+ also correlates with the downward shift in mean velocity profile (ΔB). Therefore, roughness shifts downward the mean velocity profile more under FPG than under ZPG (Fig. 4.14). From Eq. (3.1), friction coefficients for rough surfaces ZPG and FPG boundary layers have also been estimated using measured shape factors. Surface roughness increases both C_f and *H*. In Eq. (3.1), however, C_f decreases with increasing *H*. Therefore, Eq. (3.1) is not applicable for rough surface boundary layers regardless of pressure gradient.

The FPG effects on turbulence production and friction coefficient are reflected in the integral boundary layer parameters, and the boundary layer thickness and momentum thickness are shown in Figs. 4.15(a) and 4.15(b), respectively. The roughness effect (the difference between a rough surface and the corresponding smooth surface) is greater under FPG than under ZPG. Table 4.2 shows the normalized momentum thickness growths from S1 to S9. Surface roughness has higher

influence on θ under FPG than under ZPG. Thus, FPG further increases roughness-induced loss.

Figure 4.16 shows the roughness and FPG effect on H and δ^*/δ. Roughness effect of increasing H and δ^*/δ is greater under FPG than under ZPG because FPG barely changes the parameters compared to ZPG for rough surfaces.

4.3 Adverse pressure gradient effects

In this section, roughness effects in the APG boundary layers are compared to those in the ZPG boundary layers. Figure 4.17 shows the APG and roughness effects on the mean velocity defects versus the normalized wall normal distance (a) y/δ and (b) y/k_r. In Fig 4.17(a), compared to the smooth surface APG boundary layer, rough surface APG boundary layer has higher mean velocity defects throughout. Thus, as in the ZPG boundary layer, roughness in the APG boundary layer increases the mean velocity defect. However, as in Fig 4.17(b), the significance of APG depends on surface condition and distance from the wall. The roughness effect of increasing mean velocity defect is weaker under APG than under ZPG for y/k_r < 23 (Fig. 4.18). The

maximum difference is found near the peaks of roughness elements (y/k_r = 2). On the contrary, the roughness effect is stronger under APG than under ZPG for y/k_r > 23. Thus, APG decreases the roughness effect of increasing mean velocity defect near the surface but increases the roughness effect in the outer region.

The reason for such APG effects can be found in the streamwise turbulence distribution. Figure 4.19 shows the normalized normal Reynolds stress $\overline{u'u'}/U_0^2$ distribution versus (a) y/δ and (b) y/k_r. In Fig. 4.19(a), the APG effect of decreasing $\overline{u'u'}/U_0^2$ is more greater in the rough surface case than in the smooth surface case. APG decreases $\overline{u'u'}/U_0^2$ more greatly in a wider region in the rough surface case than in the smooth surface case. In Fig. 4.19(b), compared to the rough surface ZPG boundary layer, rough surface APG boundary layer has lower $\overline{u'u'}/U_0^2$ for y/k_r < 28. Thus, APG decreases roughness effect on turbulence production in the rough surface boundary layer near the surface. However, compared to that in the rough surface ZPG boundary layer, $\overline{u'u'}/U_0^2$ in the rough surface APG boundary layer decreases more slowly from its maximum. Consequently, relative to ZPG, APG increases $\overline{u'u'}/U_0^2$ for y/k_r > 28. Similar trends are found at all measurement locations, and the APG effects on turbulence production

become stronger with increasing Re_θ as shown in the peak value of $\overline{u'u'}/U_0^2$ in Fig 4.20. Figure 4.19 suggests that the vortices and shearing motions, which are correlated with the strong turbulence in the rough surface boundary layer, are weakened near the surface and strengthened in the outer region by APG. With FPG, vortices are created due to the increased mean velocity gradients, and the vortices are confined to the near-surface region, increasing in the near-surface turbulence. On the contrary, APG decreases the gradients. Thus, APG weakens the strengths of the horseshoe vortices from the roughness elements. In addition, the enhanced outward vortex convection by APG contributes to the decreased turbulence for y/k_r < 28 as well as the increased turbulence for y/k_r > 28. Similar trend is observed at all measurement locations, and the APG effect on the near surface turbulence becomes bigger as Re_θ increases. The Re_θ effect is shown in plots of $\overline{u'u'}/U_0^2$ (Fig. 4.20). As Re_θ, The maximum $\overline{u'u'}/U_0^2$ decreases.

To confirm the APG effect on turbulence kinetic energy generation, *TKE* generation rate are estimated for APG flows (Table 4.1). Table 4.1 shows the APG effect on the *TKE* generatio nbetween S1 and S9. In the smooth surface boundary layer, there is little APG effect on

TKE. Thus, APG by itself reduces streamwise turbulent energy only slightly in a boundary layer. However, APG in the rough surface boundary layer decreases the *TKE* generation greatly. This result supports the argument that for a rough surface, APG not only redistributes turbulence but also reduces turbulent energy.

Figure 4.21 shows the APG effect on the friction coefficient for rough surfaces. Relative to the rough surface ZPG boundary layer, the friction coefficient is decreased in the rough surface APG boundary layer because APG reduces the strengths of vortices and associated shear. Also, as Re_θ increases, the friction coefficient decreases more rapidly in the rough surface APG boundary layer than in the rough surface ZPG boundary layer because the APG's effect of reducing the strength of the near-surface vortices increases with increasing Re_θ. Figure 4.22 shows the mean velocity profile scaled with inner coordinates. With a decreased C_f, APG in the rough surface boundary layer decreases the k_s^+ and roughness shift (ΔB). Thus, relative to ZPG, APG shifts the velocity profile upward for rough surfaces.

The APG effect on mean and turbulence structures of smooth and rough surface boundary layers are reflected in the integral boundary layer parameters. Distributions of δ and θ are illustrated versus local

Reynolds number Re_x in Fig. 4.23(a) and Fig. 4.23(b), respectively. In the smooth surface boundary layer, APG increases the growth rates of both parameters. The normalized momentum thickness growth per unit length is summarized in Table 4.2. The roughness effect, defined as the relative difference in momentum thickness between the rough surface boundary layer and smooth surface boundary layer for a given pressure gradient, is greater under ZPG than under APG. Thus, the roughness effect on momentum thickness is weaker under APG than under ZPG.

APG effects on H and δ^*/δ are shown in Fig. 4.24. As in the smooth surface case, APG increases the parameters for rough surfaces, and, it shows that APG increases mass defect greatly and moves vortices upward for rough surfaces.

4.3 Comparison of favorable and adverse pressure gradient effects

APG decreases the roughness effects on turbulent boundary layers. First, APG decreases the roughness effect of increasing mean velocity defect for y/k_r < 23, and this result is contrary to the FPG which shows that FPG increases the roughness effect of for y/k_r <30. The

reason for such effects can be found in the $\overline{u'u'}/U_0^2$ and *TKE* data. For rough surfaces, APG decreases $\overline{u'u'}/U_0^2$ for y/k_r < 28 and *TKE* generation rate while FPG increases $\overline{u'u'}/U_0^2$ for y/k_r < 25 and TKE generation rate. Figure 4.25 shows such difference between APG and FPG on turbulence distribution. Figure 4.26 shows the APG and FPG effects on friction coefficient. Due to the weakened vortices and shear near the surface, APG decreases friction coefficient for all the measuring stations while FPG increases friction coefficient with strengthened vortices and shears. Consequently, APG decreases k_s^+, ΔB and roughness effects on integral boundary layer parameters while FPG increases all of the parameters in the rough surface boundary layers. The result shows that numerical and analytical researchers should consider the additional pressure gradient effects on surface friction, wall function, and turbulence when they estimate or account for the surface roughness effects in non-zero pressure gradient applications.

4.4 Conclusions

The conclusions of this chapter can be summarized as follows.

1. The roughness effect of increasing mean velocity defect is stronger

under FPG than under ZPG near the surface.

2. With a rough surface, FPG increases the streamwise normal Reynolds stress. The additional turbulence production due to FPG increases as Re_θ increases. The increase in $\overline{u'u'}/U_0^2$ is thought to be due to the near-surface confinement of roughness-generated vortices and strengthened horseshoe vortices.
3. FPG in the rough surface boundary layer generates extra turbulence energy and further increases TKE while FPG in the smooth surface boundary layer barely changes TKE.
4. Due to the strengthened vortices and associated shear, FPG in the rough surface boundary layer increases friction coefficient, roughness Reynolds number (k_s^+), and roughness shift (ΔB).
5. The roughness-induced increases in the integral boundary layer parameters (δ, θ, H, δ/δ^*) are considerably greater with FPG than with ZPG.
6. The roughness effect of increasing mean velocity defect is weaker under APG than under ZPG near the surface.
7. With a rough surface, APG reduces the streamwise normal Reynolds stress. The reduction of turbulence production due to

APG becomes greater as Re_θ increases.

8. APG reduces TKE in the rough surface boundary layer.
9. Due to the weakened vortices and associated shear, APG in the rough surface boundary layer decreases friction coefficient, roughness Reynolds number (k_s^+), and roughness shift (ΔB).
10. The roughness-induced increases in the integral boundary layer parameters (δ and θ) are smaller with FPG than with ZPG.
11. The results shows that FPG increases the roughness effects while APG decreases them for turbulent boundary layers.

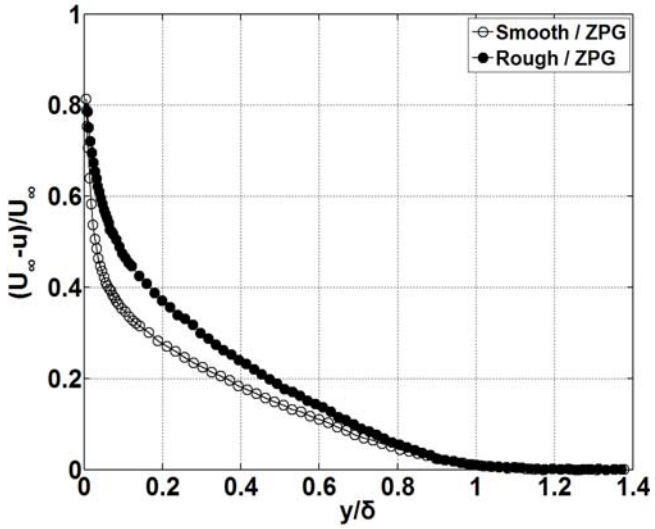

(a)

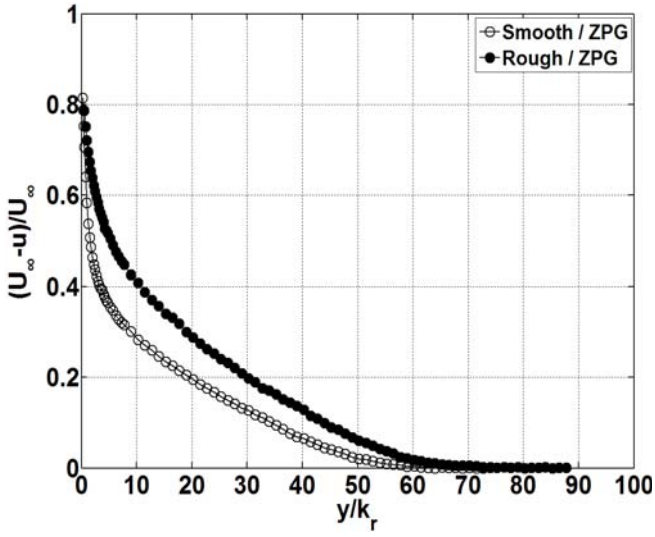

(b)

Fig. 4.1 Roughness effect on mean velocity defect profile under zero pressure gradient:
(a) Velocity defect vs. y/δ, (b) Velocity defect vs. y/k_r.
Smooth / ZPG: $K\times10^6$ = 0.01, Re_x = 729,000, Re_θ = 2,070,
Rough / ZPG: $K\times10^6$ = -0.01, Re_x = 724,000, Re_θ = 2,770.

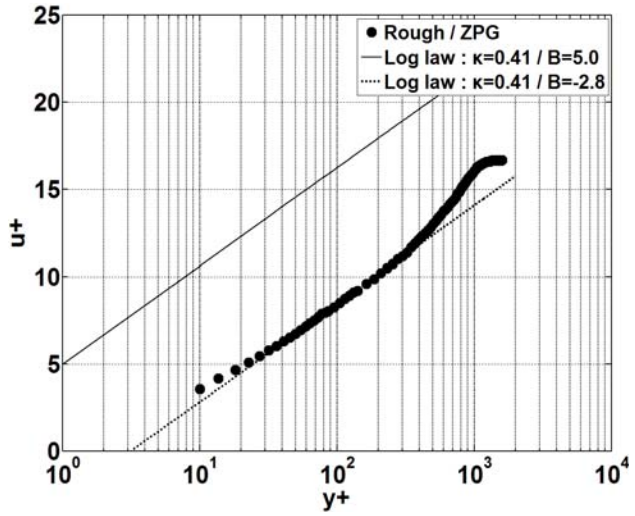

Fig. 4.2 Roughness effect on mean velocity profile in inner coordinate. K, Re_x, and Re_θ are as in Fig. 4.1.

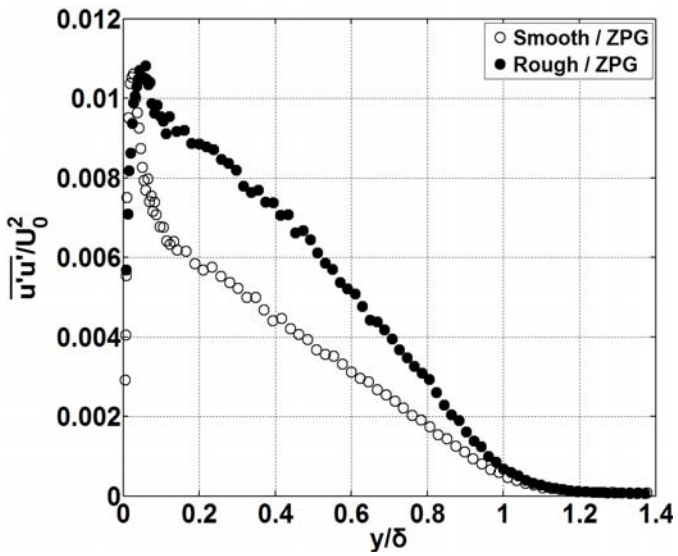

(a)

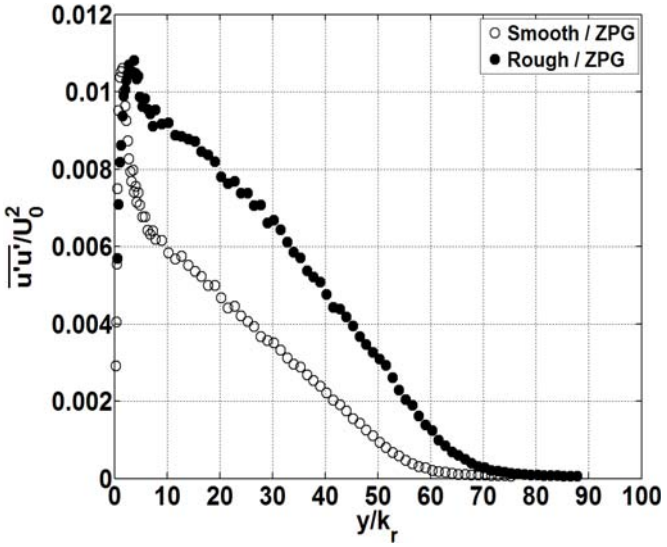

(b)

Fig. 4.3 Roughness effect on streamwise normal Reynolds stress under zero pressure gradient:
(a) $\overline{u'u'}/U_0^2$ vs. y/δ, (b) $\overline{u'u'}/U_0^2$ vs. y/k_r.
K, Re_x, and Re_θ are as in Fig. 4.1.

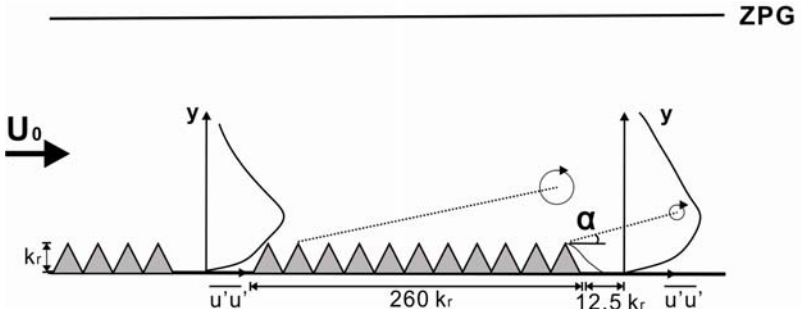

Fig. 4.4 A schematic of flow structures near the rough surface.

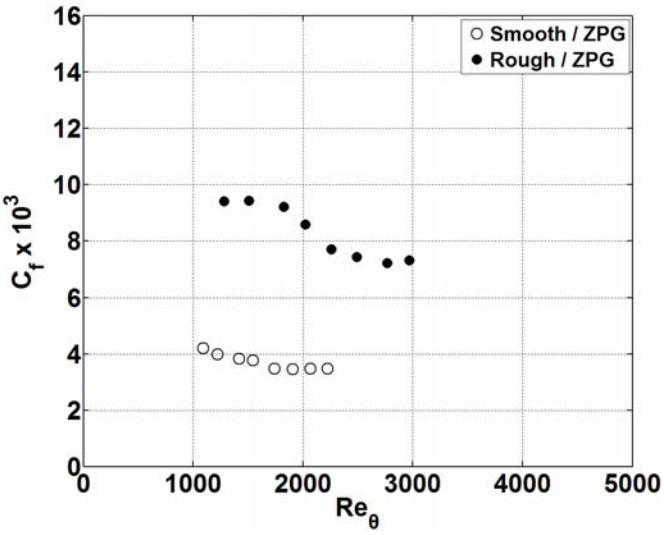

Fig. 4.5 Roughness effect on friction coefficient under zero pressure gradient.
Smooth / ZPG: $K\times10^6$ = -0.02 ~ 0.01, Re_x = 203,000 ~ 816,000,
Rough / ZPG: $K\times10^6$ = -0.03 ~ 0.04, Re_x = 201,000 ~ 809,000.

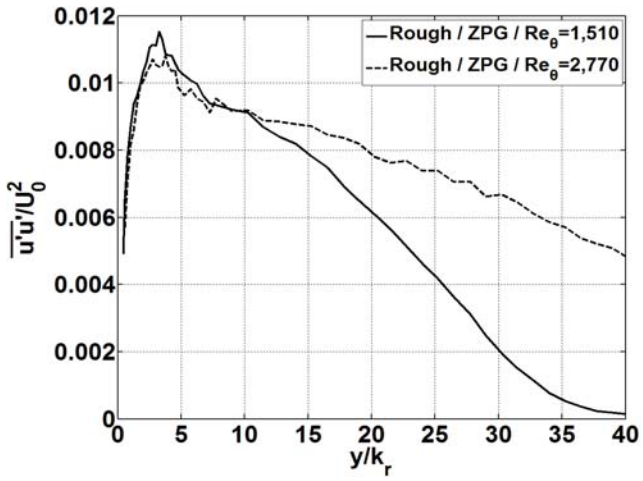

Fig. 4.6 Re_θ effect on streamwise normal Reynolds stress in the rough surface zero pressure gradient boundary layer. Rough / ZPG / Re_θ=1,520: $K\times10^6$ = 0.03, Re_x = 287,000, Rough / ZPG / Re_θ=2,770: $K\times10^6$ = 0, Re_x = 724,000.

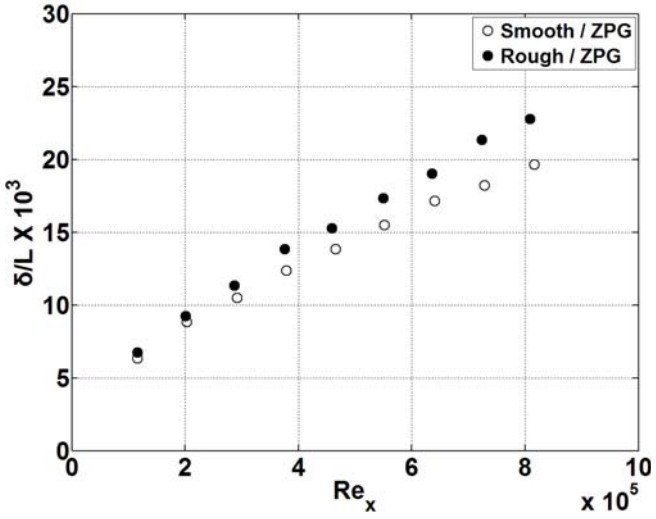

(a)

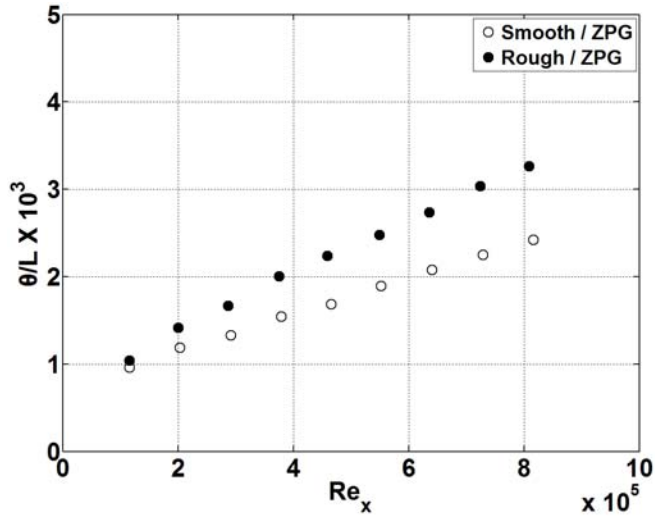

(b)

Fig. 4.7 Roughness effects on integral boundary layer parameters under zero pressure gradient: (a) boundary layer thickness, (b) momentum thickness.

Smooth / ZPG: $K \times 10^6$ = -0.02 ~ 0.01, Re_θ = 880 ~ 2,220,

Rough / ZPG: $K \times 10^6$ = -0.03 ~ 0.04, Re_θ = 950 ~ 2,970.

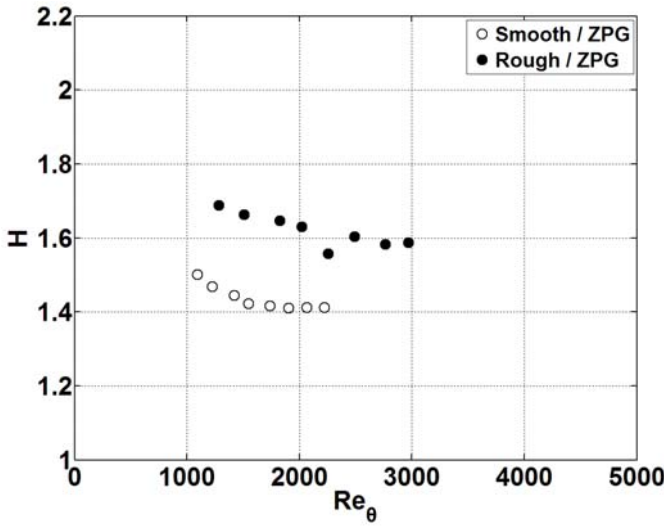

(a)

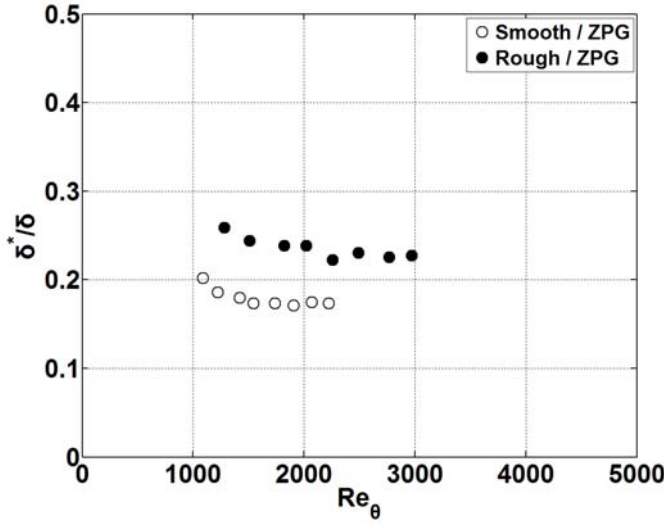

(b)

Fig. 4.8 Roughness effects on H and δ^*/δ under zero pressure gradient: (a) H, (b) δ^*/δ.
K and Re_x are as in Fig. 4.6.

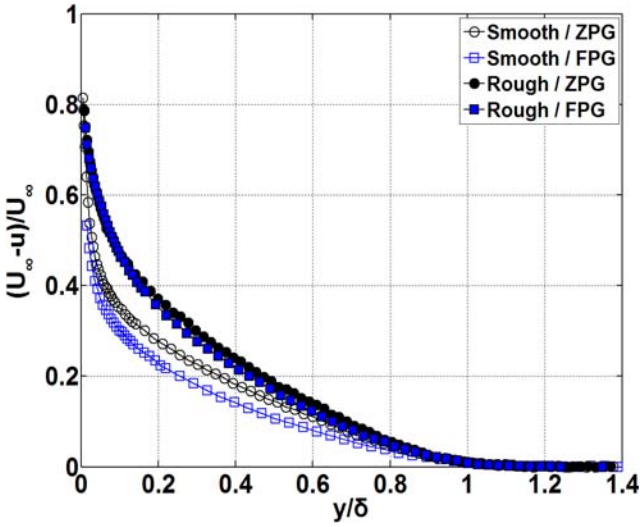

(a)

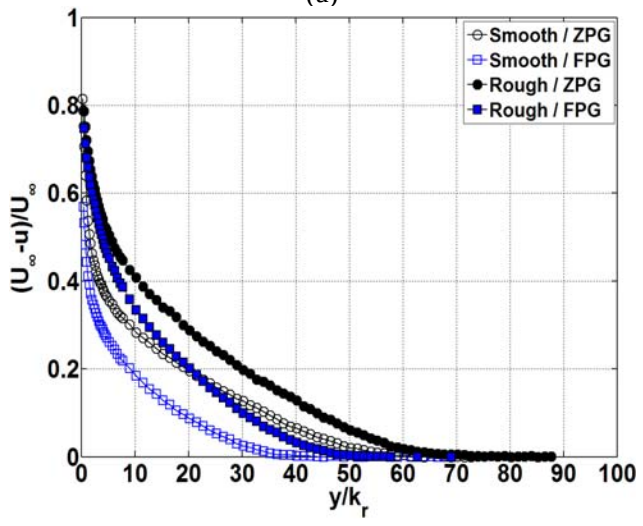

(b)

Fig. 4.9 Favorable pressure gradient effect on mean velocity defect profile in the rough surface boundary layer: (a) Velocity defect vs. y/δ, (b) Velocity defect vs. y/k_r.

Smooth / ZPG: $K\times10^6$ = 0.01, Re_x = 729,000, Re_θ = 2,070,
Smooth / FPG: $K\times10^6$ = 0.28, Re_x = 903,000, Re_θ =1,420,
Rough / ZPG: $K\times10^6$ = -0.01, Re_x = 724,000, Re_θ =2,770,
Rough / FPG: $K\times10^6$ = 0.27, Re_x = 919,000, Re_θ =2,420.

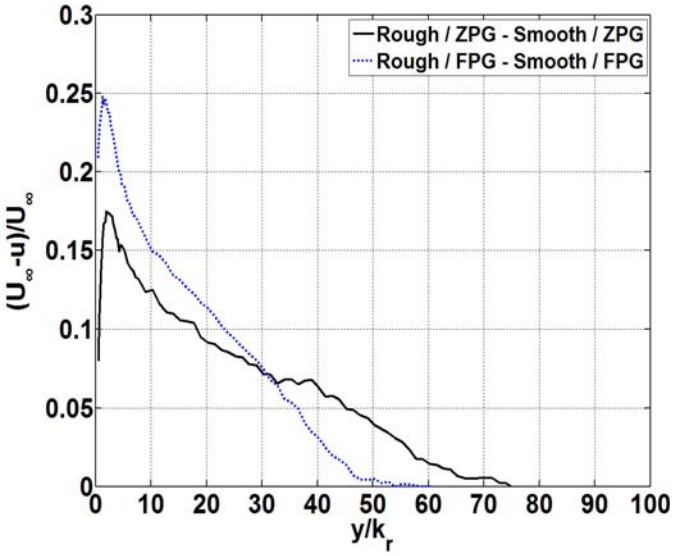

Fig. 4.10 Roughness effect on mean velocity defect under zero and favorable pressure gradients.

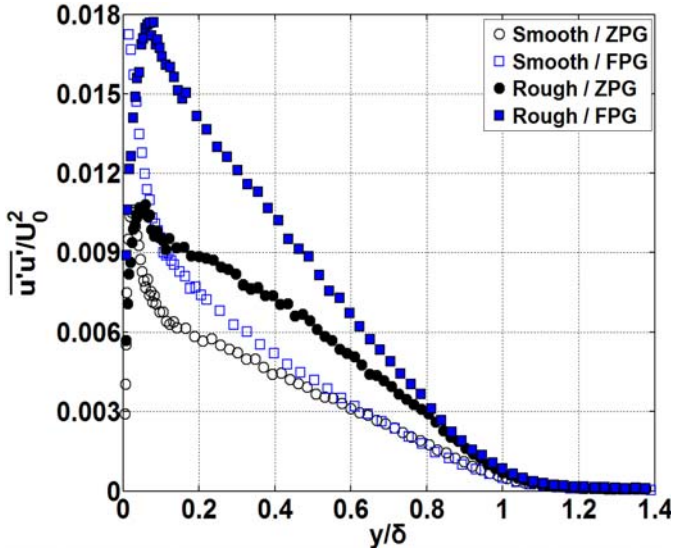

(a)

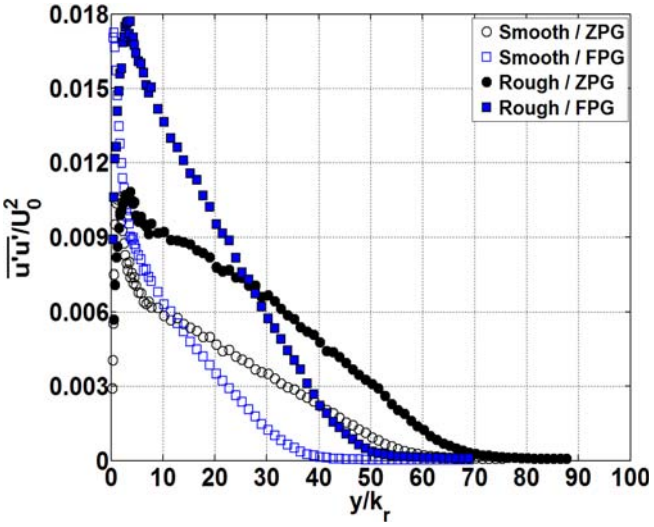

(b)

Fig. 4.11 Favorable pressure gradient effect on streamwise Reynolds stress in the rough surface boundary layer: (a) $\overline{u'u'}/U_0^2$ vs. y/δ, (b) $\overline{u'u'}/U_0^2$ vs. y/k_r. K, Re_x, and Re_θ are as in Fig. 4.9.

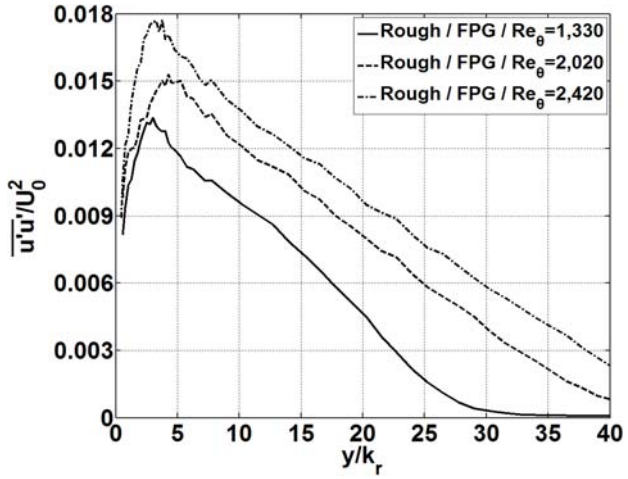

Fig. 4.12 Re_θ effect on streamwise normal Reynolds stress in the rough surface favorable pressure gradient boundary layer.
Rough / FPG / Re_θ=1,330: $K\times10^6$ = 0.32, Re_x = 312,000,
Rough / FPG / Re_θ=2,020: $K\times10^6$ = 0.32, Re_x = 656,000,
Rough / FPG/ Re_θ=2,420: $K\times10^6$ = 0.27, Re_x = 919,000.

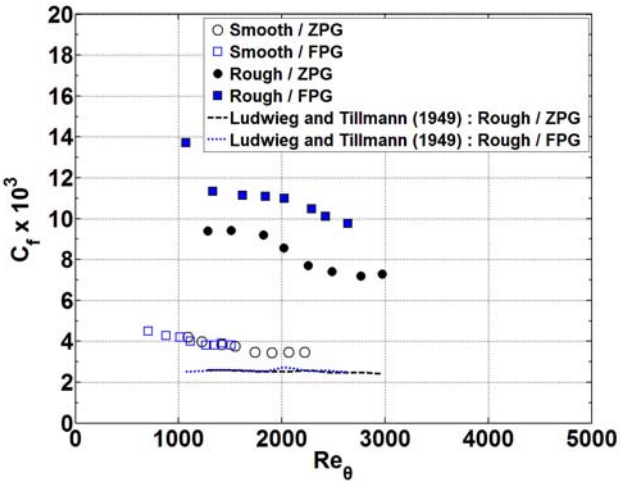

Fig. 4.13 Favorable pressure gradient effect on friction coefficient in the rough surface boundary layer.

Smooth / ZPG: $K\times10^6$ = -0.02 ~ 0.01, Re_x = 203,000 ~ 816,000,
Smooth / FPG: $K\times10^6$ = 0.38 ~ 0.28, Re_x = 207,000 ~ 1,046,000,
Rough / ZPG: $K\times10^6$ = -0.03 ~ 0.04, Re_x = 201,000 ~ 809,000,
Rough / FPG: $K\times10^6$ = 0.35 ~ 0.27, Re_x = 213,000 ~ 1,058,000.

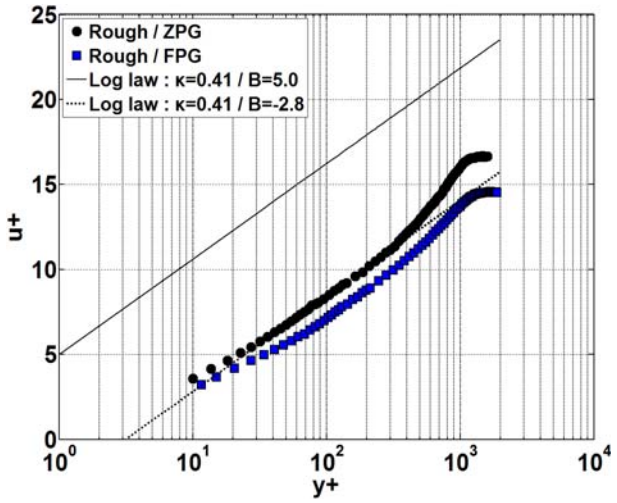

Fig. 4.14 Favorable pressure gradient effect on mean velocity (inner coordinate)
in the rough surface boundary layer. *K*, Re_x, Re_θ are as in Fig. 4.9.

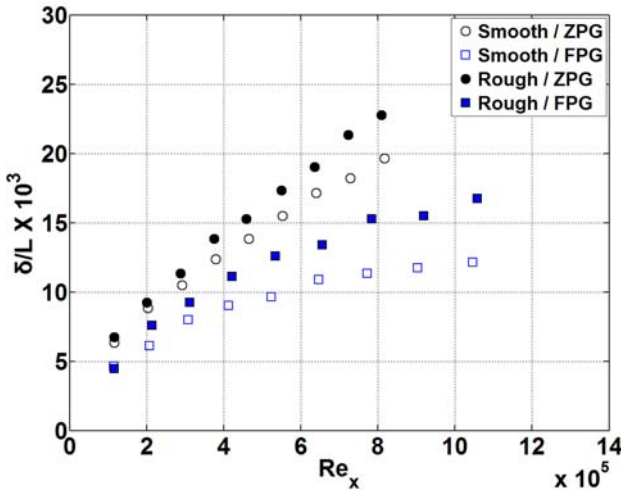

(a)

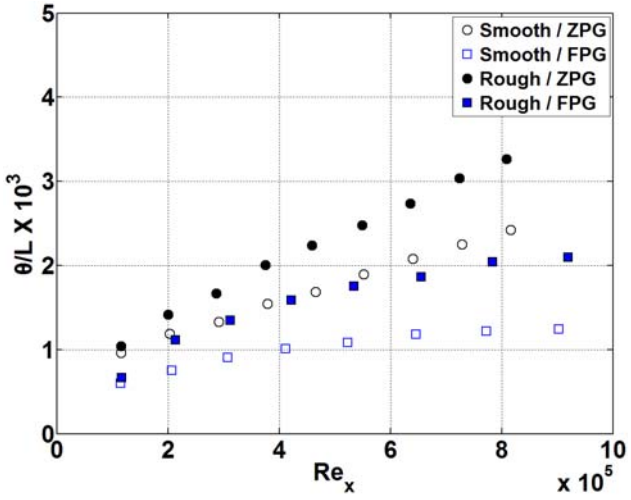

(b)

Fig. 4.15 Favorable pressure gradient effects on integral boundary layer parameters in the rough surface boundary layer: (a) boundary layer thickness, (b) momentum thickness. Smooth / ZPG: $K\times10^6$ = -0.02 ~ 0.01, Re_θ = 880 ~ 2,220, Smooth / FPG: $K\times10^6$ = 0.38 ~ 0.27, Re_θ = 540 ~ 1,510, Rough / ZPG: $K\times10^6$ = -0.03 ~ 0.04, Re_θ = 950 ~ 2,970, Rough / FPG: $K\times10^6$ = 0.35 ~ 0.27, Re_θ = 620 ~ 2,640.

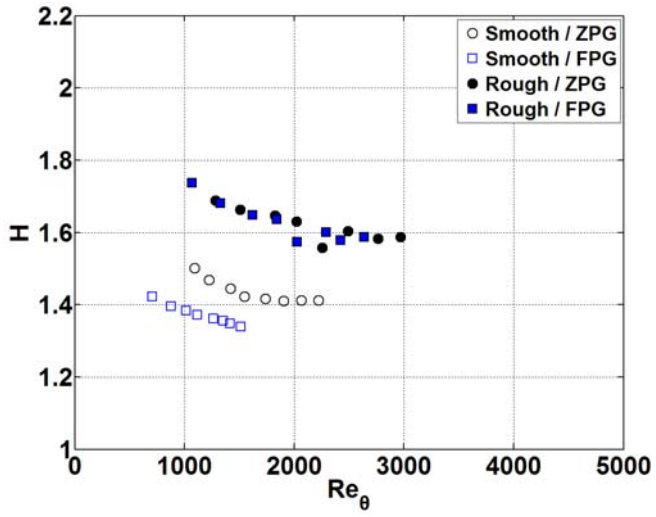

(a)

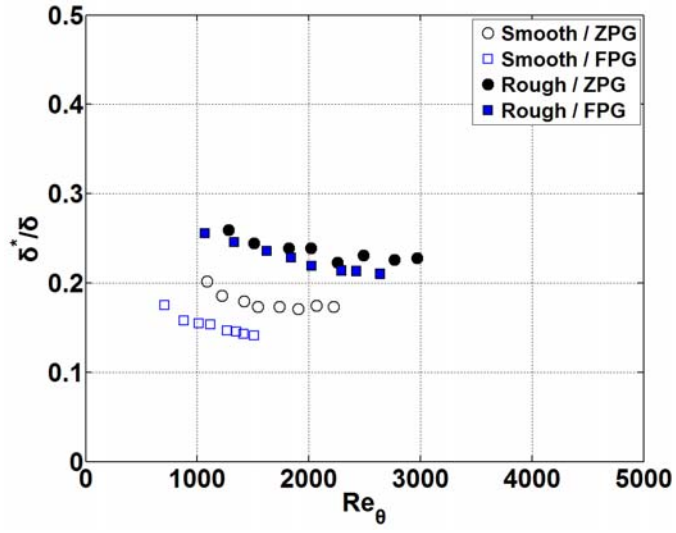

(b)

Fig. 4.16 Favorable pressure gradient effects on H and δ^*/δ in the rough surface boundary layer: (a) H, (b) δ^*/δ. K and Re_x are as in Fig. 4.13.

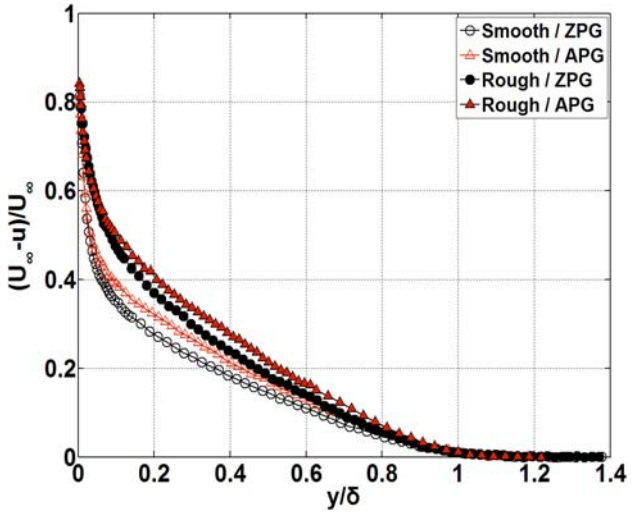

(a)

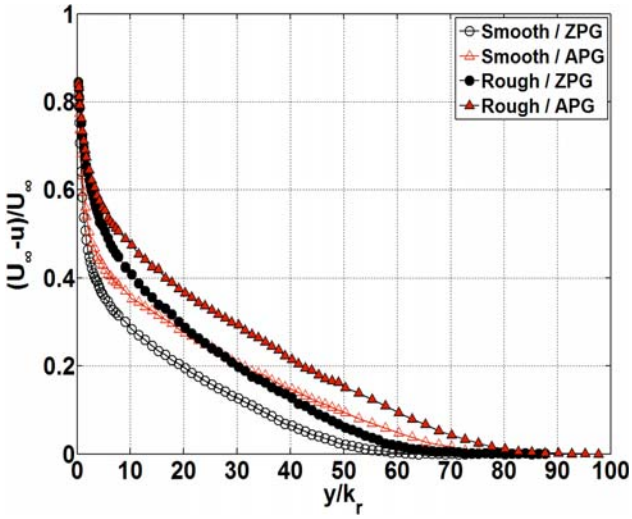

(b)

Fig. 4.17 Adverse pressure gradient effect on mean velocity defect profile in the rough surface boundary layer:
(a) Velocity defect vs. y/δ, (b) Velocity defect vs. y/k_r.

Smooth / ZPG: $K\times10^6$ = 0.01, Re_x = 720,000, Re_θ = 2,070,
Smooth / APG: $K\times10^6$ = -0.14, Re_x = 644,000, Re_θ =2,660,
Rough / ZPG: $K\times10^6$ = -0.01, Re_x = 724,000, Re_θ =2,770,
Rough / APG: $K\times10^6$ = -0.14, Re_x = 645,000, Re_θ =3,350.

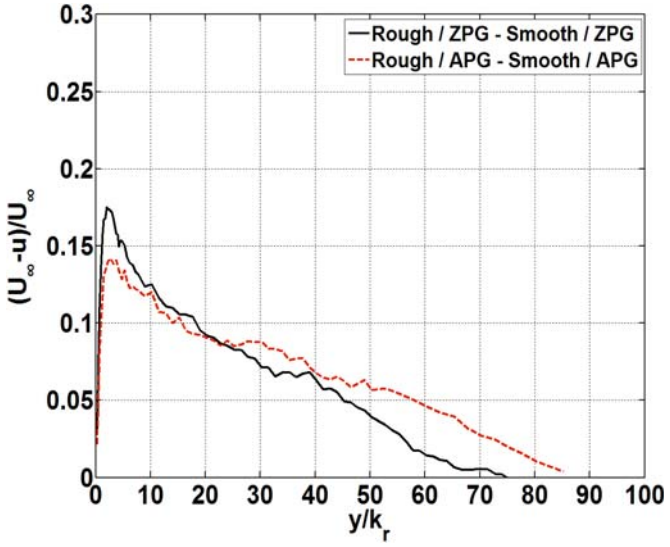

Fig. 4.18 Roughness effect on mean velocity defect under zero and adverse pressure gradients.

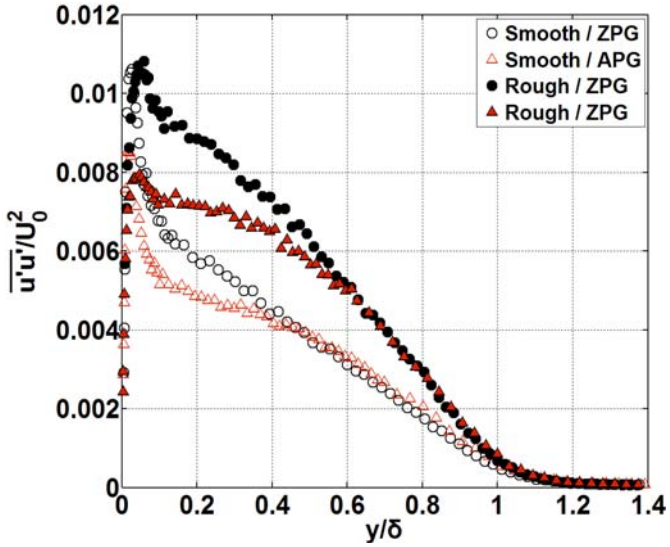

(a)

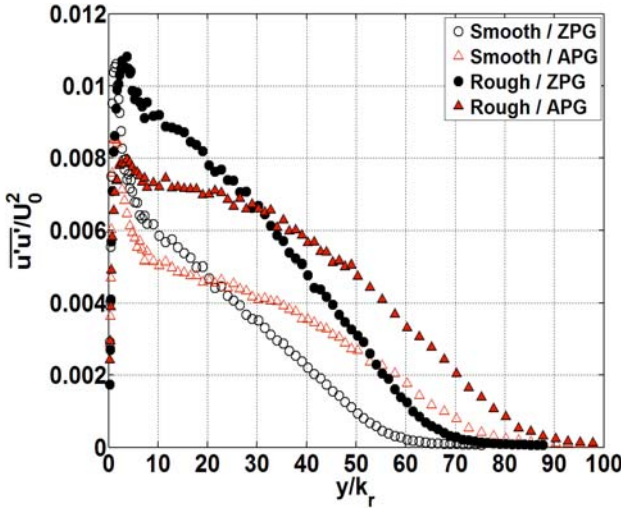

(b)

Fig. 4.19 Adverse pressure gradient effect on streamwise Reynolds stress in the rough surface boundary layer: (a) $\overline{u'u'}/U_0^2$ vs. y/δ, (b) $\overline{u'u'}/U_0^2$ vs. y/k_r. K, Re_x, and Re_θ are as in Fig. 4.17.

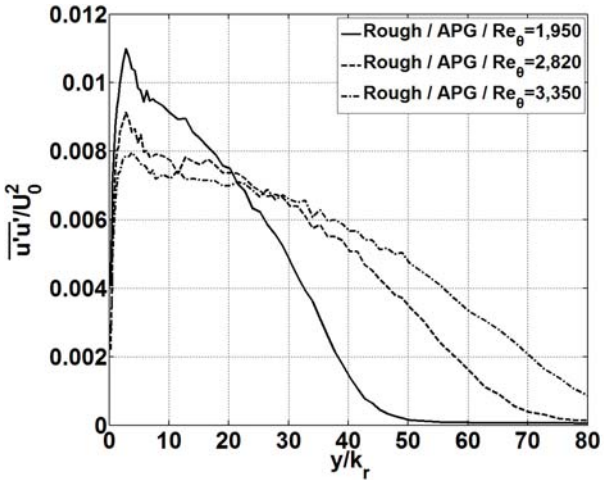

Fig. 4.20 Re_θ effect on streamwise normal Reynolds stress in the rough surface adverse pressure gradient boundary layer.
Rough / APG / Re_θ=1,950: $K\times10^6$ = -0.22, Re_x = 278,000,
Rough / APG / Re_θ=2,820: $K\times10^6$ = -0.20, Re_x = 504,000,
Rough / APG /Re_θ=3,350: $K\times10^6$ = -0.14, Re_x = 645,000.

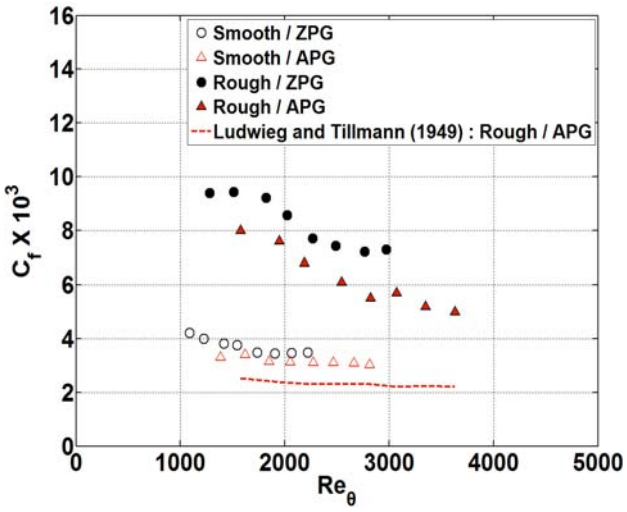

Fig. 4.21 Adverse pressure gradient effect on friction coefficient in the rough surface boundary layer.
Smooth / ZPG: $K\times10^6$ = -0.02 ~ 0.01, Re_x = 203,000 ~ 816,000,
Smooth / APG: $K\times10^6$ = -0.22 ~ -0.14, Re_x = 196,000 ~ 711,000,
Rough / ZPG: $K\times10^6$ = -0.03 ~ 0.04, Re_x = 201,000 ~ 809,000,
Rough / APG: $K\times10^6$ = -0.21 ~ -0.14, Re_x = 196,000 ~ 716,000.

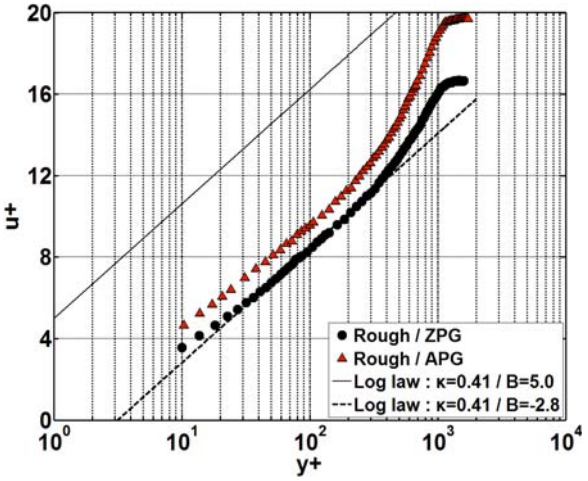

Fig. 4.22 Adverse pressure gradient effect on mean velocity (inner coordinate) in the rough surface boundary layer. K, Re_x, Re_θ are as in Fig. 4.17.

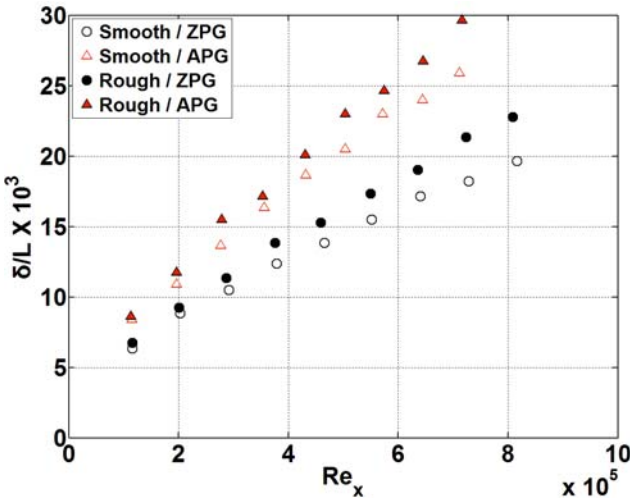

(a)

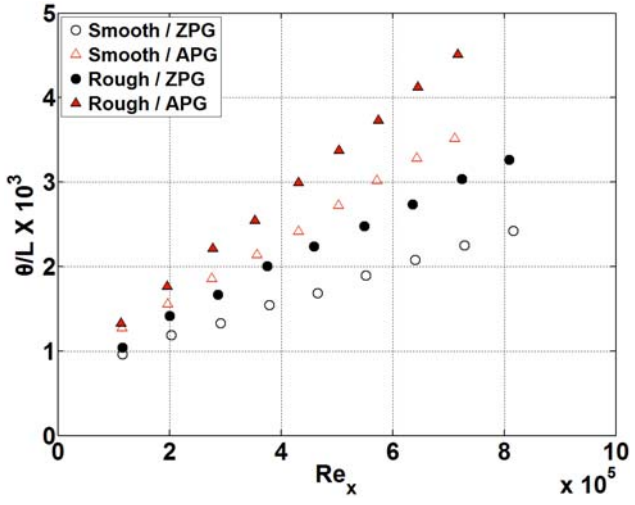

(b)

Fig. 4.23 Adverse pressure gradient effects on integral boundary layer parameters in the rough surface boundary layers: (a) boundary layer thickness, (b) momentum thickness. Smooth / ZPG: $K\times10^6$ = -0.02 ~ 0.01, Re_θ = 880 ~ 2,220, Smooth / APG: $K\times10^6$ = -0.22 ~ -0.14, Re_θ = 1,160 ~ 2,810, Rough / ZPG: $K\times10^6$ = -0.03 ~ 0.04, Re_θ = 950 ~ 2,970, Rough / APG: $K\times10^6$ = -0.21 ~ -0.14, Re_θ = 1,210 ~ 3,630.

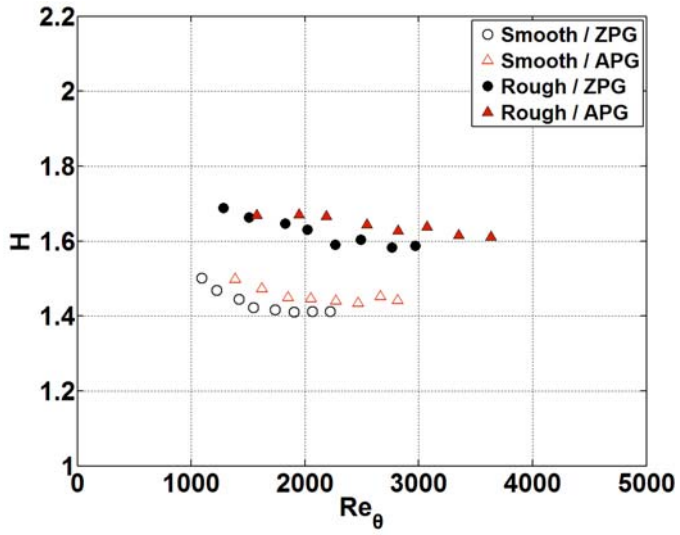

(a)

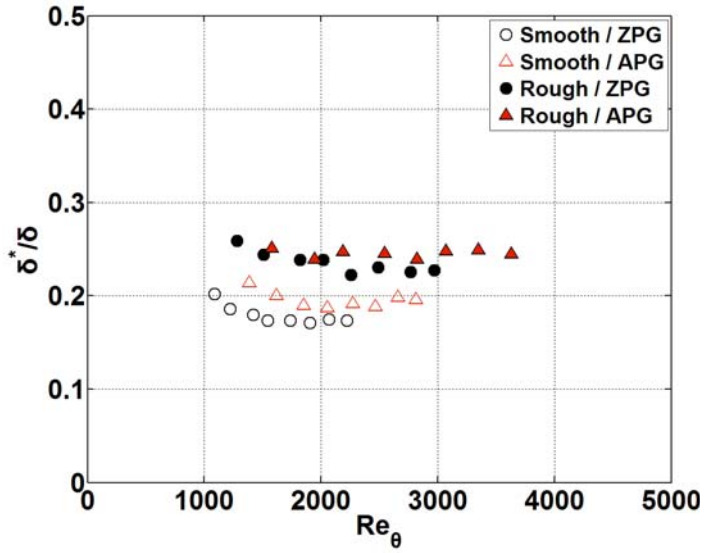

(b)

Fig. 4.24 Adverse pressure gradient effects on H and δ^*/δ in the rough surface boundary layer: (a) H, (b) δ^*/δ. K and Re_x are as in Fig. 4.21.

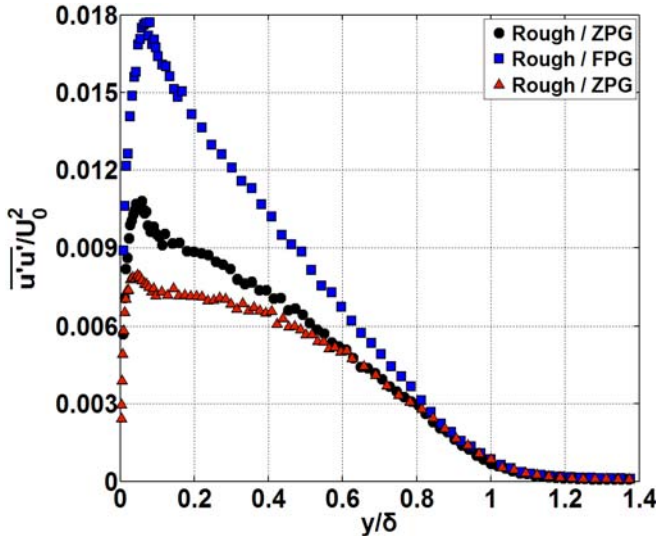

(a)

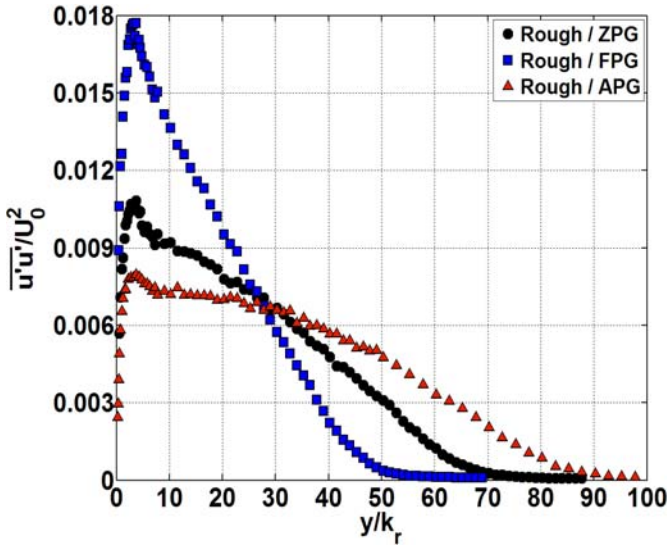

(b)

Fig. 4.25 Favorable and adverse pressure gradient effects on streamwise Reynolds stresses in the rough surface boundary layers: (a) $\overline{u'u'}/U_0^2$ vs. y/δ, (b) $\overline{u'u'}/U_0^2$ vs. y/k_r.

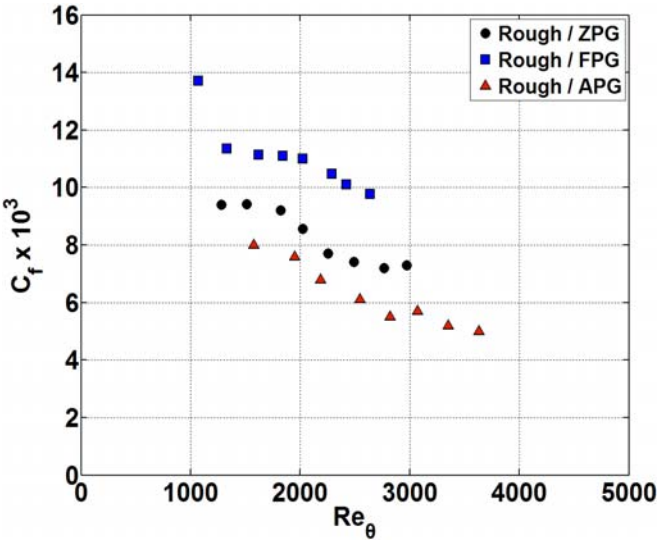

Fig. 4.26 Favorable and adverse pressure gradient effects on friction coefficients in the rough surface boundary layers.

Table 4.1 Production of *TKE* in the smooth and rough surface boundary layers.

Case	$(TKE_{S9} - TKE_{S1}) \times 10^5$
Smooth / ZPG	3.43
Rough / ZPG	8.80
Smooth / FPG	3.34
Rough / FPG	11.4
Smooth / APG	3.13
Rough / APG	7.46
Rough - Smooth (ZPG)	5.37
Rough - Smooth (FPG)	8.06
Rough - Smooth (APG)	4.33

Table 4.2 Momentum thickness growth from S1 to S9.

Case	$(\theta_{S9} - \theta_{S1})/L \times 10^3$
Smooth / ZPG	1.463
Rough / ZPG	2.228
Smooth / FPG	0.689
Rough / FPG	1.550
Smooth / APG	2.242
Rough / APG	3.181
Rough - Smooth (ZPG)	0.765 ($\Delta 52.3\%$)
Rough - Smooth (FPG)	0.861 ($\Delta 125\%$)
Rough - Smooth (APG)	0.939 ($\Delta 41.9\%$)

Chapter 5.

Mean Velocity Scaling and Power Law Velocity Profile Estimation

5.1 Mean velocity scaling for flat plate boundary layers

In Chapter 3 and 4, it is shown that pressure gradient and surface roughness changes mean velocity defect significantly. The mean velocity defect ($(U_\infty - u)/U_\infty$) profile also depends on Re_θ [73]. Figure 5.1 shows the individual effects of (a) Reynolds number (Re_θ); (b) pressure gradient (K); and (c) roughness (k). As Re_θ increases, mean velocity defect decreases slightly. The mean velocity defect also decreases as K increases. Surface roughness increases the mean velocity defect.

Figure 5.2 shows the normalized mean velocity defect ($(U_\infty - u)/(U_\infty \delta^*/\delta)$) profiles for varying (a) Re_θ; (b) K; and (c)k. All curves collapse, and thus, the individual effects of Re_θ, K, and k on flat plate boundary layers scale with δ^*/δ. In Fig. 5.3, the mean velocity profiles at S2 and S8 from all of the test cases (11 Cases) in Table 2.3 are shown. The cases also include the combined effects of

roughness and pressure gradients. For y/δ > 0.2, compared to the rough surface ZPG boundary layer, rough surface APG boundary layer has higher $(U_\infty - u)/(U_\infty \delta^*/\delta)$. On the contrary, compared to the rough surface ZPG boundary layer, rough surface FPG boundary layer has lower $(U_\infty - u)/(U_\infty \delta^*/\delta)$. For y/δ < 0.2, compared to the rough surface ZPG boundary layer, rough surface APG boundary layer has lower $(U_\infty - u)/(U_\infty \delta^*/\delta)$ and rough surface FPG boundary layer has higher $(U_\infty - u)/(U_\infty \delta^*/\delta)$. However the differences are small, and, thus, the combined effects of Re_θ, *K*, and *k* also scaled with δ^*/δ.

5.2 Application of the velocity scaling to turbomachinery blade boundary layers

Figure 5.4 shows the mean velocity defect plotted versus y/δ for smooth surface axial compressor blade boundary layers [83, 84] and mean velocity profile for smooth surface ZPG flat plate boundary layer of the present study. Deutsch and Zierke [83] presented incompressible, pressure side (*x/C*=0.979, Re_θ = 388 and FPG) and suction side (x/C=0.127, Re_θ =1,482 and APG) boundary layers developing over a double circular arc compressor blade with a positive incidence angle of

5°. The Reynolds number based on the blade chord *C* (Re_C) was 500,000. Freestream turbulence intensity has been kept below 3% and this turbulence level is common in compressor stages [85]. The suction side boundary layer profile from Deutsch and Zierke [83] is similar to the present study's smooth surface ZPG profile. However, for a given *y/δ*, compared to the smooth surface ZPG profile, the pressure side boundary layer has a relatively lower $(U_\infty - u)/U_\infty$. One reason for the lower mean velocity is FPG on the pressure side near the trailing edge. Higenfeld et al. [84] provided boundary layer data at x_{ax}/C_{ax} = 0.95 from a highly-loaded transonic compressor cascade with shock-boundary layer interactions and separation bubbles upstream of the turbulent region. Re_C and inlet Mach number *Ma* were 450,000 and 0.83, respectively. Due to the pressure jump across and APG downstream of a shock, Hilgenfeld's boundary layer has higher $(U_\infty - u)/(U_\infty \delta^*/\delta)$ than those in the smooth surface ZPG flat plate boundary layer. However, when the mean velocity defect is normalized by δ^*/δ, the measured boundary layer profiles all collapse into a single curve in Fig. 5.5. That δ^*/δ scaling works well for compressible boundary layers with shock-boundary layer interactions and upstream separation bubbles suggests that such effects are also incorporated into the δ^*/δ.

Figure 5.6 shows the mean velocity defect profiles from the smooth surface ZPG flat plate boundary layer and smooth tripped turbine boundary layer measurements of Lorenz et al. [22] and Dees and Bogard [58]. Lorenz et al. [22] presented smooth surface turbulent boundary layers measured near the trailing edge of a turbine blade. In their study, Re_C, the maximum *Ma*, and freestream turbulence intensity were 250,000, 0.6, and 1.4%, respectively. Mean velocity profile for Lorenz's tripped smooth suction side boundary layer is similar to that of the smooth surface ZPG profile. Smooth surface boundary layer profile of Dees and Bogard [58] (s/C=0.57 and freestream level is 5.2%), has lower mean velocity defect thoughout the boundary layer. However, when the mean velocity defect is normalized by δ^*/δ, the smooth turbine blade boundary layer profiles match the flat plate ZPG profile (Fig. 5.7).

Figure 5.8 shows the mean velocity defect profiles from the rough surface ZPG flat plate boundary layer and smooth tripped turbine boundary layer measurements [22, 58]. Due to their surface roughness, mean velocity defects in the rough turbine blade boundary layers are considerably greater than those in the present study's smooth surface ZPG flat plate boundary layer. Again, the roughness effect is not shown when the mean velocity defect is scaled with δ^*/δ (Fig. 5.9).

Thus, the δ^*/δ parameter can be applied to scale the mean velocity defect in both axial compressor and axial turbine blade boundary layers.

5.3 Power law velocity estimation for flat plate boundary layers

To develop a one-variable power law which estimates the outer layer velocity profiles of boundary layers, the exponent in Eq. (1.3) ought to include the effects of Re_θ, K, and k.

$$\gamma = \gamma(Re_\theta, K, k) \tag{5.1}$$

In this investigation, γ based on δ^*/δ is suggested. From the definition of δ^*, γ can be determined as follows:

$$\frac{\delta^*}{\delta} = \frac{1}{\delta}\int_0^\delta (1-\frac{u}{U_\infty})dy = \frac{1}{\delta}\int_0^\delta (1-(\frac{y}{\delta})^\gamma)dy = (1-\frac{1}{\gamma+1}) \tag{5.2}$$

$$\gamma = \frac{1}{(\delta/\delta^* - 1)} \tag{5.3}$$

Then, the power law (Eq. (1.3)) becomes:

$$u / U_{\infty} = (y/\delta)^{\frac{1}{(\delta/\delta^{*}-1)}} \tag{5.4}$$

The measured flat plate boundary layer data are compared with the velocity profile estimated by Eq. (5.4). Figure 5.10 shows the measured mean velocity profiles of flat plate boundary layers (o) at S8 and estimations of Eq. (5.4) (--). Estimations from the conventional 1/7 law and shape factor-based power law (Eq. (5.5)) are also shown in the figures.

$$u / U_{\infty} = (y/\delta)^{\frac{H-1}{2}} \tag{5.5}$$

Eq. (5.4) estimates the measured velocity profile with greater accuracy than the conventional 1/7 power law and accurately estimates the smooth surface boundary layers with FPG (Fig. 5.10(b)) and APG (Fig. 5.10(c)). For smooth surface ZPG and FPG boundary layers, Eq. (5.4) shows good agreement with Eq. (5.5). For smooth surface APG boundary layer, for y/δ > 0.2 (corresponding to logarithmic and outer layer), Eq. (5.4) estimates the mean velocity profile more accurately

than Eq. (5.5).

The mean velocity profiles for rough surface ZPG (Fig. 5.10(d)), rough surface FPG (Fig. 5.10(e)), and rough surface APG (Fig. 5.10(f)) cases are also well estimated by Eq. (5.4). For rough surface boundary layers, Eq. (5.4) estimates mean velocity profiles more accurately than Eq. (5.5) for y/δ > 0.2. Eq. (5.4) also accurately estimates the mean velocity profiles at different measuring stations (S1 ~ S7). Thus, the newly proposed power law can estimate outer layer mean velocity profiles of smooth and rough flat plate boundary layers with and without pressure gradients.

The momentum thicknesses inferred from Eq. (5.4) are also compared with the measured momentum thicknesses in Table 5.1. From Eq. (5.4), the momentum thickness can be estimated as:

$$\frac{\theta}{\delta} = \frac{1}{\delta}\int_0^{\delta}\frac{u}{U_\infty}(1-\frac{u}{U_\infty})dy = \frac{1}{\delta}\int_0^{\delta}(\frac{y}{\delta})^{\gamma}(1-(\frac{y}{\delta})^{\gamma})dy$$

$$\frac{\theta}{\delta} = (\frac{1}{\gamma+1}-\frac{1}{2\gamma+1}) \tag{5.6}$$

For all of the flat plate cases, the estimations agree with measurements to within 3%. The maximum differences in the ZPG, FPG and APG

cases are under 0.8%, 2.2%, and 2.9%, respectively. Thus, the power law (Eq. (9)) can accurately estimate the profile loss as well as the velocity profiles.

5.4 Application of the power law to turbomachinery blade boundary layers

Applicability of Eq. (5.4) to compressor and turbine blade boundary layers are evaluated. In Fig. 5.11, mean velocity profiles of smooth compressor blade boundary layers [83, 84], estimated compressor blade velocity profile from Eq. (5.4) with experimentally determined γ, and estimations from the conventional 1/7 power law are plotted. Eq. (5.4) estimates the measured mean velocity profiles well. As shown in Figs. 5.11(a) and 5.12(b), the difference between the measured data and Eq. (5.4) is much smaller than the difference between the measured data and the 1/7 power law.

Smooth and rough surface turbine boundary layer data from Lorenz et al. [22] and Dees and Bogard [58] are also shown with estimations from Eq. (5.4) and the 1/7 power law in Fig. 5.12(a) and 5.12(b), respectively. The estimations from Eq. (5.4) show good agreement with the measured velocity profiles and provides better estimation than the

1/7 power law, especially for rough surface turbine boundary layers. However, some discrepancy between the measured data and estimations (Eq. (5.4)) exists in the rough surface cases. Eq. (5.4) overestimates the mean velocity for $y/\delta < 0.5$, and underestimates the mean velocity for $y/\delta > 0.5$. This discrepancy may be due to the streamline curvature (convex) effect. For a convex surface (e.g., suction surfaces in turbomachinery), there is a pressure gradient in the wall-normal direction and the angular momentum of the mean flow increases in the wall-normal direction. Gibson et al. [86] showed that compared to the flat surface boundary layer, convex surface boundary layer has lower turbulent stress and intensity. So and Mellor [87] also found a reduction in the shear stress especially for $y/\delta > 0.5$. The reduced turbulence and shear can increase mean velocity in the outer layer, and, thus, the measured velocities are higher than the velocities estimated by Eq. (5.4). Such effect is noticeable for rough surfaces due to the higher δ/R [88].

5.5 Conclusions

The conclusions of this chapter can be summarized as follows.

1. The mean velocity profiles of smooth and rough surface turbulent

boundary layers with and without pressure gradient scale with δ^*/δ.

2. The scaling is applicable to attached turbulent boundary layers found in axial compressor and turbine blades.
3. A new single variable power law ($u/U_\infty = (y/\delta)^{\frac{1}{(\delta/\delta^* - 1)}}$) is proposed.
4. The new power law can accurately estimate the mean velocity profiles in smooth aud rough flat plate boundary layers with and without pressure gradient.
5. The new power law can also accurately estimate the mean velocity profiles in axial compressor and turbine blades.

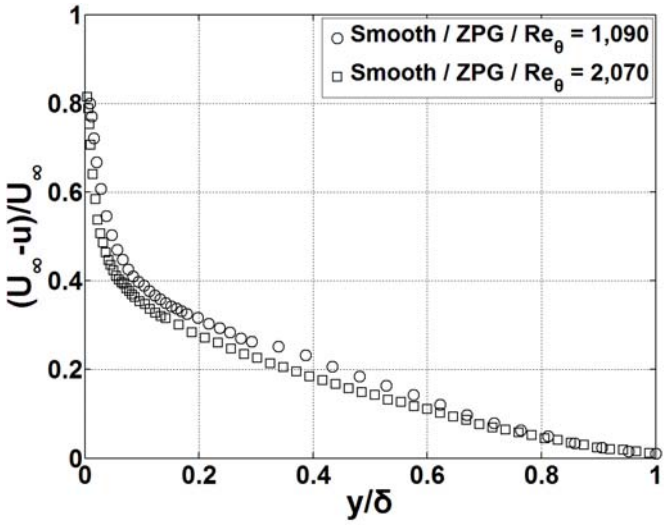
Smooth / ZPG / Re$_\theta$ = 1,090
Smooth / ZPG / Re$_\theta$ = 2,070
(U$_\infty$-u)/U$_\infty$
y/δ
0
0.2
0.4
0.6
0.8
1

(a)

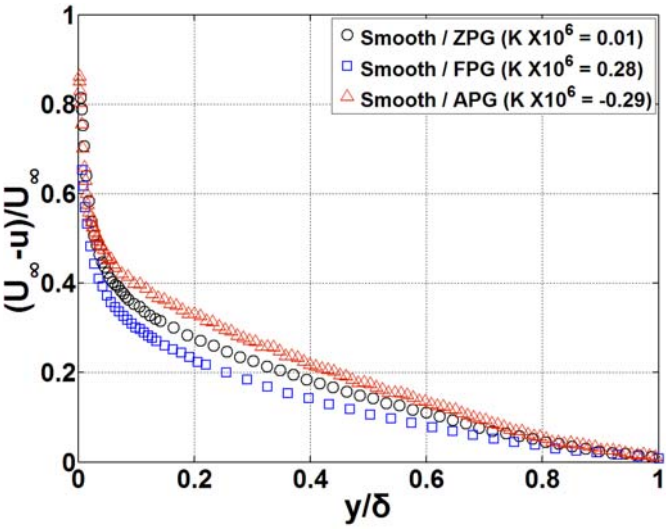
Smooth / ZPG (K X10^6 = 0.01)
Smooth / FPG (K X10^6 = 0.28)
Smooth / APG (K X10^6 = -0.29)
(U$_\infty$-u)/U$_\infty$
y/δ
0
0.2
0.4
0.6
0.8
1

(b)

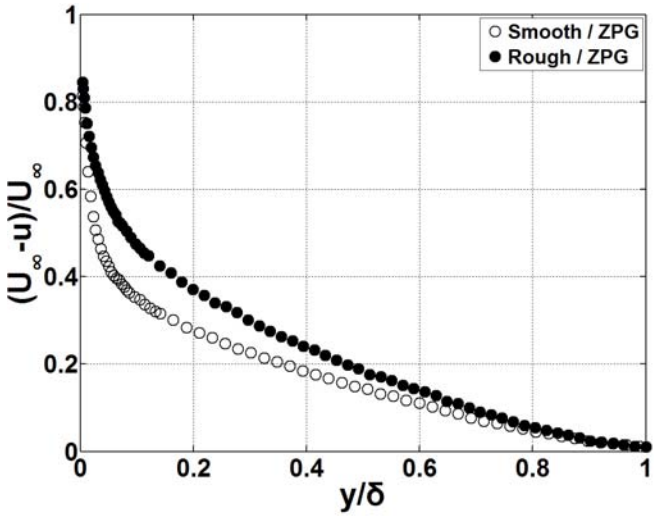

(c)

Fig. 5.1 Individual effects of Re_θ, K, k on mean velocity defect: (a) Re_θ effect, (b) K effect (c) k effect.

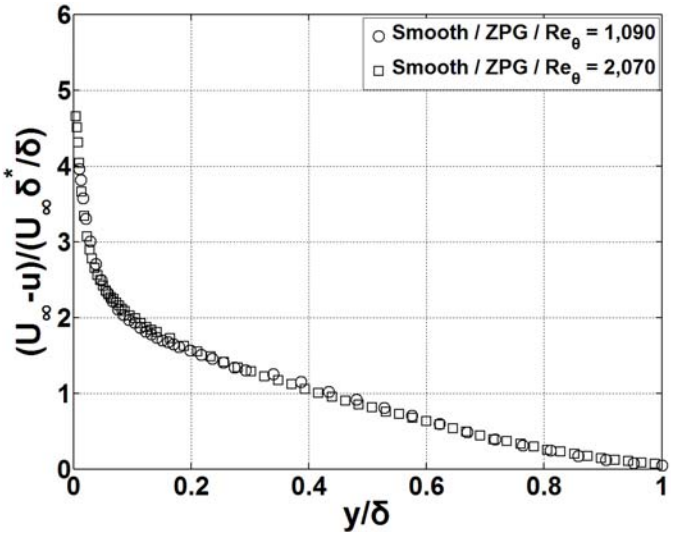

(a)

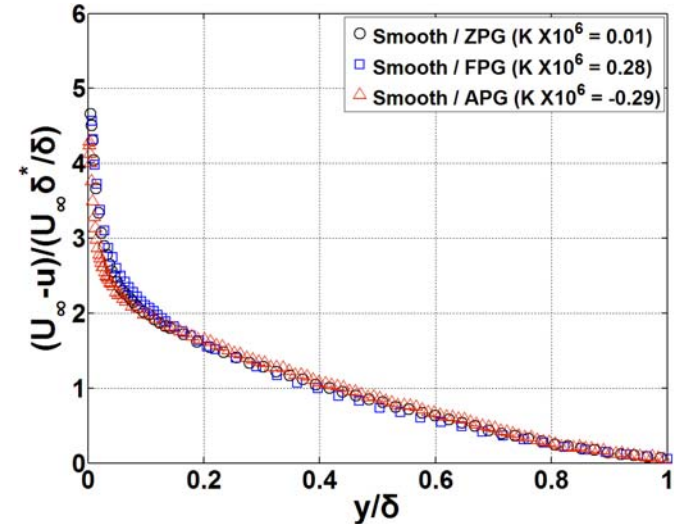

(b)

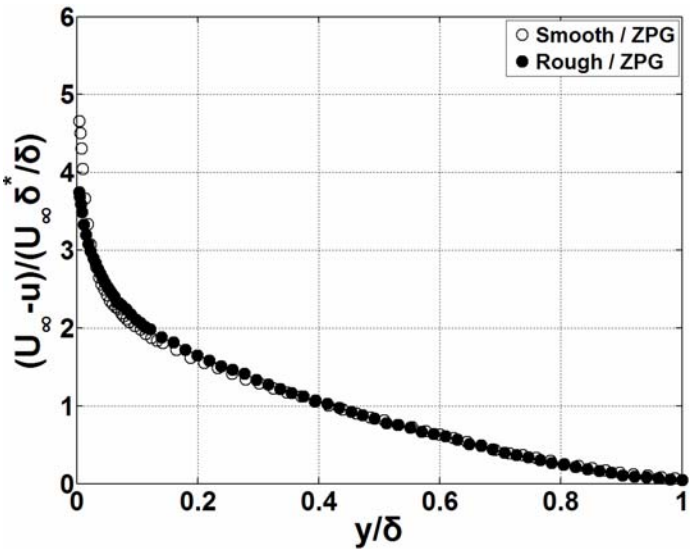

(c)

Fig. 5.2 Scaled mean velocity defect profiles with varying (a) Re_θ, (b) K, and (c) k.

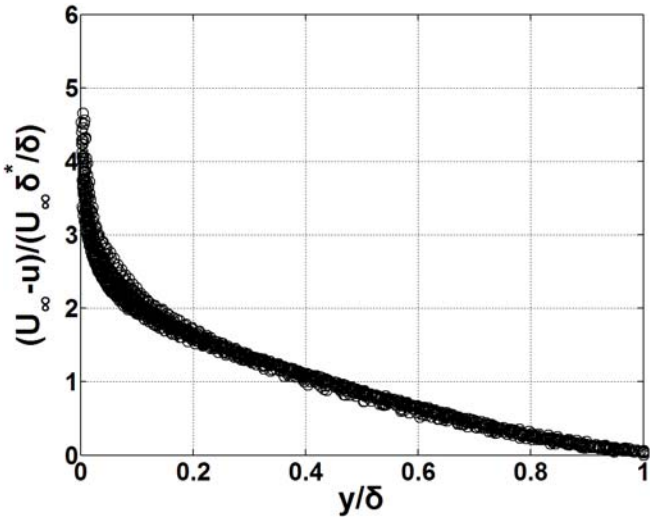

Fig. 5.3 Scaled mean velocity defect profiles in the smooth and rough surface boundary layers under zero, favorable, and adverse pressure gradients.

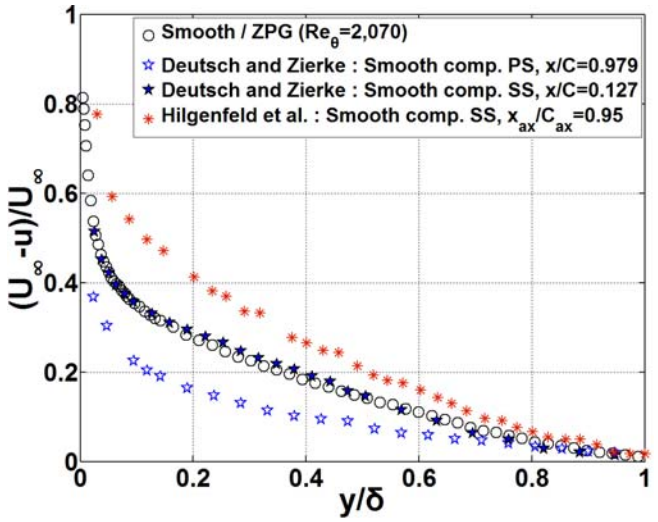

Fig. 5.4 Mean velocity defect profiles for axial compressor blade boundary layers [83, 84] and smooth surface zero pressure gradient boundary layer of the present study.

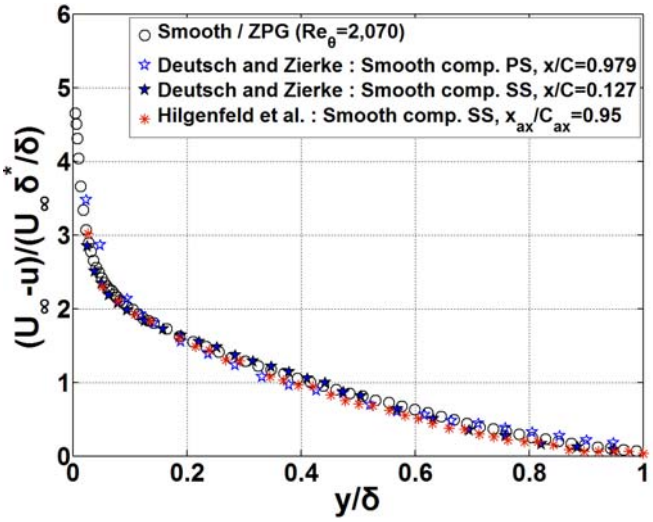

Fig. 5.5 Scaled mean velocity defect profiles for axial compressor blade boundary layers [83, 84] and smooth surface zero pressure gradient boundary layer of the present study.

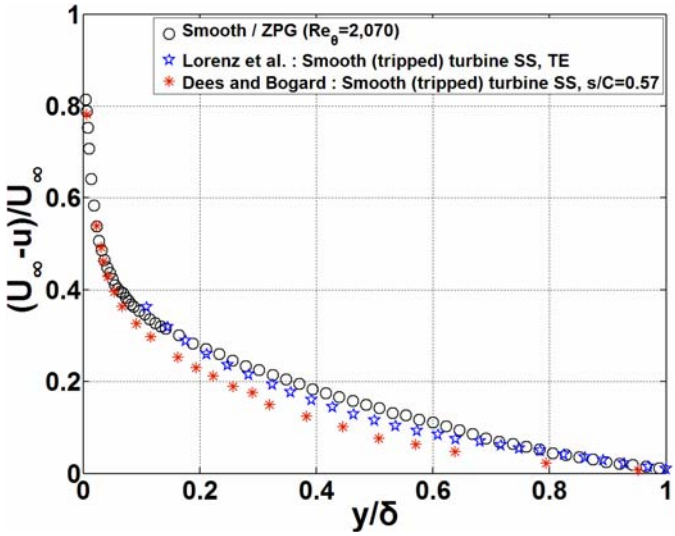

Fig. 5.6 Mean velocity defect profiles for smooth axial turbine blade boundary layers [22, 58] and smooth surface zero pressure gradient boundary layer of the present study

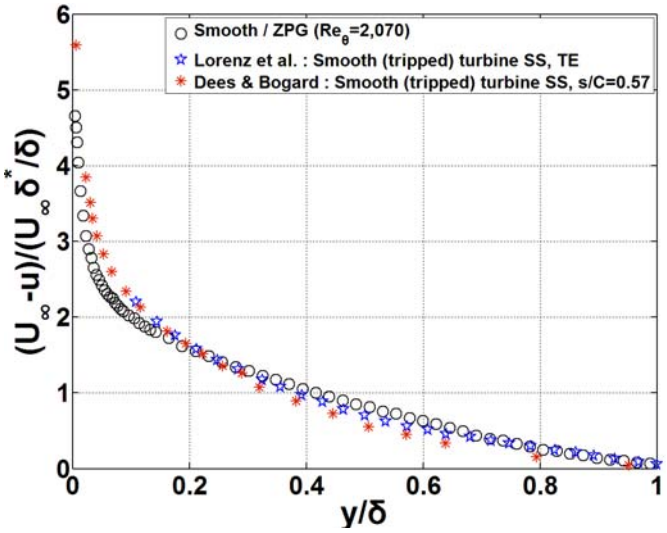

Fig. 5.7 Scaled mean velocity defect profiles for smooth axial turbine blade boundary layers [22, 58] and smooth surface zero pressure gradient boundary layer of the present study.

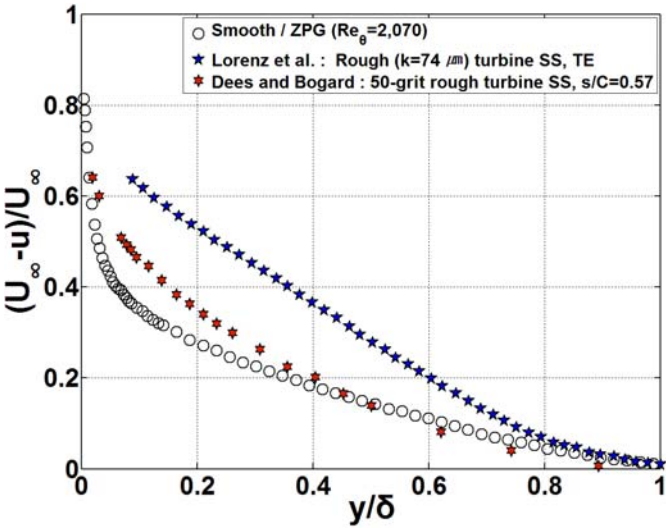

Fig. 5.8 Mean velocity defect profiles for rough axial turbine blade boundary layers [22, 58] and smooth surface zero pressure gradient boundary layer of the present study.

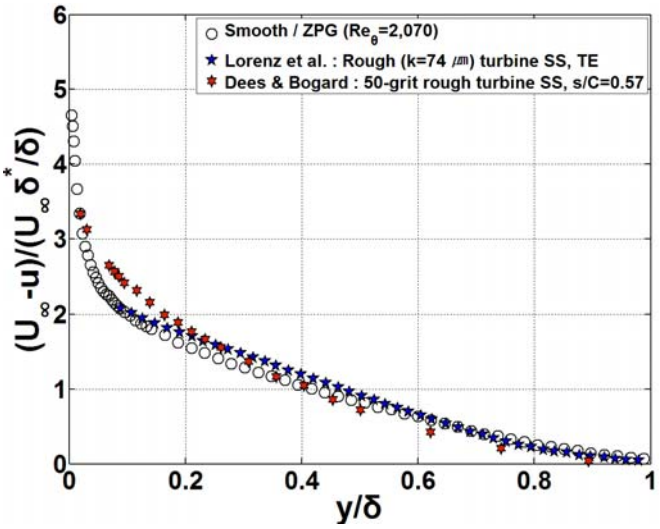

Fig. 5.9 Scaled mean velocity defect profiles for rough axial turbine blade boundary layers [22, 58] and smooth surface zero pressure gradient boundary layer of the present study.

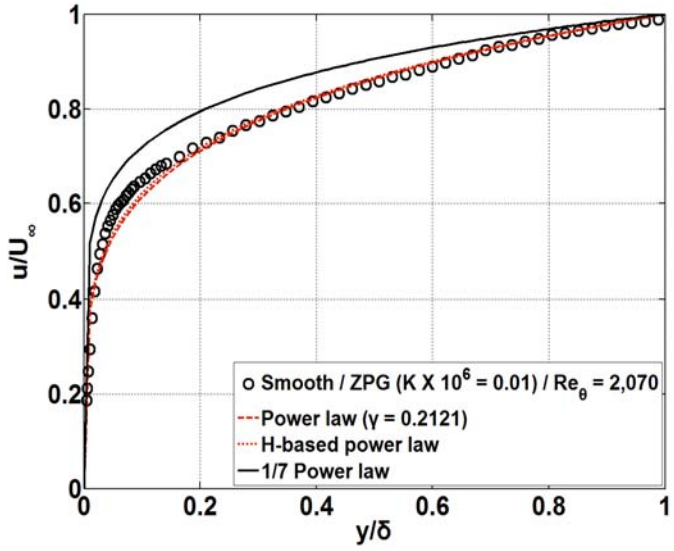

(a)

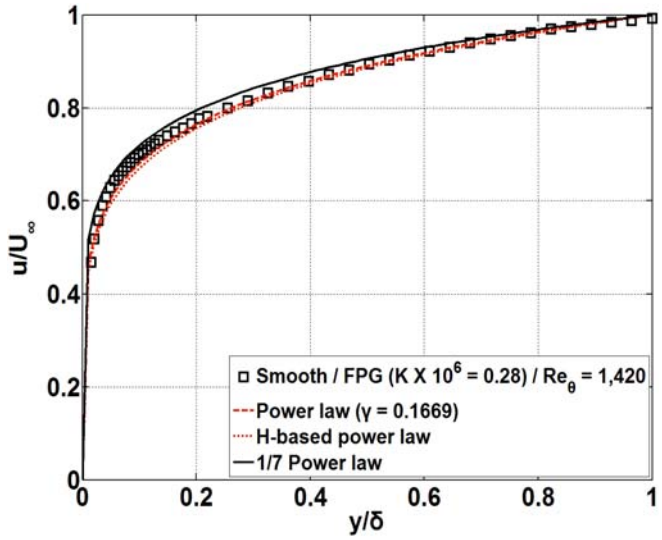
u/U∞
y/δ
Smooth / FPG (K X 10^6 = 0.28) / Re_θ = 1,420
Power law (γ = 0.1669)
H-based power law
1/7 Power law

(b)

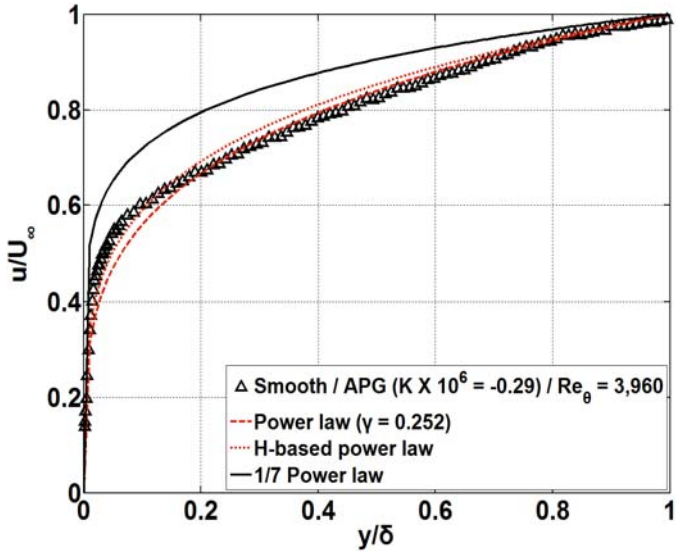
u/U∞
y/δ
Smooth / APG (K X 10^6 = -0.29) / Re_θ = 3,960
Power law (γ = 0.252)
H-based power law
1/7 Power law

(c)

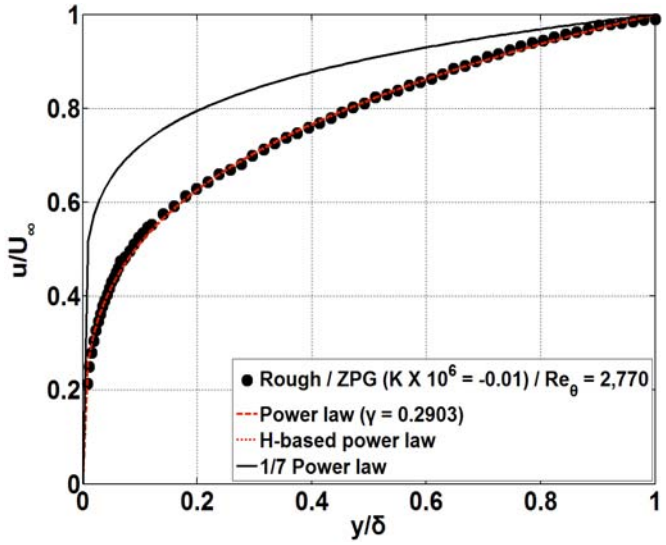
u/U∞
y/δ
Rough / ZPG (K X 10^6 = -0.01) / Reθ = 2,770
Power law (γ = 0.2903)
H-based power law
1/7 Power law

(d)

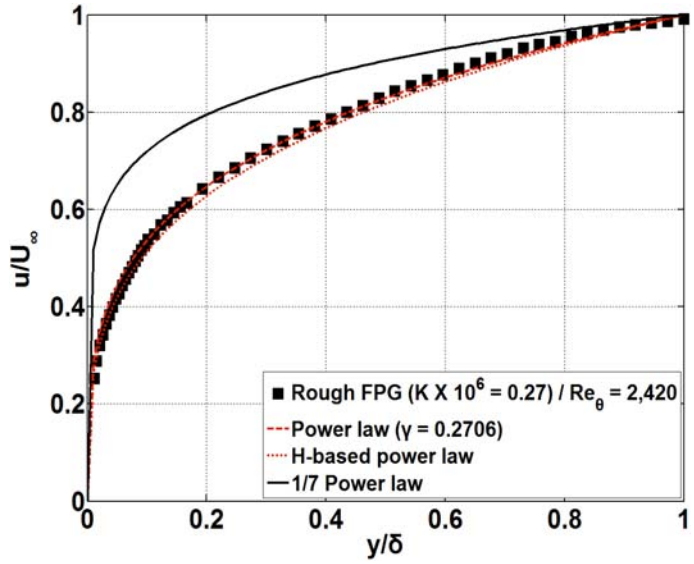
u/U∞
y/δ
Rough FPG (K X 10^6 = 0.27) / Reθ = 2,420
Power law (γ = 0.2706)
H-based power law
1/7 Power law

(e)

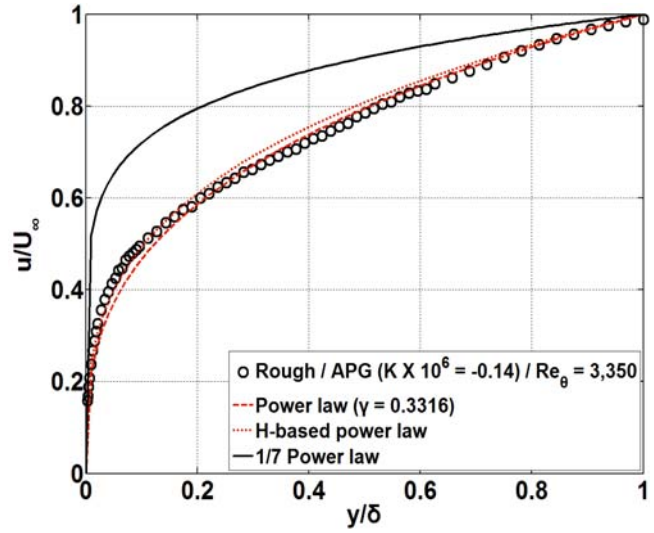

(f)

Fig. 5.10 Measured flat plate mean velocity profiles vs. Power law profiles with experimentally determined ɣ: (a) Smooth surface zero pressure gradient, (b) Smooth surface favorable pressure gradient, (c) Smooth surface adverse pressure gradient, (d) Rough surface zero pressure gradient, (e) Rough surface favorable pressure gradient, (f) Rough surface adverse pressure gradient.

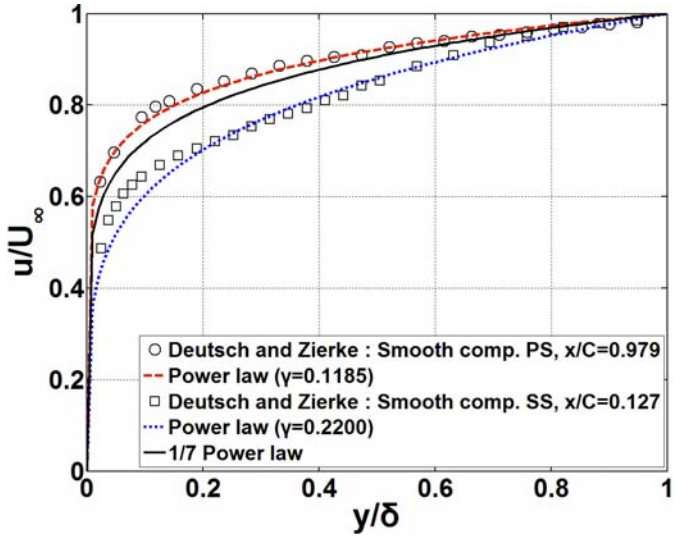

(a)

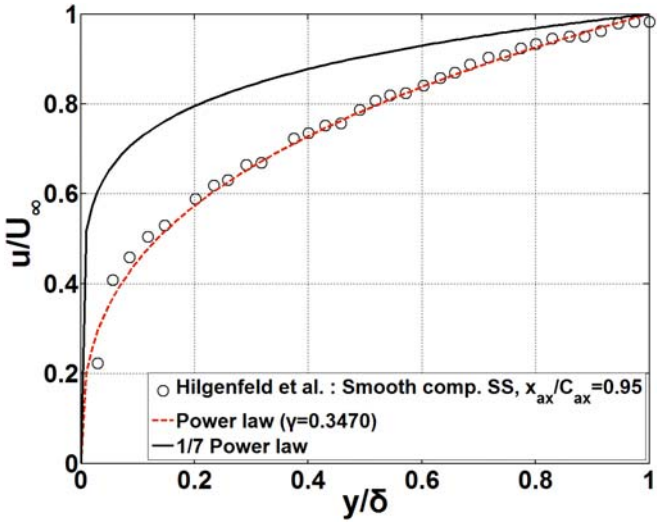

(b)

Fig. 5.11 Compressor boundary layers vs. power law profiles with experimentally determined ɣ: (a) Data from Deutsch and Zierke [83], and (b) Higenfeld et al. [84].

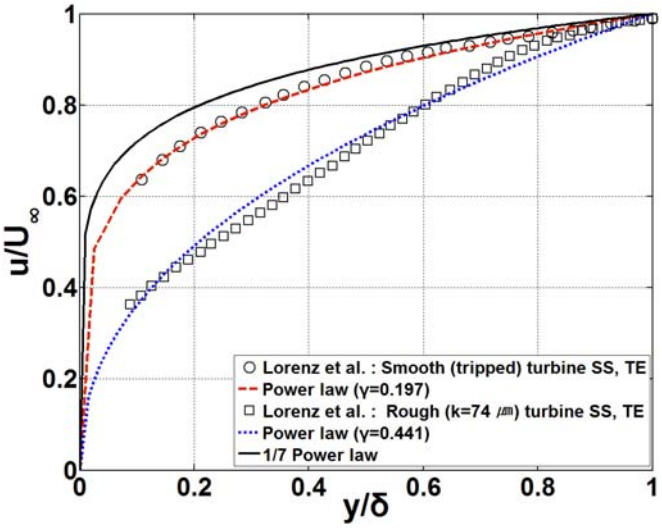

(a)

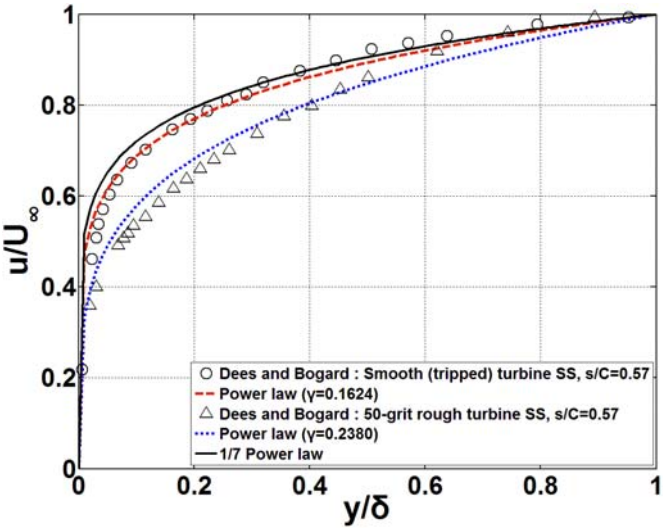

(b)

Fig. 5.12 Turbine boundary layers vs. power law profiles with experimentally determined ɣ: (a) Data from Lorenz et al. [22], and (b) Dees and Bogard [58].

Table 5.1 Measured vs. estimated momentum thickness.

Case	Smooth /ZPG	Smooth /FPG	Smooth /APG	Rough/ ZPG	Rough/ FPG	Rough/ APG
$\theta/\delta_{measured}$	0.124	0.106	0.138	0.142	0.135	0.154
θ/δ_{power}	0.124	0.107	0.134	0.142	0.135	0.150
% error	0.8	0.9	2.9	0.0	2.2	2.6

Chapter 6.

Friction Coefficient Estimation for Rough Surface Boundary Layers

6.1 Friction coefficient correlation for smooth and rough surface boundary layers under pressure gradients

Bergstrom et al. [64] proposed a C_f correlation (Eq. (1.5)) for smooth and rough surface ZPG turbulent boundary layers for 1,430 < Re_θ < 31,000. Figure 6.1 shows the C_f for the smooth and rough flat plate ZPG cases plotted versus δ^*/δ. Upper and lower dashed lines show the upper and lower bounds in Bergstrom's correlation, and the solid line represents $C_f^{0.5} = 0.360(\delta^*/\delta)$. Most of the measured smooth and rough surface ZPG ($k \times 10^3/L$ = 0.208 and 0.333) data are within the Bergstrom's correlation region, thus the correlation esimates C_f for zero pressure gradient boundary layers.

Figure 6.2 shows the estimated C_f for Smooth surface FPG, Smooth surface APG, Rough surface FPG, and Rough surface APG. For both smooth and rough surfaces, C_f in the FPG cases are higher than the

upper bound of Eq. (1.5), and C_f in the APG cases are lower than the lower bound of Eq. (1.5). Thus, Eq. (1.5) is not applicable for non-zero pressure gradient boundary layers.

Figure 6.3 shows the distribution of $C_f^{0.5}(\delta/\delta^*)$ versus *K*. The $C_f^{0.5}(\delta/\delta^*)$ increases linearly with increasing *K*. From the result, a new C_f correlation for smooth and rough surface boundary layers with and without pressure gradient is proposed (Eq. (6.1)).

$$C_f^{0.5} = [0.254(K \times 10^6) + 0.367](\delta^* / \delta) \tag{6.1}$$

Note that the new correlation is valid for low Reynolds number ($1{,}010 \leq Re_\theta \leq 4{,}680$), rough surface ($k \leq 400\mu m$) boundary layers under pressure gradients ($-0.40 \leq K \times 10^6 \leq 0.52$).

Applicability of the suggested correlation to smooth axial turbine blade boundary layer is evaluated. Figure 6.4 shows the $C_f^{0.5}(\delta/\delta^*)$ estimated from Eq. (6.1) (solid line) and $C_f^{0.5}(\delta/\delta^*)$ measured on a turbine suction surface by Dees and Bogard [58]. Eq. (6.1) estimates $C_f^{0.5}(\delta/\delta^*)$ for a ZPG turbine suction surface boundary layer to within 10%. Under FPG, Eq. (6.1) estimates $C_f^{0.5}(\delta/\delta^*)$ to within 5%. Thus,

Eq. (6.1) can accurately estimate $C_f^{0.5}(\delta/\delta^*)$ for attached boundary layers on smooth axial turbine blades. With integral boundary layer parameters, the proposed correlation can estimate friction coefficient without any shear stress measurement which is often impossible for rough surface applications.

6.2 Conclusions

The conclusions of this chapter can be summarized as follows.

1. The previous friction coefficient correlation ($C_f^{0.5} = (0.360 \pm 0.025)(\delta^*/\delta)$) is not applicable to boundary layers with pressure gradients.
2. A new friction coefficient correlation ($C_f^{0.5} = [0.254(K \times 10^6) + 0.367](\delta^*/\delta)$), applicable to rough surface flat plate boundary layers with and without pressure gradients, is proposed.
3. The new friction coefficient correlation can estimate C_f in smooth turbine blades.

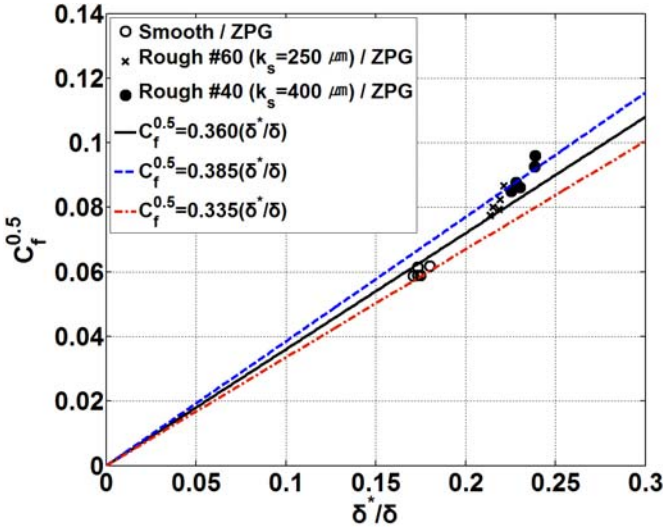

Fig. 6.1 Friction coefficient vs. δ^*/δ for the smooth and rough surface boundary layers without pressure gradient.

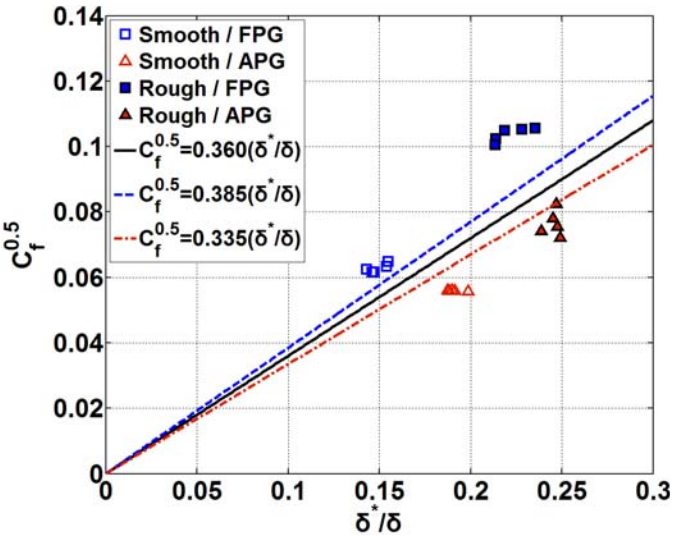

Fig. 6.2 Friction coefficient vs. δ^*/δ for the smooth and rough surface boundary layers with pressure gradients.

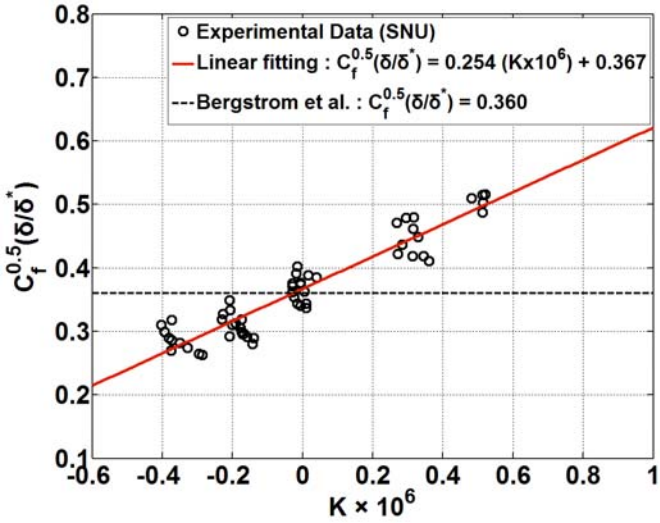

Fig. 6.3 Distribution of $c_f^{0.5}(\delta/\delta^*)$ in the flat-plate cases for varying *K*.

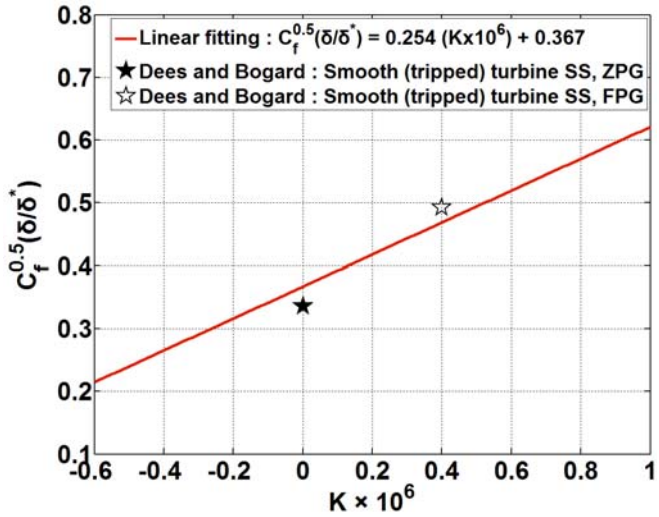

Fig. 6.4 $c_f^{0.5}(\delta/\delta^*)$ in turbine boundary layers [58].

Chapter 7. Conclusions

Individual and combined effects of pressure gradients (FPG and APG) and surface roughness on mean velocity, fluctuating velocity, friction coefficient, boundary layer integral paramaeter, and streamwise turbulent kinetic energy in flat plate turbulent boundary layers have been investigated experimentally. From the results, applicability of the δ^*/δ scaling to attached turbulent boundary layers on smooth and rough flat plates, axial compressor blades, and axial turbine blades are evaluated. A new power law mean velocity estimation method for smooth and rough flat plate boundary layers and turbomachinery blade boundary layers are proposed. Finally, a new friction coefficient correlation which is applicable to smooth and rough flat plate boundary layers with and without pressure gradient and smooth turbine blade boundary layers is proposed. New findings of this investigation are summarized as follows.

1. For smooth surfaces, FPG barely changes friction coefficient because the increased freestream velocity counteracts against the increased wall shear stress. APG decreases the friction coefficient

slightly.

2. For smooth surfaces, FPG increases streamwise normal Reynolds stress near the surface because FPG confines vortices to a narrow region near the surface. On the contrary, APG enhances outward migration of the near-surface vortices and decreases streamwise normal Reynolds stress near the surface.

3. For rough surfaces, the roughness effect of increasing mean velocity defect is stronger under FPG than under ZPG near the surface. Under APG, the roughness effect is weaker than ZPG.

4. With a rough surface, FPG increases the streamwise normal Reynolds stress near the surface. The result is thought to be due to the near-surface confinement of roughness-generated coherent unsteady vortices and strengthened horseshoe vortices. On the contary, APG decreases the streamwise normal Reynolds stress near the surface because APG enhances outward convection of near-surface vortices generated by roughness elements.

5. FPG enhances roughness effect on *TKE* generation while APG

reduces the roughness effect.

6. For rough surfaces, FPG increases friction coefficient, roughness Reynolds number, roughness shift, and roughness effect on integral boundary layer parameters. On the contrary, APG decreases the parameters.

7. The individual and combined effects of Reynolds number, pressure gradient, and roughness on mean velocity defect profile scale with δ^*/δ. The scaling is applicable to attached turbulent boundary layers found in flat plates, axial compressor blades, and axial turbine blades.

8. A new single variable power law $(u/U_\infty = (y/\delta)^{\frac{1}{(\delta/\delta^*-1)}}$ is proposed. The new power law can accurately esimate the mean velocity profiles in smooth and rough flat plate boundary layers with and without pressure gradient, axial compressor blades boundary layers, and axial turbine blade boundary layers.

9. A new friction coefficient correlation

$C_f^{0.5} = [0.254(K \times 10^6) + 0.367](\delta^* / \delta)$ is suggested for smooth and rough flat plate boundary layers with and without pressure gradient. The new friction coefficient can also estimate C_f in smooth turbine blades.

References

[1] Hill, P., Peterson, C., 1992, "Mechanics and Thermodynamics of Propulsion Second Edition," Addison-Wesley Publishing Company.

[2] Denton, J. D., 1993, "Loss Mechanisms in Turbomachines," ASME Journal of Turbomachinery, 115, pp. 621-656.

[3] Curtis, E. M., Hodson, H. P., Banieghbal, M. R., Denton, J. D., Howell, R. J., and Harvey, N. W., 1997, "Development of Blade Profiles for Low-Pressure Turbine Applications," ASME Journal of Turbomachinery, 119, pp. 531-538.

[4] Mailach, R. and Vogeler, K., 2006, "Blade Row Interaction in Axial Compressors Part Ⅱ: Unsteady Behaviour of Boundary Layer, Pressure Distribution and Excited Pressure Force of Compressor Blades," von Karman Institute for Fluid Dynamics Lecture Series 2006-06 Advances in Axial Compressor Aerodynamics.

[5] Schreiber, H. -A., Steinert, W., and Küsters, B., 2002, "Effects of Reynolds Number and Free-Stream Turbulence on Boundary Layer Transition in a Compressor Cascade," ASME Journal of Turbomachinery, 124, pp. 1-9.

[6] Mayle, R. E., 1991, "The Role of Laminar-Turbulent Transition in Gas Turbine Engines," ASME Journal of Turbomachinery, 113,

pp. 509-536.

[7] Launder, B. E., 1964, "Laminarization of the Turbulent Boundary Layer in a Severe Acceleration," ASME Journal of Applied Mechanics, 31, pp. 707-708.

[8] Bons, J. P., 2010, "A Review of Surface Roughness Effects in Gas Turbines," ASME Journal of Turbomachinery, 132, pp. 021004.

[9] Song, S. J., Sohn, J. L., and Kim, T. S., 2006, "Midterm Report on the Effect of Compressor Fouling on Gas Turbine Performance and Diagnosis," Korea Midland Power, Co. Ltd., Seoul, Technical Report No. R-2005-0-016.

[10] Millsaps, K. T., Baker, L. J., and Patterson, J. S., 2004, "Detection and Localization of Fouling in a Gas Turbine Compressor From Aerothermodynamic Measurements," ASME Turbo Expo 2004, GT2004-54173.

[11] Shin, J. H., Back, S. C., Kim, J. K., Kim, D. K., and Song, S. J., 2010, "Measurement of Surface Roughness on Gas Turbine Compressor Blade," 2010 KSME Spring Conference.

[12] Bons, J. P., Taylor, R. P., McClain, S. T., and Rivir, R. B., 2001, "The Many Faces of Turbine Surface Roughness," ASME Journal of Turbomachinery, 123, pp. 739-748.

[13] Taylor, R. P., 1990, "Surface Roughness Measurements on Gas

Turbine Blades," ASME Journal of Turbomachinery, 112, pp. 175-180.

[14] Koch C. C., and Smith, L. H., 1976, "Loss Sources and Magnitudes in Axial-Flow Compressors," ASME Journal of Engineering for Power, 98, pp. 411-424.

[15] Schlichting, H., and Gersten, K., 2000, "Boundary-Layer Theory 8th edition," Springer-Verlag Berlin Heidelberg.

[16] Bogard, D. G., Schmidt, D. L., and Tabbita, M., 1998, "Characterization and Loboratory Simulation of Turbine Airfoil Surface Roughness and Associated Heat Transfer," ASME Journal of Turbomachinery, 120, pp. 337-342.

[17] Song, S. J., Sohn, J. L., and Kim, T. S., 2007, "Final Report on the Effect of Compressor Fouling on Gas Turbine Performance and Diagnosis," Korea Midland Power, Co. Ltd., Seoul, Technical Report No. R-2005-0-016.

[18] Yun, Y. I., Park, I. Y., and Song, S. J., 2005, "Performance Degradation due to Blade Surface Roughness in a Single-Stage Axial Turbine," ASME Journal of Turbomachinery, 127, pp. 137-143.

[19] Back, S. C., Sohn, J. H., and Song, S. J., 2010, "Impact of Surface Roughness on Compressor Cascade Performance," ASME Journal of Fluids Engineering, 132, pp. 064502.

[20] Leipold, R., Boese, M., and Fottner, L., 2000, "The Influence of Technical Surface Roughness Caused by Precision Forging on the Flow Around a Highly Loaded Compressor Cascade," ASME Journal of Turbomachinery, 122, pp. 416-425.

[21] Zhang, Q., Goodro, M., Ligrani, P. M., Trindade, R., and Sreekanth, S., 2006, "Influence of Surface Roughness on the Aerodynamic Losses of a Turbine Vane," Journal of Fluids Engineering, 128, pp. 568-578.

[22] Lorenz, M., Schulz, A., and Bauer, H. -J., 2012, "Experimental Study of Surface Roughness Effects on a Turbine Airfoil in a Linear Cascade- Part Ⅱ: Aerodynamic Losses," ASME Journal of Turbomachinery, 134, pp. 041007.

[23] Back, S. C., Hobson, G. V., Song, S. J., and Millsaps, K. T., 2012, "Effects of Reynolds Number and Surface Roughness Magnitude and Location on Compressor Cascade Performance," Journal of Turbomachinery, 134, pp. 051013.

[24] Joshi, P., Liu, X., and Katz, J., 2011, "Turbulence in Accelerating Boundary Layers," ASME-JSME-KSME Joint Fluids Engineering Conference 2011, AJK2011-25010.

[25] Escudier, M. P., Abdel-Hameed, A., Johnson, M. W., and Sutcliffe, C. J., 1998, "Laminarisation and Re-transition of

a Turbulent Boundary Layer Subjected to Favorable Pressure Gradient," Experiments in Fluids, 25, pp. 491-502.

[26] Herring, H. J., and Norbury, J. F., 1967, "Some Experiments on Equilibrium Turbulent Boundary Layers in Favorable Pressure Gradients," Journal of Fluid Mechanics, 27, pp. 541-549.

[27] Piomelli, U., Balaras, E., and Pascarelli, A., 2000, "Turbulent Structures in Accelerating Boundary Layers," Journal of Turbulence, 1, pp. 1-16.

[28] Spalart, P. R., and Watmuff, J. H., 1993, "Experimental and Numerical Study of a Turbulent Boundary Layer with Pressure Gradients," Journal of Fluid Mechanics, 249, pp. 337-371.

[29] Krogstad, P. A., and Skare, P. E., 1995, "Influence of a Strong Adverse Pressure Gradient on the Turbulent Structure in a Boundary Layer," Physics of Fluids, 7, pp. 2014-2024.

[30] Nagano, Y., Tsuji, T., and Houra, T., 1998, "Structure of Turbulent Boundary Layer Subjected to Adverse Pressure Gradient," International Journal of Heat and Fluid Flow, 19, pp. 563-572.

[31] Lee, J. H., and Sung, H. J., 2008, "Effects of an Adverse Pressure Gradient on a Turbulent Boundary Layer," International Journal of Heat and Fluid Flow, 29, pp. 568-578.

[32] Acharya, M., Bornstein, J., and Escudier, M. P., 1986, "Turbulent

Boundary Layers on Rough Surfaces," Experiments in Fluids, 4, pp. 33-47.

[33] Brzek, B., Cal, R. B., Johansson, T. G., and Castillo, L., 2007, "Inner and Outer Scalings in Rough Surface Zero Pressure Gradient Turbulent Boundary Layers," Physics of Fluids, 19, pp.065101.

[34] Furuya, Y., Miyata, M., and Fujita, H., 1976, "Turbulent Boundary Layer and Flow Resistance on Plates Roughened by Wires," Journal of Fluids Engineering, 98, pp. 635-643.

[35] Leonardi, S., Orlandi, P., and Antonia, R. A., 2007, "Properties of d- and k-Type Roughness in a Turbulent Channel Flow," Physics of Fluids, 19, pp. 125101.

[36] Nikuradse, J., 1933, "Law of Flow in Rough Pipes," Technical Memorandum 1292, National Advisory Committee for Aeronautics, Washington.

[37] Krogstad, P. -A., Antonia, R. A., and Browne, W. B., 1992, "Comparison Between Rough- and Smooth-Wall Turbulent Boundary Layers," Journal of Fluid Mechanics, 245, pp. 599-617.

[38] Krogstad, P. -A., and Antonia, R. A., 1999, "Surface Roughness Effects in Turbulent Boundary Layers," Experiments in Fluids, 27, pp. 450-460.

[39] Jimenez, J., 2004, "Turbulent Flows over Rough Walls," Annual Review of Fluid Mechanics, 36, pp. 173-196.

[40] Meinders, E. R., and Hanjalic, K., 1999, "Vortex Structure and Heat Transfer in Turbulent Flow over a Wall-Mounted Matrix of Cubes," International Journal of Heat and Fluid Flow, 20, pp. 255-267.

[41] Djenidi, L., Antonia, R. A., Amielh, M., and Anselmet, F., 2008, "A Turbulent Boundary Layer over a Two-Dimensional Rough Wall," Experiments in Fluids, 44, pp. 37-47.

[42] Coleman, H. W., Moffat, R. J., and Kays, W. M., 1981, Accelerated Fully Rough Turbulent Boundary Layer," ASME Journal of Heat Transfer, 103, pp. 153-158.

[43] Chakroun, W., and Taylor, R. P., 1993, "The effect of Moderately Strong Acceleration on Heat Transfer in the Turbulent Rough-Wall Boundary Layer," ASME Journal of Heat Transfer, 115, pp. 782-785.

[44] Bons, J. P., and McClain, S. T., 2004, "The Effect of Real Turbine Roughness with Pressure Gradient on Heat Transfer," ASME Journal of Turbomachinery, 126, pp. 385-394.

[45] Coleman, H. W., Moffat, R. J., and Kays, W. M., 1977, "The Accelerated Fully Rough Turbulent Boundary Layer,"

Journal of Fluid Mechanics, 82, pp. 507-528.

[46] Cal, R. B., Brzek, B., Johansson, T. G., and Castillo, L., 2008, "Influence of External Conditions on Transitionally Rough Favourable Pressure Gradient Turbulent Boundary Layers," Journal of Turbulence, 9, pp. 1-22.

[47] Cal, R. B., Brzek, B., Johansson, T. G., and Castillo, L., 2009, "The Rough Favourable Pressure Gradient Turbulent Boundary Layer," Journal of Fluid Mechanics, 641, pp. 129-155.

[48] Tay, G. F. K., Kuhn, D. C. S., and Tachie, M. F., 2009, "Particle Image Velocimetry Study of Rough-Wall Turbulent Flows in Favorable Pressure Gradient," ASME Journal of Fluids Engineering, 131, pp. 061205.

[49] Launder, B. E., and Lockwood, F. C., 1969, "An Aspect of Heat Transfer in Accelerating Turbulent Boundary Layer," ASME Journal of Heat Transfer, 91, pp. 229-234.

[50] Perry, A. E., and Joubert, P. N., 1963, "Rough-Wall Boundary Layers in Adverse Pressure Gradients," Journal of Fluid Mechanics, 17, pp. 193-206.

[51] Moore, W. F., 1951, "An Experimental Investigation of the Boundary Layer Development Along a Rough Surface," Ph. D. dissertation, State University of Iowa.

[52] Pailhas, G., Touvet, Y., and Aupoix, B., 2008, "Effects of Reynolds Number and Adverse Pressure Gradient on a Turbulent Boundary Layer Developing on a Rough Surface," Journal of Turbulence, 9, pp. 1-24.

[53] Tay, G. F. K., Kuhn, D. C. S., and Tachie, M. F., 2009, "Influence of Adverse Pressure Gradient on Rough-Wall Turbulent Flows," International Journal of Heat and Fluid Flow, 30, pp. 249-265.

[54] Zagarola, M. V., and Smits, A. J., 1998, "Mean-Flow Scaling of Turbulent Pipe Flow", Journal of Fluid Mechanics, 373, pp. 37-79.

[55] Castillo, L., 2000, "Application of Zagarola/Smits Scaling in Turbulent Boundary Layers with Pressure Gradient," In: Brebbia, CA, and Rohnman, M (editors), Advances in Fluid Mechanics Ⅲ, WIT Press, Boston, MA, pp. 275-288.

[56] Castillo, L., Seo, J., Hangan, H., and Johansson, T. G., 2004, "Smooth and Rough Turbulent Boundary Layers at High Reynolds Number," Experiments in Fluids, 36, pp. 759-774.

[57] Dong, Y., and Cumpsty, N. A., 1990, "Compressor Blade Boundary Layers: Part 1- Test Facility and Measurements With No Incident Wakes," ASME Journal of Turbomachinery, 112,

pp. 222-230.

[58] Dees, J. E., and Bogard, D. G., 2007, "Effects of Regular and Random Roughness on the Heat Transfer and Skin Friction Coefficient on the Suction Side of a Gas Turbine Vane," ASME Turbo Expo 2007, GT2007-27285.

[59] Johnson, C. B., and Bushnell, D. M., 1970, "Power-Law Velocity-Profile-Exponent Variations with Reynolds Number, Wall Cooling, and Mach Number in a Turbulent Boundary Layer," National Aeronautics and Space Administration, Technical Note D-5753.

[60] Ching, C. Y., Djenidi, L., and Antonia, R. A., 1995, "Low-Reynolds-Number Effects in a Turbulent Boundary Layer," Experiments in Fluids, 19, pp. 61-68.

[61] George, W. K., and Castillo, L., 1997, “Zero-Pressure-Gradient Turbulent Boundary Layer,” Applied Mechanics Reviews, 50, pp.689-729.

[62] Bergstrom, D. J., Tachie, M. F., and Balachandar, R., 2001, “Application of Power Laws to Low Reynolds Number Boundary Layers on Smooth and Rough Surfaces”, Physics of Fluids, 13, pp. 3277-3284.

[63] Osaka, H., Kameda, T., and Mochizuki, S., 1998, “Reexamination

of the Reynolds-Number-Effect on the Mean Flow Quantities in a Smooth Wall Turbulent Boundary Layer," JSME International Journal Series B, 41, pp. 123-129.

[64] Bergstrom, D. J., Akinlade, O. G., and Tachie, M. F., 2005, "Skin Friction Correlation for Smooth and Rough Wall Turbulent Boundary Layers," ASME Journal of Fluids Engineering, 127, pp. 1146-1153.

[65] Castillo, L., and Johansson, T. G., 2002, "The Effects of the Upstream Conditions on a Low Reynolds Number Turbulent Boundary Layer with Zero Pressure Gradient," Journal of Turbulence, 3, pp. 1-19.

[66] Clauser, F. H., 1956, "The Turbulent Boundary Layer," Advances in Applied Mechanics, 4, pp. 1-51.

[67] Nishizawa, N., Marusic, I., and Perry, A. E., 1998, Measurement of Wall Shear Stress in Turbulent Boundary Layers Using an Optical Interferometry Method," 13th Australasian Fluid Mechanics Conference, Melbourne, Australia.

[68] Madad, R., Harun, Z., Chauhan, K., Monty, J. P., and Marusic, I., 2010, "Skin Friction Measurement in Zero and Adverse Pressure Gradient Boundary Layers Using Oil Film Interferometry," 17th Australasian Fluid Mechanics Conference, Auckland,

New Zealand.

[69] Ligrani, P. M. and Bradshaw, P., 1987, "Spatial Resolution and Measurement of Turbulence in the Viscous Sublayer Using Subminiature Hot-Wire Probes," Experiments in Fluids, 5, pp. 407-417.

[70] Robinson, S. K., 1991, "Coherent Motions in the Turbulent Boundary Layer," Annual Review of Fluid Mechanics, 23, pp. 601-639.

[71] Spalart, P. R., 1988, "Direct Simulation of a Turbulent Boundary Layer up to Re_θ=1410," Journal of Fluid Mechanics, 187, pp. 61-98.

[72] Ludwieg, H., and Tillmann, W., 1949, "Untersuchungen über die Wandschubspannung in Turbulenten Reibungsschichten," Ingenieur-Archiv, 17, pp. 288-299.

[73] Purtell, L. P., Klebanoff, P. S., and Buchley, F. T., 1981, "Turbulent Boundary Layer at Low Reynolds Number," Physics of Fluids, 24, pp. 802-811.

[74] Smith, D. W., and Walker, J. H., 1958, "Skin-Friction Measurements in Incompressible Flow," National Advisory Committee for Aeronautics, Technical Note 4231.

[75] Coles, D. E., 1956, "The Law of the Wake in the Turbulent

Boundary Layer," Journal of Fluid Mechanics, 1, pp. 191-226.

[76] Schultz, M. P., and Flack, K. A., 2007, "The Rough-Wall Turbulent Boundary Layer from the Hydraulically Smooth to the Fully Rough Regime," Journal of Fluid Mechanics, 580, pp. 381-405.

[77] Raupach, M. R., Antonia, R. A., and Rjagopalan, S., 1991, "Rough-Wall Turbulent Boundary Layers," ASME Applied Mechanics Reviews, 44, pp. 1-25.

[78] Ryu, S., Kim, S., and Yoo, J. Y., 2001, "Correlation of Wall Vorticity and Streamwise Velocity Fluctuations in a Turbulent Boundary Layer," Transaction of the KSME B, 25, pp. 523-532.

[79] Moser, R. D., and Moin, P., 1984, "Direct Numerical Simulation of Curved Turbulent Channel Flow," NASA Technical Memorandum 85974.

[80] Kim, J., Moin, P., and Moser, R., 1987, "Turbulent Statistics in Fully Developed Channel Flow at Low Reynolds Number," Journal of Fluid Mechanics, 177, pp. 133-166.

[81] Lee, J. H., Lee, S. H., Kim, K., and Sung, H. J., 2009, "Structure of the Turbulent Boundary Layer over a Rod-Roughened Wall," International Journal of Heat and Fluid Flow, 30, pp. 1087-1098.

[82] Achenbach, E., 1971, "Influence of Surface Roughness on the

Cross-Flow Around a Circular Cylinder," Journal of Fluid Mechanics, 46, pp. 321-335.

[83] Deutsch, S., and Zierke, W. C., 1986, "The Measurement of Boundary Layers on a Compressor Blade in Cascade at High Positive Incidence Angle Ⅱ- Data Report," NASA Contractor Report 179492.

[84] Hilgenfeld, L., Cardamone, P., and Fottner, L., 2003, "Boundary Layer Investigations on a Highly Loaded Transonic Compressor Cascade with Shock/Laminar Boundary Layer Interactions," Proceedings of the Institute of Mechanical Engineers, Part A: Journal of Power and Energy, 217, pp. 349-356.

[85] Camp, T. R., and Shin, H. -W., 1995, "Turbulence Intensity and Length Scale Measurements in Multistage Compressors," ASME Journal of Turbomachinery, 117, pp. 38-46.

[86] Gibson, M. M., Verriopoulos, C. V., and Vlachos, N. S., 1984, "Turbulent Boundary Layer on a Mildly Curved Convex Surface," Experiments in Fluids, 2, pp.17-24.

[87] So, R. M. C., and Mellor, G. L., 1973, "Experiment on Convex Curvature Effects in Turbulent Boundary Layers," Journal of Fluid Mechanics, 60, pp. 43-62.

[88] So, R. M. C., and Mellor, G. L., 1978, "Turbulent Boundary

Layers with Large Streamline Curvature Effects," Journal of Applied Mathematics and Physics, 29, pp. 54-74.

Appendix A. Clauser Chart Technique

The Clauser chart technique estimates the friction coefficient and friction velocity for turbulent boundary layers. In this method, the friction coefficient is extrapolated from the mean velocity profile in the logarithmic layer. Note that the technique is not applicable to very low Reynolds number turbulent boundary layer which do not have a clear logarithmic region.

In the logarithmic region, the velocity profile follows the log law (Eq. A.1).

$$\frac{u}{u_\tau} = (\frac{1}{\kappa}) \ln (\frac{y u_\tau}{\upsilon}) + B \qquad \text{(A.1)}$$

If both sides of Eq. A.1 is multiplied by u_τ / U_∞, Eq. A.1 becomes Eq. A.2.

$$\frac{u}{U_\infty} = (\frac{u_\tau}{\kappa U_\infty}) \ln (\frac{y u_\tau}{\upsilon}) + B(\frac{u_\tau}{U_\infty}) \qquad \text{(A.2)}$$

By rearranging the equation, Eq. A.2 becomes:

$$\frac{u}{U_\infty} = \left(\frac{u_\tau}{\kappa U_\infty}\right)\ln\left(\frac{yU_\infty}{\upsilon}\right) + \left[\frac{u_\tau}{\kappa U_\infty}\ln\left(\frac{u_\tau}{U_\infty}\right) + B\frac{u_\tau}{U_\infty}\right] \qquad \text{(A.3)}$$

From the definition of the friction coefficient ($C_f = 2(u_\tau / U_\infty)^2$), Eq. A.3 becomes:

$$\frac{u}{U_\infty} = \left(\frac{\sqrt{C_f}}{\kappa\sqrt{2}}\right)\ln\left(\frac{yU_\infty}{\upsilon}\right) + \left[\frac{\sqrt{C_f}}{\kappa\sqrt{2}}\ln\left(\sqrt{\frac{C_f}{2}}\right) + B\sqrt{\frac{C_f}{2}}\right] \qquad \text{(A.4)}$$

Therefore, C_f is proportional to the slope in the mean velocity profile as in Fig. B.1.

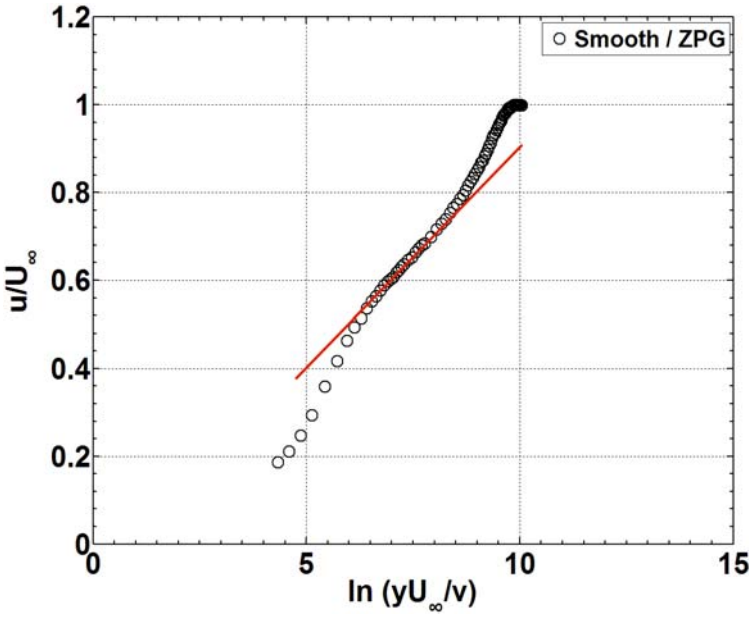

Fig. A.1 Mean velocity distribution in the logarithmic layer.

요약(국문초록)

압력구배가 거친 표면 위 난류경계층 특성에 미치는 영향

서울대학교 대학원

기계항공공학부

신 주 현

본 논문은 유동의 흐름방향 순, 역압력구배가 매끄러운 표면 및 거친 표면에서 발달하는 난류경계층의 특성에 미치는 영향을 실험적으로 연구하였다. 순압력구배는 영압력구배에 비해 매끄러운 표면 위 난류경계층의 벽마찰응력을 증가시켰으나, 자유류속도의 증가로 인해 마찰계수를 증가시키지 못한다. 한편 역압력구배는 벽마찰응력을 감소시켜 마찰계수를 감소시킨다. 또한 매끄러운 표면에 대해 순압력구배는 난류 경계층 내 와류를 표면근처에 제한함으로써 표면근처 흐름방향 정상 레이놀즈 응력을 증가시키나, 역압력구배는 벽

근처에서 발생하는 와류를 벽 외부 방향으로 이송시킴으로써 벽근처에서의 흐름방향 정상 레이놀즈 응력을 감소시킨다. 영압력구배에서 표면거칠기는 강한 난류강도를 갖는 비정상 와류를 발생시킴으로써 경계층 전영역에서 속도 결핍을 야기하고 흐름방향 정상 레이놀즈 응력을 증가시키며, 마찰계수를 증가시킨다. 표면거칠기가 표면 근처 속도 결핍 및 흐름방향 정상 레이놀즈 응력에 미치는 영향은 영압력구배의 경우에 비해 순압력구배가 있을 때 커진다. 또한 순압력구배는 거친 표면 위 난류 경계층의 흐름방향 난류 에너지를 증가시키며, 마찰계수를 증가시킨다. 이는 순압력구배가 표면거칠기에 의해 발생하는 추가적인 고난류 와류를 벽근처에 위치시키고, 벽근처 속도 구배를 증가시켜 표면거칠기에 의한 와류의 강도를 증가시키기 때문이다. 한편 순압력구배와는 반대로 역압력구배는 표면거칠기에 의한 와류를 벽 외부영역으로 이송시키며, 벽 근처 속도 구배를 감소시켜 표면거칠기에 의한 와류 강도를 감소시킨다. 따라서 거친 표면에 대해 역압력구배는 표면거칠기에 의한 속도 결핍 및 표면거칠기의 흐름방향 정상 레이놀즈에 미치는 영향력을 감소시킨다. 또한 거친표면에서 역압력구배는 표면거칠기에 의한 흐름 방향 난류 에너지 생성량 및 마찰계수를 줄인다. 본 결과는 순압력구배가 난류경계층에서 표면거칠기의 영향력을 증가시키며, 역압력구배는 표면거칠기의 영향력을 감소시킴을 나타낸다. 한편 위와 같은 결과로부터 유체기기의 프로파일 손실, 마찰력 및 열전달 예측을 위한 방법들이 제시되었다. 경계층 배제두께와 경계층 두께의 비는 평판, 축류 압축기 블레이드 및 축류 터빈 블레이드 난류경계층 속도 결

펍 프로파일에서 레이놀즈 수, 압력구배, 표면거칠기 효과를 스케일링하는데 사용될 수 있다. 이로부터 평판 경계층 속도 프로파일을 추산하기 위한 새로운 방법을 제안하였으며, 이는 압력구배하에 매끄럽고 거친 평판 위 난류경계층의 속도 프로파일을 정확히 예측한다. 또한 같은 방법이 축류 압축기 및 터빈 블레이드 위 난류경계층 속도 프로파일을 예측하는데 이용될 수 있음을 확인하였다. 마지막으로 순, 역압력구배하에 매끄럽고 거친 평판 위 난류 경계층의 마찰계수를 추산하기 위한 상관식을 제안하였으며, 이 상관식이 매끄러운 터빈 표면 난류 경계층의 마찰계수를 정확히 추산할 수 있음을 확인하였다.

주요어 : 평판, 마찰계수, 평균 속도, 압력구배, 스케일링, 표면 거칠기, 터보기계 블레이드, 난류경계층

학 번 : 2009 - 20692